Universidade de Aveiro

Secção Autónoma de Ciências da Saúde

2013

Inês Castro Fernandes

Identificação e classificação de tecidos tumorais da próstata por FTIR

Identification and classification of prostate tumour tissues by FTIR

Universidade de Aveiro

Secção Autónoma de Ciências da Saúde

2013

Inês Castro Fernandes

Identificação e classificação de tecidos tumorais da próstata por FTIR

Identification and classification of prostate tumour tissues by FTIR

Tese apresentada à Universidade de Aveiro para cumprimento dos requisitos necessários à obtenção do grau de Mestre em Biomedicina Molecular, realizada sob a orientação científica da Doutora Carla Alexandra Pina da Cruz Nunes, Professora Auxiliar Convidada da Secção Autónoma de Ciências da Saúde da Universidade de Aveiro e co-orientação científica da Doutora Margarida Sâncio da Cruz Fardilha, Professora Auxiliar Convidada da Secção Autónoma de Ciências da Saúde da Universidade de Aveiro.

This work was co-financed by Fundação para a Ciência e Tecnologia (PTDC/QUI-BIQ/118492/2010) and FEDER (FCOMP-01-0124-FEDER-020895).

Dedico este trabalho ao meu pai e à minha mãe, que me proporcionam estabilidade e que sempre me apoiaram e incentivaram durante todo o meu percurso académico, ao qual só tive o privilégio de ter acesso graças aos seus esforços.

"Há sem dúvida quem ame o infinito,
Há sem dúvida quem deseje o impossível,
Há sem dúvida quem não queira nada
Três tipos de idealistas, e eu nenhum deles:
Porque eu amo infinitamente o finito,
Porque eu desejo impossivelmente o possível,
Porque quero tudo, ou um pouco mais, se puder ser,
Ou até se não puder ser..."

(excerto do poema "O que há em mim é sobretudo cansaço" de Álvaro de Campos)

"Sou feliz só por preguiça. A infelicidade dá uma trabalheira pior que a doença:
é preciso entrar e sair dela…"

(Mia Couto)

o júri

presidente

Prof. Doutora Odete Abreu Beirão da Cruz e Silva
professora Auxiliar com Agregação da Secção Autónoma de Ciências da Saúde, Universidade de Aveiro

Professora Doutora Ivonne Delgadillo Giraldo
professora Associada com Agregação do departamento de química, Universidade de Aveiro

Professora Doutora Carla Alexandra Pina da Cruz Nunes
professora Auxiliar Convidada da Secção Autónoma de Ciências da Saúde, Universidade de Aveiro

agradecimentos

Um grande agradecimento à Professora Doutora Alexandra Nunes pelo apoio e confiança no meu trabalho. Obrigada pelos concelhos e pela orientação sempre disponibilidade.

À Professora Doutora Margarida Fardilha, obrigada pela co-orientação, apoio e disponibilidade.

À Professora Doutora Odete da Cruz e Silva obrigada pela confiança no projeto.

Ao Grupo de Química dos produtos naturais e alimentares da Universidade de Aveiro, em especial à Professora Doutora Ivonne Delgadillo pela disponibilização do FTIR.

Ao Centro de Biologia Celular da Universidade de Aveiro, obrigada pelo material disponibilizado.

À Joana Vieira obrigada pela disponibilidade e sugestões.

A todos os pacientes que aceitaram fazer parte deste estudo.

Aos Urologistas António Patrício e Nuno Maio do Hospital Infante Dom Pedro, responsáveis pela colheita das amostras, obrigada pela ajuda neste projecto.

À Rafaela, obrigada por me acompanhares durante esta etapa final do nosso percurso académico, pela amizade e pelo teu espírito alegre e otimista contagiante.

À Rita, à Sónia, à Rita Ribeiro e à Cindy pela amizade e companheirismo e pelos momentos marcantes que partilharam comigo durante o nosso percurso universitário, que me ajudaram a crescer e a moldar a pessoa que sou hoje. Obrigada Rita, minha companheira de quarto, por todos os bons momentos e rotinas que passamos juntas.

Ao Filipe, obrigada pelo companheirismo e por me fazeres sorrir, pela confiança em mim e por me incentivares a trabalhar mais e melhor para realizar os meus objetivos.

A todos os meus colegas de mestrado, obrigada pelo apoio.

A todos os meus amigos, obrigada pela amizade e pelos bons momentos de descontração.

Aos meus pais, obrigada por fazerem de mim a pessoa que sou hoje. Obrigada pelo amor e orientação, por sempre acreditarem em mim e estarem sempre do meu lado em todas as fases da minha vida.

A toda a minha família, obrigada pelo amor e pela força.

A Deus, que sei que está sempre a olhar por mim.

palavras-chave Cancro da Próstata, espectroscopia de infravermelho, tecidos, tumor, análise multivariada

resumo

O desenvolvimento do cancro da próstata (CaP) ainda não é inteiramente compreendido, mas já se reconhece que este se desenvolve a partir de estágios pré-malignos. Assim, o fator mais importante na prevenção do cancro é a deteção precoce, que facilita a erradicação destas células pré-malignas antes de uma invasão sistémica. Há uma grande necessidade clínica de técnicas que possam detetar essas alterações bioquímicas pré-malignas que podem avançar para cancro.

A espectroscopia de infravermelho é uma poderosa ferramenta analítica para fornecer informações detalhadas sobre a composição química de amostras biológicas complexas, como tecidos. Esta técnica baseia-se nas vibrações entre os átomos de uma molécula. As moléculas absorvem luz infravermelha e dão origem a padrões espectrais distintos de luz transmitida. Esta é uma técnica analítica não-destrutiva, altamente sensível e específica que permite a identificação de sinais associados ao cancro da próstata ao nível bioquímico, proporcionando um melhor diagnóstico e facilitando a identificação de tumores com biopotencial agressivo.

Esta dissertação é um estudo exploratório que pretende testar a capacidade da espectroscopia de infravermelho por transformada de Fourier (FTIR) em discriminar amostras de CaP de amostras controlo e identificar sinais espectroscópicos relacionados com grupos funcionais de compostos bioquímicos presentes nos tecidos malignos.

Amostras de biópsias prostáticas foram recolhidas de peças de prostatectomia radical de 8 pacientes caracterizados com antigénio específico da próstata (PSA) elevado e/ou exame de toque rectal (TR) anormal. Também foram fornecidas outras informações histopatológicas relevantes sobre os pacientes, como o score de Gleason e a classificação TNM. Amostras de CaP e controlo foram analisadas por FTIR e os espectros resultantes foram submetidos a análise em componentes principais (ACP) nas regiões 3000-2800 cm^{-1}, 1200-900 cm^{-1} e 1800-1700 cm^{-1}.

O diagrama das coordenadas fatoriais (scores) discriminou os espectros das amostras de CaP dos espectros das amostras controlo. O diagrama das contribuições fatoriais (loadings) permitiu a identificação de sinais espectroscópicos associados a modificações bioquímicas patológicas esperadas em tecidos malignos, nomeadamente desregulações no metabolismo lipídico, com base num elevado conteúdo em ácidos gordos e em alterações nas cadeias lipídicas da membrana; também se verificou um menor conteúdo em polissacarídeos (glicose) e em glicogénio e num aumento nos ácidos nucleicos.

No futuro, novas investigações irão possibilitar o desenvolvimento de um modelo universal de classificação multivariada por FTIR para o cancro da próstata.

keywords Prostate cancer, infrared spectroscopy, tissues, tumour, multivariate analysis

abstract

The development of prostate cancer (PCa) is not yet fully understood, but it is already recognized that it develops through pre malignant stages. Thus, the most important factor in the prevention of cancer is early detection, facilitating eradication of these pre-malignant cells prior to systemic invasion. There is a great clinical need for techniques that can detect these pre-malignant biochemical changes that can advance to cancer.

The infrared (IR) spectroscopy is a powerful analytical tool to provide detailed information on the chemical composition of complex biological samples, such as tissues. This technique is based on the vibrations between the atoms of a molecule. The molecules absorb infrared light and give rise to distinctive spectral patterns in transmitted light. This is a non-destructive, highly sensitive and specific analytical technique that allows the identification of signals associated with prostate cancer at a biochemical level, providing an improved diagnosis of cancer and also facilitating the identification of tumors with aggressive biopotential.

This dissertation is an exploratory study that intends to test the ability of the Fourier transform infrared spectroscopy (FTIR) to discriminate between control and PCa samples and to identify spectroscopic signals related to functional groups of biochemical compounds present in the malignant tissues.

Prostate biopsy samples were collected from radical prostatectomy pieces of 8 patients characterized with elevated prostate specific antigen (PSA) and/or abnormal digital rectal examination (DRE). Also relevant histopathological information about the patients has been provided, including the Gleason grade and the TNM staging. PCa and control samples were analysed by FTIR and the resulting spectra were submitted to Principal Component Analysis (PCA) in the ranges 3000-2800 cm^{-1}, 1200-900 cm^{-1} and 1800-1700 cm^{-1}.

The diagram of the factorial coordinates (scores) discriminated the spectra of PCa samples from the spectra of controls samples. The diagram of the factorial contributions (loadings) allowed the identification of spectroscopic signals associated with biochemical pathologic modifications expected in malignant tissues, mainly dysregulations in lipid metabolism, based on higher content in fatty acids and increased disorder of the chains of membrane lipids; also a lower polysaccharide (glucose) and glycogen content and an increase in the nucleic acids.

In the future, further investigations would make possible the development of a universal FTIR multivariate classification model for prostate cancer.

Index

Figures Index

Tables Index

Abbreviations

Acetyl-CoA	Acetilcoenzima A
ADT	Androgen deprivation therapy
AFMS/AFS	Anterior fibromuscular stroma
AKT	Protein kinase B
ANNS	Artificial neural networks
AR	Androgen receptor
ASAP	Atypical small acinar proliferation
ATR	Attenuated total reflectance
BM	Basement membrane
BNI	Bladder neck incision
BPH	Benign prostatic hyperplasia
CA	Cluster analysis
CBP	CREB-binding protein
C-CAMs	Cell-cell adhesion molecules
CT	Computed tomography
CZ	Central zone
DHT	Dihydrotestosterone
DRE	Digital rectal examination
EGF	Epidermal growth factor
EZH2	Polycomb repressor complex 2
FDA	Fisher Discriminant Analysis
FHIT	Fragile histidine triad protein
FTIR	Fourier Transform Infrared Spectroscopy
HGF	Hepatocyte growth factor
IGF	Insulin-like growth factor
IL-6	Interleukin 6
IR	Infrared
KLK	Kallikrein-like serine protease
LDA	Discriminant analysis
LV	Latent variables
MAPK	Mitogen-activated protein kinase
Mid IR	Mid infrared region
MMP's	Matrix metalloproteinases
MRI	Magnetic resonance imaging
PAP	Prostatic acid phosphatase
PCa	Prostate cancer
PCA	Principal component analysis
PCA3	Prostate cancer gene 3
PCR	Principal components regression
PI3 kinase	Phosphatidylinositol 3 kinase
PIA	Proliferative inflammatory atrophy

PIN	Prostatic intraepithelial neoplasia
PLS	Partial least squares regression
PSA	Prostate specific antigen
PSCA	Prostate stem cell antigen
PSDA	Prostate specific antigen density
PSMA	Prostate-specific membrane antigen
PZ	Peripheral zone
RBp	Retinoblastoma protein
RMSECV	Root mean square error of cross-validation
RT	Radiotherapy
SNV	Standard Normal Deviates
STAT3	Signal transducer and activator of transcription 3
SVI	Seminal vesicle involvement
TCA	Tricarboxylic acid
TGF	Tumour growth factor
TNM	Tumour – Lymph node –Metastasis
TRPM-2	Testosterone-repressed prostate message-2
TRUS	Transrectal ultrasonography
TZ	Transitional zone
VEGF	Vascular endothelial growth factor
ZPD	Zero path difference

Chapter one

This chapter describes the normal anatomy and function of the prostate gland. The current diagnostic modalities of prostate cancer are outlined in addition to an overview of the prostate cancer epidemiology and aetiology. Also an introduction about the technique Fourier Transform Infrared Spectroscopy as a new diagnostic modality of prostate cancer and its biomedical applications are included in this chapter. To conclude, the aims and objectives of this thesis are stated.

A. Introduction

1. Prostate Gland
   1.1. Anatomy of the Normal Prostate

The term 'prostate' was first used by Herophilus of Alexandria in 335 B. C. to describe the small organ situated in front of the bladder and derived from the Greek word *prohistani* which means "to stand in front of".(1)

The prostate gland is a small firm organ, about the size of a chestnut, has the shape of a pyramid and lies on the pelvic musculofascial floor, located below the bladder and in front of the rectum – see Figure 1.

The prostate is surrounded by a thin, filmy layer of connective tissue, which separates posteriorly the prostate and seminal vesicles from the rectum - Denonvilliers' fascia. Anteriorly, the puboprostatic ligaments fix the prostate to the pubic bone, being the gland held in the dorsal vein plexus between these structures.(2-4) It consists of a fibromuscular glandular part and the stroma and has a base at the bladder neck and an apex at the urogenital diaphragm, anterior and posterior surfaces and two inferior-lateral surfaces. Skeletal muscle fibers from the urogenital diaphragm extend into the prostate at the apex and, anteriorly, up to the midprostate. The urethra passes from the bladder and through the prostate and penis. About 3 cm long, the prostatic urethra hugs anterior portion of prostate gland and is divided into proximal and distal segments by an abrupt anterior angulation of 30º in its mid portion. Distal to the urethral angulation it has a midline longitudinal ridge in its posterior wall, the Verumontanum.(1, 2) Located superior to the base of the prostate, the seminal vesicles undergo confluence with the vas deferens on each side to form the ejaculatory ducts – see Figure 2. The ejaculatory duct complex consists of the two ejaculatory ducts along with a second loose stroma rich in vascular spaces. The two ejaculatory ducts open in distal urethral segment that also receives about 95% of the ducts of glandular prostate. When present, the utricle is located between the ejaculatory ducts and its remnants occasionally form cystic structures in the midline posteriorly. Seminal vesicle involvement (SVI) by prostate cancer (PCa) is one of the most important predictors for PCa progression.(1, 3, 4) – see Figure 2.

The term "capsule" is used in the current literature, but there is no consensus about the presence of a true capsule in the prostate. This prostatic "capsule" is composed of fibrous tissue surrounding the gland and is best appreciated posteriorly and posterolaterally, between the prostatic stroma and extraprostatic fat (2).

The prostatic branches of the inferior vesical artery are the main arterial supply to the prostate gland. It is also supplied by small branches from the middle rectal and pudendal vessels. The veins are situated mainly in the prostatic "capsule" and the lymphatic vessels from the prostate drain into internal iliac lymph nodes.

Being the largest accessory reproductive gland in man, the prostate contracts with the ejaculation and has as primary function to provide enzymes to maintain the fluid nature of seminal fluid and to nourish sperm.(2, 4) – see Figures 1 and 2.

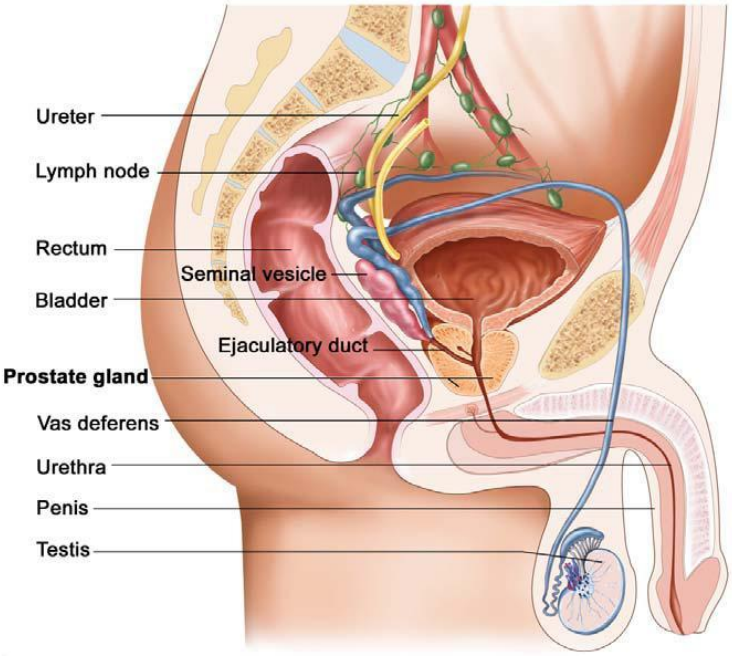

Figure 1 Median sagittal section of the male pelvis. Adapted from (5)

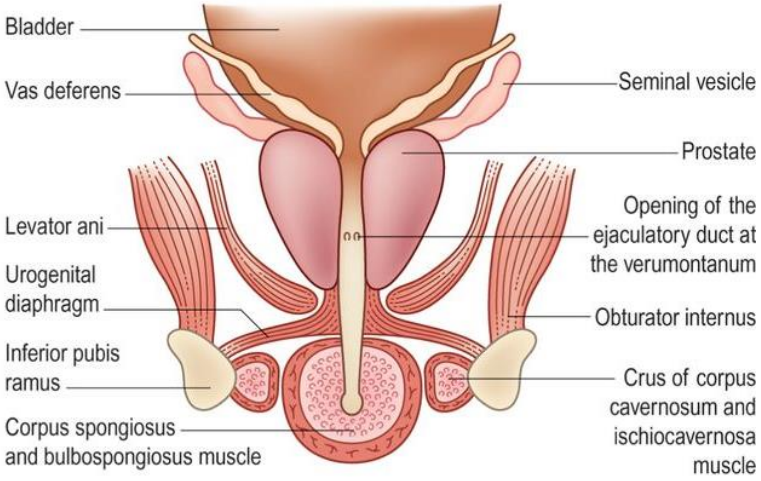

Figure 2 Illustration of the prostate gland localization. Adapted from (6)

1.2. Zonal Anatomy and Histology of the Normal Prostate

McNeal JE introduce the concept that the prostate gland was composed of diverse zones rather than lobes and established the current and most widely accepted division of the prostate gland into four basic anatomic zones, on the basis of biological and histological concepts, the peripheral zone (PZ), the central zone (CZ), the transitional zone (TZ) and the anterior fibromuscular stroma (AFMS/AFS). (2, 7, 8) – see Figure 3.

The peripheral zone constitutes about 70% of the glandular part of the prostate, comprising all the glandular tissue at the apex and all of the tissue located posteriorly near the capsule. Its ducts open into prostatic urethra distal to verumontanum. The glands of the peripheral zone have rounded contours and its stroma is loosely woven with randomly arranged smooth muscle.

Diseases of the prostate, such as carcinoma, chronic prostatitis and postinflammatory atrophy, are more common in this zone than in the others. (1, 2, 7, 9)
The central zone is cone-shaped and comprises 25% of the glandular prostate. The apex of the cone is at the confluence of the ejaculatory ducts and the prostatic urethra at the verumontanum. This zone is surrounded by the peripheral zone in its distal part, surrounds the ejaculatory ducts and is relatively resistant to carcinoma and other diseases. Central zone glands are larger, more complex and often located in lobules around central ducts, ridges and arches. The stroma in this zone is less abundant but contains compact smooth muscle fibres. Biochemically, the CZ is the only zone which produces pepsinogen II and tissue plasminogen activator. (1, 2, 9)
The transitional zone consists of two equal and independent lobes of glandular tissue. Its ducts open in the postrolateral part of urethra. The glands of this zone have rounded contours and its stroma contains more compact, interlacing smooth muscle bundles. This zone is clinically important as it is involved in the development of age-related benign prostatic hyperplasia (BPH). (2, 9)
The anterior fibromuscular stroma forms the convexity of the anterior external surface and consists of a band of fibromuscular tissue contiguous with the bladder muscle and the external sphincter. Its distal portion is important in voluntary sphincter functions and its proximal portion in involuntary sphincter functions.(1, 2, 9)
Zonal anatomy has replaced lobar anatomy with one exception. The term “median lobe” was originally designated as a third lobe occasionally palpable on digital examination above and between the two lateral lobes. It can be visualized on cystoscopy as a posterior encroachment, as opposed to lateral encroachment from TZ hypertrophy and it is visible on ultrasound, magnetic resonance imaging (MRI) and Computed tomography (CT) as a distinct form of hypertrophy with a large intralumen component. The median lobe has a unique behaviour and its presence has implications to radiation treatment planning and treatment selection.(9)

Histologically, two cells layers can be found in the prostate gland. A luminal secretory columnar cell layer line the entire tubulo-alveolar organisation of the prostate, with the exception of the main lateral ejaculatory ducts that are lined by transitional cell epithelium just before they enter the urethra.(2) The typical gland is lined by a basement membrane (BM) composed of type IV collagen, fibronectin, laminin, heparin sulphate and entactin. An underlying basal cell layer separates the columnar secretory cells from the BM. The basal cells have little discernible cytoplasm and darkly stained nuclei. The function of these basal cells is poorly understood, but they are histologically important as their presence differentiates between benign disease and adenocarcinoma when they are not present. The secretory cells (epithelium) secrete proteins such as prostate specific antigen (PSA) and prostatic acid phosphatase (PAP) into the seminal plasma. The glands secrete mucins and produce lipofuscin. They also secrete citric acid and acid phosphatase.(2, 10)

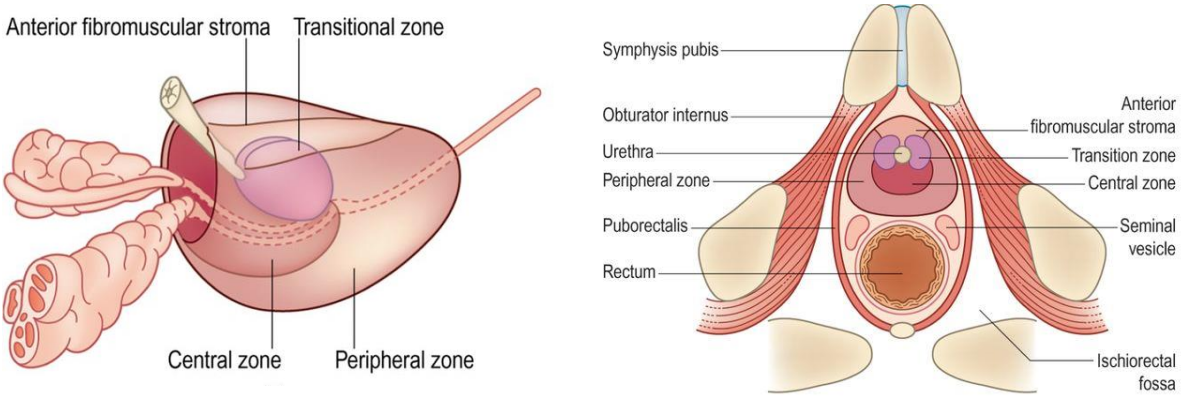

Figure 3 Prostate illustrations of McNeal's zonal anatomy. Adapted from (6)

1.3. Neural Anatomy of the Normal Prostate

The prostate gland is an extraordinarily well-innervated organ that receives dual autonomic innervation, both parasympathetic and sympathetic. The cholinergic innervation is from the hypogastric and pelvic nerves and the noradrenergic innervation from a peripheral hypogastric ganglion. Two neurovascular bundles are located posterolaterally adjacent to the gland and form the superior and inferior pedicles on each side. (2) – see Figure 4.

Both autonomic fibres innervate the prostate stroma. Cholinergic nerves innervate the smooth muscle of the capsule and the space around the blood vessels, being responsible for the secretory function of the epithelial part. Sympathetic nerves control the prostatic musculature and their excitation closes the bladder neck during ejaculation of the seminal fluid into the urethra. There is an increasing interest on nerve-sparing surgical treatment of PCa, because of the demonstrated importance of these nerves in penile erection. (2)

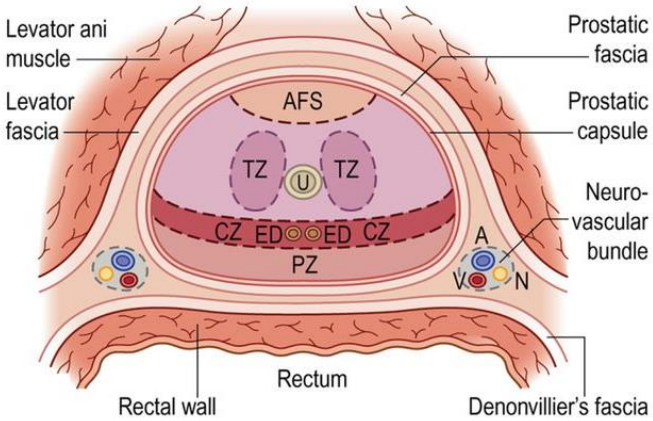

Figure 4 Illustration of the prostate gland, showing the zonal anatomy and the neuro-vascular anatomy. Abbreviations: AFS, anterior fibromuscular stroma; TZ, transitional zone; U, Urethra; CZ, central zone; ED, ejaculatory duct; PZ, peripheral zone. Adapted from (6)

1.4. Relevance of Prostate Zonal Anatomy and Histology in Clinical Practice

A sound knowledge and application of prostate gland histology and anatomy is required for the diagnosis of different pathological conditions including benign prostatic hypertrophy (BPH) and allow a more scientifically based selection of medical therapy for men with prostate disease.
A key landmark for endoscopic procedures of the lower urinary tract is the verumontanum. To avoid damage to the external urethral sphincter and preserve continence, when an endoscopic surgery such as transrectal ultrasonography (TRUS) of the prostate or bladder neck incision (BNI) is performed to relieve bladder outflow obstruction, resection is not pursued distal to the verumontanum. The obturator nodes are usually the first to be involved in metastatic spread. So, during radical prostatectomy, the obturator nodes or other pelvic lymph nodes can be sampled to provide useful tumour staging information. (11)
The origin of the tumours can be established according to the sample technique used. When a transrectal ultrasound guided core biopsy is performed, the regions of the prostate sampled are likely to consist of tissue from the peripheral zone, seldom the central or transitional zones. When a TRUS is performed, the specimens will mostly consist of tissue from the urethra, bladder neck, periurethral zone, transitional zone and anterior fibromuscular stroma.(8) On one hand, a well differentiated carcinoma found in TRUS specimens is more likely to represent carcinoma originating in the transitional zone. On the other hand, a poorly differentiated carcinoma in TRUS specimens may represent tumour originating in the peripheral zone that invades the transitional zone.(11)

Based upon the concept of a prostate gland divided into four basic anatomic zones, it has been possible to establish the different neoplastic potential of the zones and the effect of the zonal origin on prognosis.
The predominant thought was that PCa arose nearly exclusively in the posterior part of the prostate (peripheral zone) close to the prostatic capsule. But more recent studies confirmed that in prostates removed for PCa a significant minority of PCa foci arise in the transition zone and central zone.(2) Has been also described the unique well-differentiated nature of tumors arising in the transition zone (Gleason pattern 1 and 2), which are characterized with a low risk of progression and being rarely associated with capsular invasion or seminal vesicle involvement (SVI). (2)
It is also known that the parenchymal components of the prostate vary in the size, shape and the number of acini in different zones. So, the greater number of acini in PZ can explained the higher incidence of adenocarcinoma in this zone. The loosely woven stroma in PZ and compact stroma in TZ can also explained the occurrence of adenocarcinoma from the acini of PZ and the BPH in TZ.(2, 7)

2. Prostate Cancer

2.1. Epidemiology

2.1.1. International Prostate Cancer Epidemiology

Being the second most frequently diagnosed cancer of men and the fifth most common cancer overall, there are 899 000 new cases of prostate cancer every year (13.6% of the total) and nearly three-quarters of the registered cases occur in developed countries (644 000 cases). (12)
Prostate cancer is the sixth leading cause of death from cancer in men (6.1% of the total), with an estimated 258 000 deaths in 2008 and the second leading cause of cancer-related death of men in the United States. Incidence rates of prostate cancer vary by more than 25-fold worldwide. Australia/New Zealand, Western and Northern Europe, Northern America have the highest rates because of the widespread practice of prostate specific antigen (PSA) testing and subsequent biopsy in those regions. Certain developing regions (Caribbean, South America and sub-Saharan Africa) have incidence rates relatively high, while South-Central Asia has the lowest age-standardised incidence rate (4.1 per 100,000). (13)
Adenocarcinoma, which accounts for about 95% of prostatic neoplasms, has frequently no specific presenting symptoms. Prostate cancer (PCa) is often clinically silent and sometimes mimics obstructive symptoms of Benign Prostate Hyperplasia (BPH). Consequently, has come to the forefront of focus the diagnostic value of patient screening by using early detection programs like the widespread screening with serum prostate specific antigen (PSA). PSA testing has a much greater effect on incidence than on mortality. With the introduction of this test, the incidence of stage IV PCa at presentation has dramatically lessened, although the number of PCa detected has increased as well. There is less variation in mortality rates worldwide than is observed for incidence, and the number of deaths from PCa is almost the same in developed and developing regions. Mortality rates are generally high in predominantly black populations (Caribbean, sub-Saharan Africa), very low in Asia and intermediate in Europe and Oceania. (14)

2.1.2. Portuguese Prostate Cancer Epidemiology

Prostate cancer is the second most common cancer among Portuguese men in 2000 (2973 new cases). There is a cumulative risk (0–74 years) of 3.2 % of a Portuguese individual developing prostate cancer and a total cumulative risk of 3.0 % of dying from prostate cancer.(15)
During the period of 1988 to 1998 the overall age-standardised cancer mortality rate for men in Portugal increased (1.4 % annually), with prostate cancer (3.6 % annually) mostly contributing. In the middle of 1990s the level of prostate cancer mortality in Portugal was similar to the EU average and approximately 35 % higher than in Southern European countries. However, in the years 1978 to 1994, the increase in prostate cancer mortality in Portugal and other Southern European countries such as Italy and Spain was lower than in most Northern European countries, and similar to those of Western Europe such as France, Austria and Germany. As mentioned before, the introduction of some prostate-screening programmes, based on PSA testing, may be the cause of the gradual reduction in mortality (due to an earlier diagnosis) in some countries of Europe (Austria, France, Germany, Italy), where the decreasing in mortality trends in the age group 50–79 years began in the 1990s. (15)

2.2. Aetiology of Prostate Cancer

The currently established risk factors for prostate cancer are increasing age, family history and ethnicity.

Age is the most significant risk factor of all for prostate cancer. More than half of all cases of PCa are diagnosed in men over 70 and it is quite rare in men under 50. In old age, up to 8 out of 10 men have prostate cancer cells in the prostate.(16, 17)

Family history is also an important risk factor for PCa. If you have a father or brother diagnosed with prostate cancer you are 2 to 3 times more likely to get prostate cancer yourself, compared to the average man. And with more than one first degree relative diagnosed, your risk is about 4 times that of the general population.(17, 18) Also an important factor is the age that your relative is diagnosed with prostate cancer. The younger they were diagnosed (before the age of 60), the higher your risk for developing PCa. A case of an inherited faulty gene can be the cause of having several relatives with prostate cancer, especially if they were diagnosed when they were young. For example, men who have relatives with breast cancer may have a higher risk of prostate cancer, mainly caused by an inherited faulty gene called BRCA2. Men who have a mutation in the BRCA2 gene can have a risk 5 times higher than men in the general population and this risk increase (7 times) in men under the age of 65.(18)

As mentioned before, ethnicity also influences the risk for prostate cancer. PCa is more common in black populations than in white or Asian men, being the black African and black Caribbean men 2 or 3 times more likely to develop prostate cancer than white men. Asian men have a lower risk than white men. A mixture of inherited genes and environmental factors seem to be the cause of these differences. When men move from a country where the prostate cancer risk is low to one where it is higher their risk increases.(19)

There is a keen interest in establishing potentially modifiable factors, such as diet, lifestyle, endogenous hormones and medical conditions/interventions, but no definitive evidence to support a change in treatment strategy currently exists. For example, many studies have looked at dietary factors and prostate cancer risk. This type of research is difficult and much of the research has not found any definite links between particular foods and the risk of prostate cancer. Recently, though, has been found that foods containing lycopene and selenium probably reduce the risk of prostate cancer.(20, 21) Lycopene is found mainly in tomatoes and tomato based foods and selenium is a naturally occurring chemical found in plant foods, fish, shellfish, some meats, grains, eggs, Brewer's yeast, and wheat germ. Diets high in calcium and dairy protein may increase the risk of prostate cancer.(21) Hormone levels may or may not play a part in the risk of developing prostate cancer. The prostate gland is a sex organ that needs the sex hormone testosterone to work. In the past, it was thought that having higher levels of testosterone in the blood may increase the risk of prostate cancer. But, in 2008 an analysis of 18 separate studies found no link between levels of sex hormones and prostate cancer risk.(22)

2.3. Androgen Receptor Pathway in Prostate Cancer

Androgens serve as a most important ligand for prostate cancer (PCa), stimulating growth via the androgen receptor action pathway. The androgen receptor action pathway includes the androgen receptor, the 5-alpha-reductase gene and the various members of the cytochrome p450

family.(23) About 10 to 20% of PCa specimens have mutations within the AR gene, with mutations more common in hormone escape than hormone sensitive specimens. The androgen receptor (AR) has three important domains: N-terminal transactivation domain, DNA binding domain and C-terminal steroid binding domain.(23, 24)

Several studies have already shown that the action of AR in prostate development is mediated by the local stroma. Also, it has been shown that oestrogens have a role in cancer development, yet the oestrogen receptor is predominantly localized in stromal cells. . Animal models have demonstrated prostatic cell proliferation occurs in androgen deficient mice due to exogenous oestrogen. In addition, elevated androgen levels in oestrogen deficient mice induced prostatic hyperplasia. Therefore, neither of these hormones alone induced prostate cancer, but combined androgen and oestrogen therapy did evoke prostatic dysplasia and adenocarcinoma. Thus, both androgens and oestrogens influence the process of prostate carcinogenesis.(25-27)

The androgen deprivation therapy (ADT) is used to prevent activation of AR regulated genes. And the failure of ADT, as in hormonally resistant prostate cancer, was linked to genetic modification of the AR.(26) More recently, the effect of post-translational modifications on the AR has been recognized. The phosphorylation of the AR in response to binding by the ligand DHT (dihydrotestosterone) has been demonstrated. This phosphorylation can stabilize the active AR homodimers and also influence AR mediated gene activation.(28) In addition, the phosphorylation of AR by MAPK (serine-threonine kinase) and AKT (protein kinase B) sensitizes AR to low levels of DHT, which allow low levels of androgens, or alternative steroids, to induce translocation of the AR to the nucleus, facilitating gene activation. MAPK has been shown to be activated in cell lines derived from hormone-refractory tumors and is correlated with advanced stage and grade in PCa. AKT can be activated via PI3 kinase pathway and specifically phosphorylates AR at Ser210 and Ser790 (25, 27-29) – see Figure 5.

It is also important to notice that the control of AR function also involves interaction of the receptor with a number of co-factors or proteins that increase (co-activators) or inhibit (co repressors) the transcriptional activity of the AR. Co-activators include CBP (CREB-binding protein), beta-catenin, ARA55 and ARA70. They all act to alter ligand specificity of the AR and these mechanisms include allowing the antiandrogens such as hydroxyflutamide (CBP, ARA70) and bicalutamide (ARA70) to act as agonists and/or by permitting low concentrations of adrenal androgens or oestradial to activate AR. In addition, others co activators activate AR in the absence of ligands, such as SRC-1, SRC-3, p300, Tip60, and c Jun. Lastly, there is a less well understood mechanism of AR co-activators which involves movement of AR to the nucleus. It is via this mechanism that the STAT3/AR complex activates AR-dependent genes (in the absence of androgens) in response to IL-6 stimulation.(25, 30)

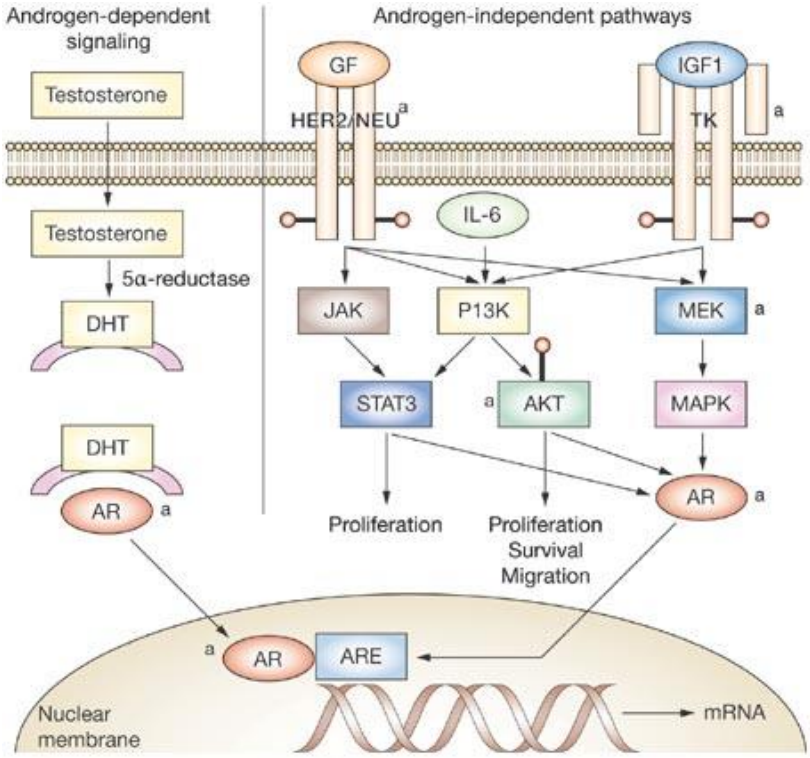

Figure 5 Illustration of the Androgen-receptor signalling in prostate cancer. The left panel illustrates the hormone-dependent androgen signaling that takes place through dihydrotestosterone stimulation of the androgen receptor; The right panel illustrates the hormone-refractory prostate cancer cells that survive through stimulation of multiple signaling pathways, including the PI3K and the MAPK pathways, which culminate in androgen-receptor signaling, or alternate pathways that lead to cell proliferation, migration and survival.

Abbreviations: AKT, protein kinase B; AR, androgen receptor; ARE, androgen response element; DHT, dihydrotestosterone; GF, growth factor; IGF1, insulin-like growth factor 1; IL-6, interleukin 6; JAK, Janus kinase; MAPK, mitogen-activated protein kinase; MEK, upstream kinases of mitogen-activated protein kinases, also known as MAP2Ks; P13K, phosphatidylinositol 3 kinase; mRNA, messenger RNA; STAT3, signal transducer and activator of transcription 3; TK, tyrosine kinase. Adapted from (31)

2.4. The Gleason Grading System

Currently, the strongest prognostic factor of a patient's time to progression is the Gleason grading system, being the 'gold standard' for classifying prostate cancer (PCa).(32) The histologic analysis of PCa based on the Gleason system describes the histologic appearance of PCa under low magnification. It assigned a rating between 1 and 5 to the tumour, based on architectural patterns, with higher numbers representing less differentiated, more aggressive tumours. Well-differentiated PCa (Gleason grade 1 or 2) is characterized by a proliferation of microacinar structures lined by prostatic luminal cells without an accompanying basal cell layer. Some of the neoplastic cells contain prominent nucleoli, defined as at least 1 µm in diameter. Gleason pattern 5 is the highest grade and includes a solid pattern with central necrosis or infiltrating individual cells – see Table 1.(2, 32)

A single prostate can harbour multiple foci of different histologic patterns of adenocarcinoma, and it is possible to have two or more grades in the same specimen (85% of prostate tumours are multifocal). The Gleason score (or Gleason sum) incorporate both a primary (dominant) and a secondary (subdominant) grade into the system. The primary pattern is added to the secondary grade to arrive at a Gleason score, i.e.: in a tumour with mostly Gleason grade 3 and some

Gleason grade 4 disease, the Gleason score will be 3+4=7. Consequently, the Gleason score possibilities range from 2 (1 + 1) up to 10 (5 + 5), assessed by the uropathologist using low-power light microscopy.(2, 33)

There are several limitations concerning Gleason system as a grading system. First, Gleason grading is observer dependent and may vary depending on the level of experience. Second, the majority of patients diagnosed today fall into the Gleason 6–7 category, an intermediate prognostic range limiting the potential usefulness of a 10-point scale. (2)

Grade	Histology	Biological Behaviour
1, 2	Closely-packed glands forming a nodule	Indolent disease, rarely progressive
3	Small infiltrating glands, complete lumen formation	Most common pattern; less aggressive than pattern 4
4	Fused glands, incomplete lumen formation	Indicates tumour progression
5	Solid sheet or single cells, no lumen formation	Very aggressive, late stage

Table 1 Gleason grading system. Adapted from (32)

2.5. Limitations of Conventional Histopathology

Pathology is the gold standard for prostate cancer diagnosis and obtaining prostate tissue specimens with the disease present is necessary for prostate cancer diagnosis. However, as mentioned before, prostate cancers are often multifocal and heterogeneous in pathology. So, prostate core biopsies may contain limited carcinoma within the sample and cancer diagnoses can be missed on account of human error. This fact means that negative biopsies do not exclude the possibility of prostate cancer, likewise that positive biopsies may not contain or reflect the degree and severity of prostate cancer present. In a case of a positive biopsy for PCa, there is also an inter-observer variation in applying Gleason grade, being the variability in interpretation the main problem.(33, 34) Recognise the border areas between Gleason patterns and that microscopic foci of carcinoma do not necessarily represent low grade carcinoma are important difficulties faced by the uropathologists. Some improvements in Gleason grading have been achieved by online tutorials and regular refresher courses. However, the subjectivity in interpretation of the Gleason grade continuous to be a concern because of the pathological assessment guides treatment.(35-37)

3. Diagnostic modalities of Prostate Cancer

3.1. Clinical Signs and Symptoms

Early localized prostate cancer is often asymptomatic. However, PCa may cause prostate gland enlargement, which leads men to present a number of unique symptoms, related to the prostate's location in the body. As the prostate enlarges, the prostatic urethra is pinched tighter and tighter within the prostate. As the tube narrows, urine has a much harder time making its way through the urethra and out of the body. This results in four primary urinary symptoms: Frequency, that is the need to urinate much more often than normal; Urgency, that is the

sensation that you need to urinate immediately; Nocturia, that is the need to urinate multiple times during the night; and Hesitancy, that is the difficulty to start the urine stream. (38-40)
It is important to realize that PCa is not the only disease that can cause the prostate to swell and, consequently, these urinary symptoms. A much more common cause of an enlarged prostate is Benign Prostatic Hyperplasia (BPH). (40) Also, the majority of prostate cancers arise in the peripheral zone; however, it is unusual that sufficient enlargement will occur in the PZ to cause urinary symptoms. Transitional zone tumours and large PZ tumours may cause urinary outflow symptoms, but it is the coexistence of transitional zone enlargement secondary to hyperplasia that may contributes to most men presenting these symptoms. (40-42)
Cancer of the prostate gland often grows slowly, especially in older men and symptoms may be mild and occur over many years. If the prostate cancer is advanced, other less common symptoms may develop, which are less specific to problems with the prostate (problems with other organs such as the bladder can also cause them). These include blood in the urine (Hematuria), blood in the semen (Haematospermia), perineal discomfort and new-onset erectile dysfunction (Impotence). Advanced prostate cancer commonly spreads to the bones, and cancers cells in the bone may cause pain in the hips, back (spine), ribs (chest), or other areas. A cancer that has spread to other areas of the body is called metastatic or secondary prostate cancer. If the cancer spreads to the bones of the spine, it will usually press on the spinal cord or its nerves, leading to weakness or numbness in the legs or feet and even loss of bladder or bowel control.(40-42)

3.2. Digital Rectal Examinations

Palpation of the prostate by digital rectal examination (DRE) allows assess the external contour of the prostate gland. (43) By itself, DRE is a poor method for diagnosing PCa, as it is not specific for cancer, both prostatitis and benign prostatic hypertrophy (BHP) may cause an abnormal examination.(43, 44) However, up to 50% of palpable masses are attributable to prostate cancer and can be detected by DRE, especially cases of prostate cancer with a palpable volume of 0.2 ml or more and originating in the peripheral zone (PZ).(41, 45) It is also particularly important the detection of a palpable mass/nodule at the prostatic apex. Its presence is often indicative of extraprostatic extension at that location and tends to foreshadow a positive surgical margin or poorer result post-radiotherapy. (46, 47)
Unfortunately, when a PCa is diagnosed based on a palpable tumour, there is a high risk of the patient already harbours metastatic or locally advanced malignancy. That is why the risk of a positive DRE turning out to be a prostate cancer should be evaluated together with the results of the PSA value: the higher the PSA value the more likely the DRE assessment will be positive. DRE still have an important diagnostic role, as 30% of tumours are detected by abnormal DRE in men with normal PSA levels, < 4.0ng/ml. DRE is also important for the clinical staging of the disease.(48, 49)

3.3. Prostate Specific Antigen

Prostate specific antigen (PSA) is a kallikrein-like serine protease produced almost exclusively by the epithelial cells of the prostate and secreted into the ductal system. In serum, it is normally in complex with α-1-anti-chymotrypsin and α-2-macroglobulin, only a small percentage of serum

PSA is in its free form. Serum PSA is determined by immunoassay techniques and monoclonal antibodies have been designed to detect the free form of PSA, the complex of PSA and α-1-anti-chymotrypsin and the total PSA.(50-52)

Prostate specific antigen (PSA) was discovered in 1979 by Wang *et al* and since then PSA testing has revolutionized the detection of prostate cancer and monitoring of its treatment.(52, 53) The PSA testing was initially approved by the FDA in 1986 for monitoring the disease status of prostate cancer patients and in 1994 it was endorsed as a screening method for PCa. Although many studies demonstrate benefits for PSA screening in reducing mortality, the benefits for screening in improving survival are yet to be proven.(54, 55)

The PSA screening has many strengths, as it can precede the appearance of a palpable mass by as many as ten years, tumour-induced symptoms by 5-10 years and, on average, death by prostate cancer by 17 years. However, it is important to notice that PSA is not a test for prostate cancer and an abnormal serum PSA only indicates that something is likely to be awry in the prostate that includes cancer as one possibility.(56-58) It is also important to recognize that there are non-malignant causes that can produce an elevated PSA (>4.0ng/ml): these include infection, benign prostatic hyperplasia (BPH), ageing endorsing age-based reference ranges and instrumentation of the prostate and urinary tract.(59-61) Also certain drugs, such as finasteride, can lower PSA values by approximately 50%. (62)

There is no universally accepted cut off point or upper limit of a normal PSA. Values over an arbitrary cut off point of 4.0ng/ml are inferred to be abnormal; however, many men may harbour prostate cancer with a low serum PSA. The Table 2 shows the risk of prostate cancer in relation to low serum PSA values. In the large majority of cases of PCa an elevated serum PSA levels, mostly between 4.0-10.0 ng/ml, are present.(63) In these cases, usually the next step in elucidating the cause of an elevated PSA is a prostatic biopsy. However, most men undergoing prostatic biopsies have negative histology for cancer, even when more than 8 TRUS-guided biopsies are taken, with biopsies repeated if suspicion of an undetected malignancy is high.(64, 65) A serum “cut-off” of 3.0ng/ml has been advocated to increase the likelihood of detecting PCa. However, it has been reported that approximately 15% of PCas detected by investigating a serum PSA level between 3.0-4.0 ng/ml had extraprostatic growth and with this PSA threshold of 3.0ng/ml, the negative biopsy rate has increased. (48, 66-69)

Improving the characteristics modifications of the PSA has been considered and there are different tests that can be performed in a PSA screening: the free/total PSA, the PSA velocity and the PSA density.(51, 70) The first one, the free/total PSA (f/t PSA), measures the percentage of free/unbound PSA in the blood, and compares it with the percentage bound to proteins, with its application most useful in younger men. As in PCa most of the PSA in blood is bound, the lower the ration of free to total PSA or the percentage of free PSA, the higher the likelihood that the patient has PCa. The free/total PSA test can help to discriminate between patients with indeterminate PSA levels (4.0-10.0 ng/ml) who are at the greatest risk of having prostate cancer, in particular aggressive disease.(70-72) The PSA velocity measures the speed at which a series of PSA values increases in value over a period of time and any change in PSA >0.75 ng/ml in a year is concerning for PCa.(73) The PSA density (PSDA) measures the concentration of PSA in a man’s prostate by comparing the value of his PSA and the size of his prostate. As most neoplastic prostate glands produce higher serum PSA levels than do non-malignant glands, a serum PSA of

5.0ng/ml in a patient with a 20 gram prostate is more worrisome for cancer than that a PSA of 5.0ng/ml in a patient with a 60 gram prostate. In order to determinate the PSA density, a PSA level is obtained and is divided by the volume of the prostate, estimated by transrectal ultrasonography (TRUS). A value >0.15 ng/ml per gram of prostate tissue concerning for PCa. As the transition zone (TZ) is the site in which BPH develops and about 25% of PCas also arise in this zone, it is also important to include TZ measurements in relation to the overall size of the prostate. Therefore, the larger the TZ in relation to the overall size of the gland, the lower the likelihood of prostate cancer, other things being equal.(74-76)

PSA level (ng/ml)	Risk of Prostate Cancer (%)
0-0.5	6.6
0.6-1	10.1
1.1-2	17
2.1-3	23.9
3.1-4	26.9

Table 2 Risk of prostate cancer in relation to low serum PSA values. Adapted from (77)

3.4. Molecular Markers (Biomarkers) for Prostate Cancer Detection

Prostate cancer (PCa) is a phenotypically heterogeneous disease and alterations in cancer cells occur at many levels, both pre and post transcriptionally (in the genome and transcribed RNA), and post translational protein modifications. So, there is an increasing interest in establish reliable prostate cancer biomarkers to identify cancer cells in blood, bone marrow, urine, prostatic tissue and semen. A biomarker is a biological molecule that can be found in both body fluids or tissues and that is a sign of a normal or abnormal process or of a condition or disease. It can also be used to see how well the body responds to a treatment for a disease or condition.

It has been noted that the genes, their transcription rates and subsequent proteins altered in prostate cancer can be grouped into a number of cellular pathways: cell adhesion, cell-cycle regulation, cell signalling, angiogenesis and apoptosis. The main molecular aberrations in prostate cancer are summarized in Table 3.

Cellular pathway	Molecular markers	Process
Cell Adhesion	E-cadherin, metalloproteinases, kallikreins, CD151	The aberrant expression of cell-cell adhesion molecules (C-CAMs), including E-cadherin, is associated with the development of tumors and the decreasing of its expression have been associated with the progression of PCa and several other types of neoplasm.(78) CD44 is also a cell adhesion molecule that has been associated with prostate cancer. However, the molecular based profiling may depend more on overexpressed molecules and the activity of MMP's 2 and 9, uPA and uPAR, and KLK2, 3 (PSA) and 4 in interfering with cell adhesion may be more relevant. The efficacy of both KLK2 mRNA and its protein product, hK2, as stand-alone biomarkers or in combinations with other known biomarkers (PSA), has been studied.(79-81) Both KLK4 and its protein product, hK4, have also been associated with prostate cancer. KLK4 expression is regulated by androgens, oestrogen and progesterone in prostate cancer cells and seems to be

		overexpressed in prostate cancer. (82) CD151 is a cell adhesion associated molecule plays a role as a link between extracellular matrix and intracellular structures and may be relevant prognostically as the increase of its protein levels in well and moderately differentiated prostate cancers is correlated with disease relapse subsequent to radical prostatectomy. (83)
Cell-cycle regulation	Cyclin family, RBp, p16, p21, p27, p53, Smad4, FHIT, and PTEN/MMAC1	Cyclin family, RBp (retinoblastoma protein), p16, p21, p27, p53, Smad4, FHIT, and PTEN/MMAC1 are some of the molecules involved in the control of progression in the cell cycle that have its expression altered in PCa.(78) Poor prognostic outcomes are related with increased expression of p16 and p21. Also some prognostic value is given to the loss of RBp and p27. (78, 84) In clinically localized PCa, the strong expression of a catalytic subunit of the polycomb repressor complex 2, EZH2, is associated with poor prognostic. In hormone refractory PCas its overexpression is also observed.(85) The E2F3 transcription factor is responsible for EZH2 regulation and its shown nuclear expression in 20% or more of prostate epithelial cells may also be an indicator of an unfavourable clinical outcome.(86)
Cell Signalling	TGF-beta, EGF, IGF Caveolins	Cell-cell signalling is mediated by a number of soluble and insoluble proteins and factors, including growth factors (TGF-beta, EGF and IGF) and cytokines (Il-6).(87) Caveolins are major structural proteins of the Caveolae[1]. Caveolin-1 is an important caveolin, demonstrated to be implicated in oncogenic cell transformation and subsequent metastasis. In PCa, caveolin-1 seems to function as a tumour promoter, via both genetic and post-translational modifications.(88) c-Myc and caveolin-1 immunopositivity are correlated positively with Gleason score (P = 0.0253) and positive surgical margin (P = 0.0006). So, the combination of positive c-Myc and caveolin-1 in patients with clinically confined PCa may be a significant prognostic marker for disease progression after surgery.(89)
Angiogenesis	VEGF, VEGF receptors, PSMA	VEGF is a key component in angiogenesis and has prognostic value, since it is highly expressed in most PCas. It has been used as target for therapeutics, which has been demonstrated to be a very important targeting pathway, since hypoxia is a known important factor that induces VEGF production.(90, 91) PSMA (prostate-specific membrane antigen) is expressed by both tumour epithelium and tumour associated endothelial cells and neovasculature.(92) PSMA has also been used as a target for therapeutics, being made a series of antibodies against the external domain of this protein.(93, 94) Some studies proposed that PSMA may function as a ligand internalizing receptor, an enzyme playing a role in nutrient uptake, and a peptidase involved in signal transduction in prostate epithelial cells.(95-97) So, a specific PSMA transcript may have applicability as a biomarker for PCa, particularly when used in combination with other gene transcripts, such as

[1] Specialized plasma membrane invaginations that are abundant in smooth muscle cells, adipocytes and endothelium, and act as regulators of signal transduction.

		DD3/PCA3. (95, 98)
Apoptosis	p53, Bcl-2, Clusterin	Some key regulators of apoptosis, which can be pro-apoptotic (p53) or anti-apoptotic (Blc-2), show abnormal function and expression in cancer cells. p53 regulates transcription of genes important for G1-phase growth arrest of cells in response to DNA damage and mutations in p53 are a common event in early stage, organ-confined PCa.(99) Its use as a diagnostic marker is controversial due to the heterogeneity of expression within tumours. Since metastatic, recurrent and androgen resistant cancers show higher number of cells with p53 immunoreactivity compared with primary tumours, this pro-apoptotic protein has great potential as a prognostic marker.(78, 100) The value of Bcl-2 as a diagnostic marker is unclear, since some groups have shown that only limited numbers of prostatic tumours express Bcl-2.(101, 102) However, some studies have demonstrated correlation with Bcl-2 and poor prognostic outcomes, with increased numbers of high-grade and metastatic tumours having Bcl-2 immunoreactivity.(103, 104) Bcl-2 overexpression in tumours has also been associated with resistance to radiotherapy. (105) TRPM-2 (testosterone-repressed prostate message-2) or clusterin or sulfated glycoprotein-2. An increased expression of TRPM-2/clusterin protein is evident in PCa (96%) compared with BPH (73%) and normal prostate epithelium (17%).(106, 107) TRPM-2/clusterin has a well-documented anti-apoptotic function.(108) However, it seems to have many functions, some of them with pro-survival effects. (109)
Others	Hepsin, PSCA, non-coding RNA's DD3/PCA3	Hepsin is a type II transmembrane serine protease that is differentially expressed in PCa compared with normal and BPH affected prostate tissue.(110) Some in-vitro studies had demonstrated that Hepsin overexpression had growth inhibitory effects.(111) It has also been found a model for Hepsin and tumour progression when the soluble form of Hepsin was found to activate HGF (hepatocyte Growth Factor).(112) Therefore, there is an increasing interest in the development of antagonists to Hepsin and subsequently HGF activation, which could be useful therapeutically. (112, 113) Prostate stem cell antigen (PSCA) is a prostate specific glycoprotein that is expressed by PCa cells as a cell surface antigen and is regulated by the androgen receptor.(114-116) It has a central role in the development of the prostate gland and could provide a new diagnostic and therapeutic target for PCa, as its increase expression has been related to an increased PCa risk. (115, 117) DD3/PCA3 was identified by differential display technology in 1999 as a non-coding RNA highly specific to PCa. Since then, the Prostate Cancer Gene 3 (PCA3) has been used in clinical practice albeit only in certain institutions in the United Kingdom. It is present in urine and expressed in prostatic secretions, semen and prostate tissue.(118, 119) This biomarker is usually measured in urine after DRE and prostatic massage which allows shedding of prostate epithelial cells and is evaluated using reverse transcriptase polymerase chain

		reaction (PCR).(119, 120) In 95% of prostate cancers PCA3 is over expressed, with studies to date showing sensitivity and specificity of 66% and 89% respectively. In patients with a PSA less than 4.0ng/ml, the sensitivity of PCA3 is increased.(118, 121) However, there is a need for further refinement of this test before it would replace PSA in routine practice for screening.

Table 3 The main molecular aberrations in prostate cancer.

3.5. Transrectal Ultrasonography-guided Prostate Biopsies

The second part of the contemporary two-step early-diagnostic approach for prostate cancer is the transrectal ultrasonography (TRUS)-guided prostate biopsy. It is usually performed after the possibility of a prostate cancer is raised, whether by rectal examination, PSA parameters, or a combination of both. The American Urologic Association established guidelines that recommend prostate needle biopsies for any man with a PSA value greater than 4.0ng/ml, or an abnormal prostate on DRE.(122)

TRUS imaging allows spatial positioning of spring-loaded biopsy needles, providing a methodical approach for obtaining tissue cores for standard histopathology. TRUS imaging is usually non-diagnostic by itself, but enables the operator to measure gland volume and delineate obvious focal lesions. When a standard sextant biopsy is performed, there is approximately 25% chance of missing a PCa.(123) Therefore, the number of biopsy cores taken is an important feature, being recommended at least 8 and preferably a minimum of 10 biopsy cores. Routinely, many urologists take 12 biopsy cores to minimize the likelihood of missing cancer. It is also advocated that biopsies should be directed laterally and that they should include the anterior horns of the peripheral zone.(124-126) Currently, indications for re-biopsy are rising in cases of a persistently high PSA, a suspicious DRE, or findings of Atypical small acinar proliferation (ASAP) or extensive Prostatic intraepithelial neoplasia (PIN).(127)

Since TRUS biopsies are unpleasant and uncomfortable, many urologists routinely use anesthesia (local or general). The routine clinical practice also involves peri-operative antibiotic prophylaxis with a pre-procedural enema and not proceeding if any faeces at all are present in the rectum, as determined by DRE. This procedure has minor morbidity associated, with well over 50% of patients experiencing at least one complication. The dreaded complication of life-threatening sepsis is uncommon and blood in the urine, ejaculate and faeces are not infrequent sequelae with some men having difficulty voiding immediately following the procedure.(128-130)

An accurate measurement of tumour volume based on biopsy findings is very difficult technically. However, it has been proposed that the biological aggressiveness of prostate cancer is a direct function of the tumour volume, which can implied that the larger the volume with biopsies, the greater the likelihood of extracapsular disease.(131-133) Therefore, the quantification of the amount of cancer on the needle biopsy, number of positive cores and core location give valuable information about individual tumour characteristics.(132, 134)

3.6. Suspicious results: Benign Prostatic Hyperplasia (BPH), Prostatic intraepithelial neoplasia (PIN), Atypical small acinar proliferation (ASAP) and Proliferative inflammatory atrophy (PIA)

Sometimes the diagnosis of prostate cancer is difficult. The existence of signs and symptoms related to PCa or an elevated serum PSA levels do not necessarily indicate a case of prostate cancer, as there are other pathologies associated with these alterations. Even when a pathologist looks at the prostate cells under the microscope, they sometimes may not look cancerous but do not look normal either and these results are usually reported as suspicious.

Benign prostatic hyperplasia (BPH) is a common pathological diagnosis that can only accurately be made after prostate tissue analysis. It is characterised by voiding and storage symptoms of variable severity and the progression of this disease may lead to recurrent urinary tract infections, bladder calculi or urinary retention.(135, 136) BPH is intimately related to ageing and although it is not life threatening, the effect of the lower urinary tract symptoms on patient quality of life can be significant.(137, 138) Histologically, BPH represents specific deviations in architecture rather than simply an increase in cell population. The macroscopic identification of hyperplastic glandular acini separated by fibrous stroma in a nodular pattern confirms the pathological diagnosis. In the transitional zone (TZ), glands may display architectural complexity and papillary infolding. The acini are microscopically tightly packed, lined by tall columnar epithelial cells with small basal and the epithelium has a distinct double layer of secretory and basal cells. In the BPH cells the nuclei remain aligned in a single row, which differs from Prostatic intraepithelial neoplasia (PIN), where the nuclei are irregularly arranged. The cytoplasm is clear and abundant. (137, 139)

Prostatic intraepithelial neoplasia (PIN) is diagnosed when there are changes in how the prostate cells look under the microscope, but the abnormal cells do not look like they have grown into other parts of the prostate.(140, 141) PIN is often divided into low-grade and-high grade. The low-grade begin to develop at an early age and do not necessarily indicate that the patient will develop prostate cancer. If a finding of low-grade PIN is reported on a prostate biopsy, the follow-up for patients is usually the same as if nothing abnormal was seen. In the cases of a high-grade PIN there is about a 20% to 30% chance that cancer may already be present somewhere else in the prostate gland. Therefore, these cases are watched more carefully and a prostate biopsy may be repeated, especially if the original biopsy did not take samples from all parts of the prostate.(140, 142)

In the atypical small acinar proliferation (ASAP) or just *atypia,* the cells look like they might be cancerous when viewed under the microscope, but there are too few of them to be sure. Therefore, there is a high chance that cancer is also present in the prostate and an appropriate follow-up of the patients is necessary. (143, 144)

In cases of proliferative inflammatory atrophy (PIA), the prostate cells look smaller than normal and signs of inflammation are present. PIA is not cancer but is believed that it may sometimes lead to high-grade PIN or to prostate cancer directly.(145)

3.7. Magnetic Resonance Imaging, Computed Tomography and Nuclear Medicine

Routinely, clinical staging of patients with prostate cancer is performed with cross sectional imaging techniques such as magnetic resonance imaging (MRI) and computed tomography (CT).
The CT scan (or CAT scan) is a special kind of x-ray test that gives detailed, cross-sectional images of your body. A CT scanner takes many pictures of the part of the body being studied, and not just one picture like a standard x-ray, creating detailed images of the soft tissues in the body. CT scans rarely provide useful information about newly diagnosed prostate cancers, so it is not always performed at baseline in men with a PCa diagnosis. However, this test can help tell if the prostate cancer has spread into nearby lymph nodes, which made it the usual first-line investigation for detecting soft-tissue metastases. (146-148)
The MRI scan uses radio waves and strong magnets instead of x-rays and is a technique that can be helpful in looking at prostate cancer.(149) MRI scans can produce a very clear picture of the prostate and show whether the cancer has spread outside the prostate into the seminal vesicles or other nearby structures. To improve the accuracy of the MRI, a probe called endorectal coil can be used to help in the detection of extracapsular disease. However, in the overall context of patient assessment, this test adds little to clinical staging and is currently predominantly a research technique. (147, 149, 150)
Finally, technetium labelled phosphate radioisotope bone scanning is used for diagnosing bone metastases and is a sensitive method for prostate cancer staging. Routine bone scanning is usual prior to treatment, as a bone scan at this time serves as a baseline reference for subsequent monitoring. Sites of increased radio-tracer uptake are those with greater metabolic activity, called ‘hot-spots’, and a malignant cause has to be differentiated from non-malignant diagnoses. The predilection for PCa metastases to strongly favour the axial skeleton, with a much less common limb involvement (apart from upper femora), helps in this differentiation.(147, 150)
There are some other techniques, which use is not yet well established, such as positron emission tomography (PET) and ProstaScint scanning.(149, 150) Like the bone scan, the ProstaScint scan uses an injection of low-level radioactive material to find cancer that has spread beyond the prostate. The material used for the ProstaScint scan is attracted to prostate cells in the body, since it contains a monoclonal antibody specific to the prostate-specific membrane antigen (PSMA), a substance found at high levels in normal and cancerous prostate cells. This test can find prostate cancer cells in lymph nodes and other soft (non-bone) organs. However, the test is not always accurate, with 70-80% sensitivity in detecting lymph node metastases and the results can sometimes be confusing.(150)

3.8. TNM Staging of the Prostate

Staging is a method of describing the extent of local and distant spread of a tumour, being very important in clinical practice since it enables an assessment of prognosis and thus guides patient management.
In the twentieth century, different staging systems for PCa were established; being the first internationally accepted staging system introduced by Whitmore in 1956, which classified the stages in letters (A-D). Posteriorly, Jewett had modified this staging system, subdividing level B. (2)

In 1950, staging systems for solid tumours began to consider the TNM (Tumour – Lymph node – Metastasis) classification to analyse patient's prognosis and to determine the tumour's definite level of development.(2, 151) Currently, TMN staging can be made either based on examination and radiological finding (clinical) or based on pathology specimen analysis (pathological). The clinical and pathological stages are designated by the letters 'c' and 'p', respectively, preceding the stage denotation. The T-stage describes the extent of local spread and is assessed by DRE and imaging; the N-stage is assessed by imaging or biopsy of suspicious lymph nodes; and the M-stage is assessed by examination, imaging and biochemical investigations. Within each category of TNM, there are several sublevels based on tumour volume or extent (T1–T4), amount and/or size of lymph node metastases (N0–N3), and distant metastases (M0–M1). (151, 152) The Table 4 describes the definitions of each stage.

The development and improvement of staging systems is a complex procedure and clinical subspecialties are now focusing on the improvement of staging systems for different neoplastic disease to precisely demonstrate each patient's prognosis.

T – Primary Tumour	
Tx	Primary tumour cannot be accessed
T0	Evidence of primary tumour
T1	Clinically inapparent tumour not visible by imaging
T1a	Tumour incidental histological finding in 5% or less of tissue resected
T1b	Tumour incidental histological finding in more than 5% of tissue resected
T1c	Tumour identified by needle biopsy
T2	Tumour confined within the prostate
T2a	Tumour involves one half of one lobe or less
T2b	Tumour involves more than half of one lobe, but not both lobes
T2c	Tumour involves both lobes
T3	Tumour extends through the prostatic capsule
T3a	Extracapsular extension (unilateral or bilateral), including microscopic bladder neck involvement
T3b	Tumour invades seminal vesicle(s)
T4	Tumour is fixed or invades adjacent structures, other than seminal vesicles: external sphincter, rectum, levator muscles, and/or pelvic wall
N – Regional Lymph Nodes	
Nx	Regional lymph nodes cannot be accessed
N0	No regional lymph node metastasis
N1	Regional lymph node metastasis
M – Distant Metastasis	
Mx	Distant metastasis cannot be accessed
M0	No distant metastasis
M1a	Non-regional lymph node(s)
M1b	Bone(s)
M1c	Other site(s)

Table 4 TMN staging of adenocarcinoma of the prostate. Adapted from (151)

3.9. Molecular Profiling Techniques for Prostate Cancer

One of the challenges in diagnosing prostate cancer is the heterogeneity of the disease phenotypically. As described before, alterations occur in cancer cells at many levels; so many methods have been used to identify potential markers for PCa, including analysis of gene expression (microarrays and quantitative PCR) and protein marker changes between disease and non-disease states (histopathology, Mass-spectrophotometry).

In samples which are difficult to classify, most commonly prostatic biopsies, immunohistochemistry is used to determine the presence of prostate cancer. A high molecular weight basal cell-specific cytokeratin, which preferentially stains basal cells, is useful in the diagnosis of small acinar carcinoma, confirming the presence of basal cells or absence. The use of specific antibodies for prostate specific markers such as PSA or PAP has a limited application in identifying prostate tumours, since they are present in both primary and secondary lesions and also sometimes in benign glands.(153) Some neuroendocrine markers can also be used to identify prostate tumours, since they are focally expressed in many adenocarcinomas, but their role in carcinoma is unknown.

There are many published papers describing genetic alterations present in PCa; some that appear to be random and others seem to be consistently present. The DNA micro array technology has been used to quantitatively elucidate genes expressed by prostate cancer cells. This technique enable identify genes that could act as biomarkers for PCa.(154, 155) However, the heterogeneity of prostate tissue and conflicting results are limiting characteristics in the establishment of markers as providers of predictive or prognostic information.

3.10. Management of Patients with Prostate Cancer

As already mentioned before, the routine PSA-based detection has increased the percentage of newly-diagnosed cases potentially curable by surgery or radiotherapy. However, a considerable proportion of patients are not candidates for such intervention, being unresectable (locally-advanced) disease, ‘poor tumour pathology’, the presence of demonstrable metastases and advancing age in association with a limited life-expectancy, common exclusionary factors.(156) As prostate cancer is has a relatively slow growing; only men with at least a 10-year life expectancy are usually considered for aggressive, potentially-curative treatment. Radical retropubic prostatectomy (RRP) is not offered to men with cT3 or cT4 disease. However, radiotherapy in combination with androgen deprivation therapy has a more recognised role in locally advanced disease, especially with neo-adjunctive or adjunctive androgen suppressive treatment.(157-159) Also, a proportion of patients with cT1 or cT2 tumours that are upstaged to pT3 at time of surgery have been reported to have durable cancer remissions.(160)

There are 3 management options for cases of a clinically localised disease: those include RRP, radiotherapy in the form of either external beam radiotherapy or brachytherapy and watchful waiting. These cases also need on-going support and counselling and to be monitored for disease progression and for potential future therapeutic intervention.

4. Fourier Transform Infrared Spectroscopy – a new diagnostic modality of Prostate Cancer

Since its commercial introduction in 1970 infrared (IR) spectroscopy has been recognized as a non-destructive, label free, and highly sensitive and specific analytical method with many potential useful applications in different fields of biomedical research and in particular cancer research.
In the past decades many technological improvements have been made to facilitate biomedical applications of Fourier Transform Infrared Spectroscopy (FTIR) extensively reviewed in which has been successfully applied to samples from a variety of cell lines(161), blood cells(162, 163), and tissues(164, 165), including cervix(166), breast(167), prostate(168-170), lung(171), colon(172, 173), brain(174, 175), skin(176, 177), esophagus(178), liver(179), lymph system(180, 181) and stem cells(182-184). The results of many studies have clearly indicated that FTIR associated with the use of some appropriate statistical data analysis methods has a strong accuracy in classifying normal and malignant tissues/cells.(185) However, the application of FTIR to cancer research and clinical diagnostics continues to be “under strong development” or “promising”.

4.1. FTIR, Cancer and Prostate Cancer

The development of most cancers is not yet fully understood, but it is now recognised that many develop through pre malignant stages. Thus, the most important factor in the prevention of cancer is early detection, facilitating eradication of these pre-malignant abnormal cells prior to systemic invasion. Therefore, there is great clinical need for techniques that can detect these pre-malignant biochemical changes that can advance to cancer. Currently, cancer diagnostics is highly reliant on histopathology, which is somewhat subjective, associated with inter-observer disagreement and in the main part relies on morphological information. Sampling errors can severely restrict the effectiveness of biopsy and lead to the unnecessary removal of tissue.(186) The ideal diagnostic test would provide rapid, non-invasive diagnosis at the point-of-care with high throughput and without prior tissue processing.
Since the early 1990s several groups have used FTIR spectroscopy to distinguish normal from neoplastic tissues. Comprehensive studies using Fourier transform infrared (FTIR) have demonstrated potential for rapid, high resolution, non-destructive, molecular histopathology without staining and possibly additional prognostic information. In combination with chemometric techniques, spectroscopy can provide a more objective diagnostic assessment in comparison to the subjectivity associated with histopathology.(186) Biochemical changes extracted from the spectral dataset enable the researcher to potentially detect molecular changes that precede any morphological change, thus enabling earlier diagnosis of tissue dysplasia. Development of technology and analytical methods is now enabling moves toward diagnosing neoplastic change at progressively earlier stages and potential to do so in vivo.

Prostate tissue is complex and heterogeneous and the diagnosis of prostate cancer (PCa) in individual patients can be problematic, which can lead to inappropriate treatment. The Gleason grading system, which is used by pathologists as an enumeration of the disease state based on the appearance of fixed and stained tissue sections, has many well-recognized flaws, as already mentioned before.(32, 33, 187, 188) Therefore, the limitation with these diagnostic modalities has

led to an interest in the development of spectroscopic analytical techniques for the diagnosis of PCa. FTIR analysis might provide an improved diagnosis of cancer and could also facilitate the identification of tumours with aggressive biopotential. Many published studies already showed that FTIR methods can discriminate tumours that are clinically confined to the prostate from those that are clinically invasive.(168, 169, 188-191) Infrared spectra of biomolecules allow the measurement of complex molecular vibrational modes that contain valuable information on changes occurring due to diseases such as cancer.(186, 188, 190) Thus, when used together with pathology reports, FTIR methods could lead to an increase in the accuracy of diagnosis.

B. Significance of the Study

Prostate cancer (PCa) is the second most common cancer among men and the fifth most common cancer overall, being the sixth leading cause of death from cancer in men.(14, 15)

Despite the dramatic rise in PCa incidence over the last decade and its demonstrated clinical significance, its etiology and natural history remain poorly understood. Currently, the diagnosis of PCa only relies on histopathological analysis. However, the prostate tissue is complex and heterogeneous and the pathological interpretation of prostate specimens can be time consuming and subjective due to inter observer variation.(32, 33, 187, 189) Therefore, there is an urgent need for more sophisticated and objective techniques that can detect these biochemical changes that can advance to cancer, improving the cost, speed and accuracy of prostate cancer diagnosis.

FTIR is a recognized non-destructive, label free, highly sensitive and specific analytical method which might provide an improved diagnosis of PCa and could also facilitate the identification of tumors with aggressive biopotential.(189)

This pilot study intends to investigate the potential application of FTIR as a tissue diagnostic technique to complement histopathology and to identify where FTIR may create a niche in clinical practice. The small sample size of this study makes difficult to define if the obtained data constitute a biologically relevant effect. Therefore, the present study constitutes an exploratory study or pilot study that will generate hypotheses for more intensive and targeted confirmatory experiments in the future.

The exploratory study aims to:

1) observe if FTIR analysis can be correlated to the histopathological analysis of prostate tissue samples;
2) test if FTIR together with multivariate analysis can distinguish objectively normal prostate tissue from PCa tissue samples;
3) test if FTIR together with multivariate analysis can classify PCa tissues samples;
4) identify spectroscopic signals responsible for the discrimination and classification of prostate tissue samples.

Chapter two

This chapter starts with an overview of the Fourier Transform Infrared Spectroscopy principles, including the theory of the infrared spectroscopy and the FTIR equipment. The second part of this chapter includes the sample characterization and the methods used in this study are described.

C. Method Overview

5. Infrared Spectroscopy

Infrared (IR) Spectroscopy is a powerful analytical tool to probe the structure of lipids, nucleic acids, carbohydrates and the primary and secondary structure conformation of proteins. It can also be used to study the composition of other complex biological materials such as body fluids, cell cultures and tissues, as we did in this study. IR spectroscopy is a technique based on the vibrations of the atoms of a molecule. An infrared spectrum is commonly obtained by passing infrared radiation through a sample and determining what fraction of the incident radiation is absorbed at a particular energy. The energy of each peak in an absorption spectrum corresponds to the frequency of a vibration of a part of a sample molecule.(192)
Infrared (IR) Spectroscopy enables the rapid, non-destructive molecular specific interrogation of clinical samples with high throughput. The ability to undertake studies on samples already characterized provide information on patient outcomes, enabling any prognostic information within the IR data to be elucidated as well as correlations with histopathology.(189)

5.1. Theory of Molecular Spectroscopy

The electromagnetic waves contained within a continuous range of frequencies known as the electromagnetic spectrum have been extensively used in cancer research and diagnosis. These waves differ from each other in the length and frequency. The frequency of vibration, ν, is the number of wave cycles that pass through a point in one second and it is measured in Hz. The wavelength, λ, is the length of one complete wave cycle and it is often measured in cm (centimeters). Wavelength and frequency are inversely related. The energy is related to wavelength and frequency, being directly proportional to frequency and inversely proportional to wavelength.(192-194) The energy values fit the quantized vibrational transitions of intra- and intermolecular bonds of bonded atoms in molecules and, therefore, photons can be absorbed by molecules that are in periodic (sinusoidal) motion.(189)
The infrared (IR) radiation is invisible to the naked eye and comprises an interval of electromagnetic spectrum between the red end of the visible region (λ~780 nm) and the beginning of microwaves region (λ=1 mm). The most commonly used spectroscopic unit in the IR region is the reciprocal of the wavelength, 1/λ, called wavenumber, with unit of reciprocal centimeter (cm^{-1}). The spectrum has dimension of wavenumbers extending from ~14000 cm^{-1} to ~4 cm^{-1}, and three regions of increasing wavenumbers have been recognized within this interval: near-IR (14 000 to 4 000 cm^{-1}), mid-IR (4 000 to 400 cm^{-1}), and far-IR (400 to 4 cm^{-1}) – see Figure 6.(192, 193, 195, 196)
In IR absorbance spectroscopy the loss of IR radiation transmitted through a sample across an interval of frequencies of electromagnetic spectrum is measure and near-IR spectroscopy, mid-IR spectroscopy, and far-IR spectroscopy (THz spectroscopy) can be performed depending on the selected interval of wavelengths. Molecular spectroscopy is the quantitative and qualitative analysis of the spectra produced by this interaction between the radiation and the sample.(189, 196)

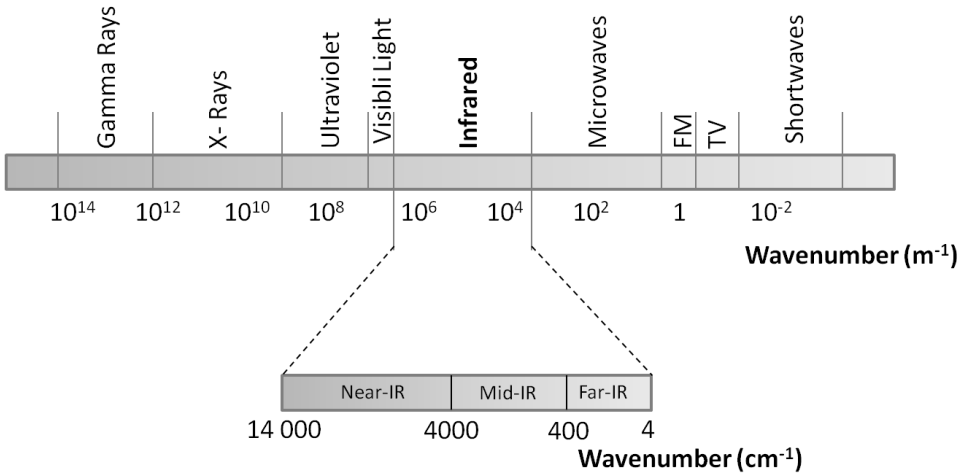

Figure 6 The electromagnetic spectrum, showing the three infrared (IR) regions. Adapted from (197, 198)

5.2. Molecular vibrations

Infrared spectroscopy is an absorption spectroscopy in which IR radiation is absorbed by organic molecules and converted into energy of molecular vibration. An organic molecule is exposed to infrared radiation and when the radiant energy matches the energy of a specific molecular vibration, absorption occurs. In other words, if incident IR radiation corresponds to the appropriate ΔE (amount of energy emitted or absorbed by the system) to cause a molecule to be promoted to a higher energy state, it will be absorbed. The change in energy state is represented in infrared spectroscopy by a change in vibrational mode.(192, 194)

Therefore, infrared spectroscopy is possible because molecules are not static; they vibrate/oscillate when they interact with radiation. A molecule in its resting stable energy state will have a number of degrees of freedom - the potential to change position in space and rotation. Being N the number of atoms in the molecule, a molecule consisting of N atoms has a total of 3N degrees of freedom, corresponding to the Cartesian coordinates of each atom in the molecule. The number of degrees of freedom in a polyatomic nonlinear molecule is: 3N-6 (3 translational and 3 rotational) and in a linear molecule is: 3N-5 (3 translational and 2 rotational). For example, oxygen (O_2) is a diatomic linear molecule with only one stretch vibration ((3x2)-5 = 1). The nonlinear molecule water (H_2O) has 3 degrees of freedom ((3x3)-6 = 3).(194-196)

The simplest types (modes) of vibrational motion in a molecule that are infrared active (give rise to absorptions) are the stretching and bending modes. Stretching (axial deformation) involves a change in the bond length. Some bonds stretch in-phase (symmetrical stretching) or out-of-phase (asymmetric stretching), and, in general, asymmetric stretching occur at higher frequencies than symmetric stretching – see Figure 7.(193-196) Bending (angular deformation) involves a change in the bond angle in relation to an arbitrary coordinate ensemble of the molecule. There are four types of bending vibrations: two of them are bending vibrations in one plane, which involve changes in bond angles and but leaving bond lengths unaltered, and they include scissoring (symmetrical bend in-plane) and rocking (asymmetrical bend in-plane); the other two are bending vibrations out of plane, in which one atom oscillates through a plane defined by at least three neighbouring atoms, and they include wagging (symmetrical bend out-of-plane) and twisting

(asymmetrical bend out-of-plane) – see Figure 7. Also, bending vibrations occur at lower frequencies than corresponding stretching vibrations.(192, 194-196)

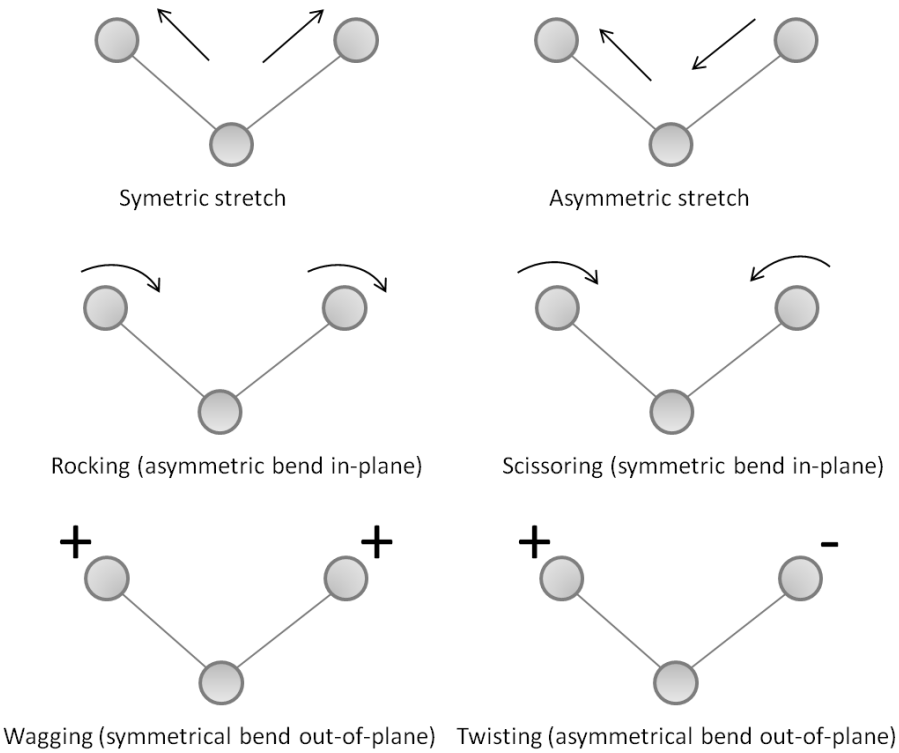

Figure 7 The vibrational modes of stretching and bending. Adapted from (192)

However, not all the molecular vibrations are infrared active i.e. show infrared absorptions. The key to a substance being infrared active is that an electric dipole moment of the molecule must change during the vibration. This change in moment is stimulated by the electrical field interaction with the molecules' dipole moment and may be either parallel or perpendicular to the line of symmetry axis. HCl, NO, and CO are examples of heteronuclear diatomic molecules that are infrared active. The dipole moment of such molecules changes as the bond expands and contracts. By comparison, H_2, N_2, and O_2 are examples of homonuclear diatomic molecules that are infrared inactive because its dipole moment or net charge remains zero no matter how long the bond and therefore there will be no detectable IR activity. Stretching vibrations of N_2, O_2 as well as of many other non-IR active modes can be detected by Raman spectroscopy.(192, 195, 196)

Furthermore, the same molecule can have vibrations that are IR active and others inactive. For example, if we consider carbon dioxide (CO_2) as a linear molecule with essentially one degree of freedom in the mode of vibration 'symmetric stretch'. The molecule is symmetrically stretched and compressed with both CO bonds changing simultaneously. Therefore, the dipole moment remains unchanged throughout and this vibration is IR inactive. However, if we consider CO_2 in the linear asymmetric stretch mode, there is a periodic alteration in dipole moment and this vibration is IR active.(192, 194-196)

A complex molecule will have a large number of vibrational modes involving the whole molecule. Infrared spectroscopists have defined frequencies at which characteristic bond vibrations will occur when known chemical groups are present within a sample.

5.3. The Infrared spectrum

Figure 8 shows two typical IR spectra. As we can see, the wavenumber, plotted on the X-axis, is proportional to energy, being the highest energy vibrations on the left. The left spectrum is plotted as T on the Y-axis, being T the percentage transmittance (%T) with 100% at the top of the spectrum. Absorption of radiant energy is therefore represented by a "trough" in the curve: zero transmittance corresponds to 100% absorption of light at that wavelength. Band intensities can also be expressed as absorbance (A), from 0 to 1. Absorbance is the logarithm, to the base 10, of the reciprocal of the transmittance – see Figure 8. It comes down to personal preference which of the two modes to use, but the transmittance is traditionally used for spectral interpretation, while absorbance is used for quantitative work and multivariate analysis. For this study we use spectra plotted as absorbance (A).(192-194)

The complexity and the wavenumbers of the peaks in the spectra give information about the molecule. The complexity is useful to match an experimental spectrum with that of a known compound with a peak-by-peak correlation. The wavenumbers (or frequencies) at which an organic molecule absorbs radiation give information on functional groups present in the molecule.

Certain bonds absorb energy at the same wavelength range, regardless of the structure of the molecule, and give rise to bands at approximately the same frequencies. For example the C=O stretch of a carbonyl group occurs at approximately 1700cm^{-1} in ketones, aldehydes and carboxylic acids. This is the principle upon which infrared spectroscopy can be used for chemical identification. Spectroscopists refer to the fingerprint region of a spectrum (<1500cm^{-1}) which is unique for a molecule and the functional group region (1500-4000cm^{-1}) which may be similar for molecules within the same group. With the help of tables which correlate frequencies with functional groups is possible to analyse a spectrum.(192)

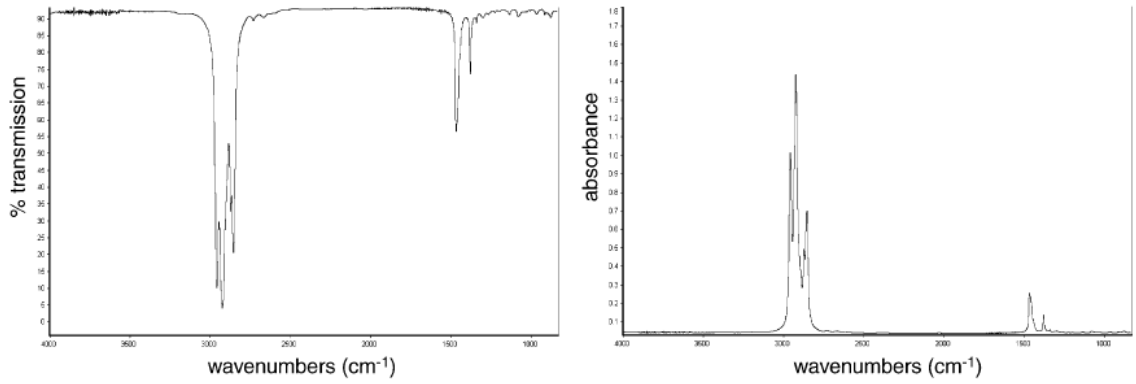

Figure 8 The IR spectrum of octane, plotted as transmission (left) and absorbance (right). Adapted from (193)

5.4. FTIR Instrumentation

All modern IR spectrometers use Fourier transform (FT) and are composed of the following common elements: an infrared light source, an interferometer, a single element detector, an optical system with a motorised x-y-z stage and a computer to process the data. The radiation emerging from the source is passed through an interferometer to the sample before reaching a detector. (189, 192, 193)

FTIR spectroscopy is based on the idea of the interference of radiation between two beams to yield an interferogram. An interferogram is a signal produced as a function of the change of path length between the two beams. The two domains of distance and frequency are interconvertible by the mathematical method of Fourier transformation.

The four arms Michelson interferometer, which is the most common interferometer used, consists of a top arm that contains the infrared source and a collimating mirror that collects the light from the source and makes its rays parallel; a bottom arm that contains a stationary mirror; a right arm that contains a moving mirror; and a left arm that contains the sample and detector. At the centre of the interferometer there is a semi-reflecting film, the beamsplitter, which bisects the planes of the two mirrors.(192, 193, 199) When a parallel beam of radiation is directed from a source to an interferometer the following happens: the beamsplitter splits the beam into two separate light paths. 50% of the incident radiation is reflected to one of the mirrors and the remaining 50% is transmitted to the other mirror. The radiation reflected from these mirrors comes back along the same path to the beamsplitter where it recombines and interferes. The recombinant radiation that emerges from the interferometer at 90º to the input (IR) beam is called the transmitted beam.(189, 192) This is the beam detected in FTIR spectrometry, as it will interact with the sample and then will reach the detector – see Figure 9.

The moving mirror in the interferometer produces an optical path difference between the two arms of the interferometer. Destructive interferences in the case of the transmitted beam or constructive interferences in the case of the reflected beam are generated. The resultant interference pattern is called an interferogram. This represents the summation of all the cosine functions of all the individual wavelengths present in the source and zero path difference (ZPD) positions where all interferences will be in phase (the centre-burst).(189)

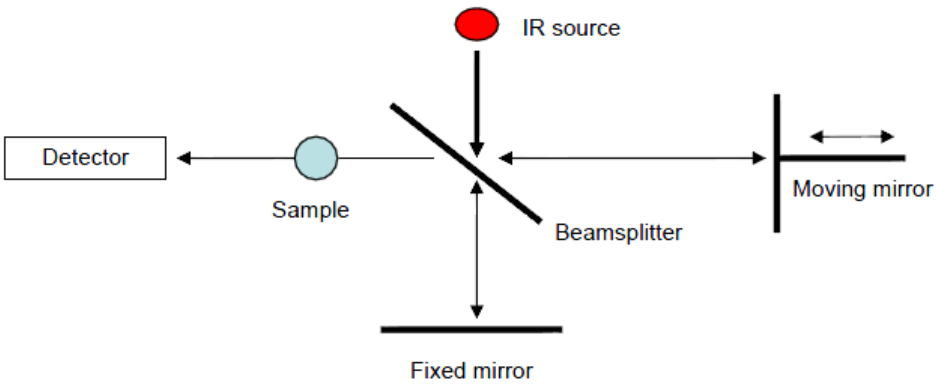

Figure 9 Scheme of an interferometer of a Fourier transform spectrometer. Adapted from (192)

The application of the Fourier transformation will convert this interferogram into an IR single-beam spectrum where the number of peaks will reflect the number of detectable components in the sample. The intensity in peaks, reflecting the amount of different molecular bonds absorbing in specific regions of the IR spectrum, will be in relation with the relative abundance of different sample constituents. The spectral resolution is the minimum wavenumber difference that can be distinguished between two lines in a spectrum.
The FT-IR absorbance spectrum is one of the most information-rich and concise way to represent the whole "…omics" of a sample and, as such, fits all the characteristics for the development of a clinically useful biomarker.(189)

5.5. Sampling Method: Attenuated total reflectance (ATR) spectroscopy

Despite the traditional sampling approach in infrared (IR) spectroscopy have been the transmission techniques, various reflectance and microsampling techniques have emerged as valuable methods for samples that are difficult to analyse by the conventional transmittance methods.(192, 194)
The reflectance method attenuated total reflection (ATR) spectroscopy is especially useful for samples which do not let light through either because they are highly absorbing or they cannot be cut into thin enough sections. ATR spectroscopy utilizes the phenomenon of total internal reflection. An ATR objective containing an ATR crystal - made of an infrared transparent material like diamond used in this study - fitted to the FTIR spectrometer. The ATR crystal is used to probe the sample and must be in contact with the sample to work.(192) The beam of radiation entering the ATR crystal will undergo total internal reflection when the angle of incidence at the interface between the sample and crystal is greater than the critical angle[2]. The beam penetrates a fraction of a wavelength beyond the reflecting surface and loses energy at the wavelength where the material absorbs. Therefore, there is a reflection loss (evanescent waves) and a reflection loss spectrum can be created and adjusted for the depth of penetration of the sample.(189, 192, 194)
The resultant attenuated radiation is measured, plotted as a function of wavelength by the spectrometer and gives rise to the absorption spectral characteristics of the sample.(189)
Different designs of ATR cells allow both liquid and solid samples to be examined. In this study we use the Golden Gate™ ATR – see Figure 10.
The ATR technique requires little sample preparation. However, it can be time consuming when used with biological tissues like in this study, as the objective had to be cleaned between spectral measurements at different points.

[2] Function of the refractive indices of the two surfaces.

Figure 10 Golden Gate™ ATR. Adapted from (200)

5.6. Advantages of the method

FTIR instruments have several significant advantages over older dispersive instruments.
The main advantage of rapid-scanning instruments is the ability to increase the signal-to-noise ratio (SNR) by signal-averaging, leading to an increase of signal-to-noise proportional to the square root of the time. This is the Fellgett (or multiplex) advantage and is due to an improvement in the SNR per unit time, proportional to the square root of the number of resolution elements being monitored. This results from the large number of resolution elements being monitored simultaneously. Furthermore, because FTIR spectrometry does not require the use of a slit or other restricting device, the total source output can be passed through the sample continuously. This results in a substantial gain in energy at the detector, hence translating to higher signals and improved SNRs. This is known as Jacquinot's (or throughput) advantage.(192, 194)
Another strength of FTIR spectrometry is its speed advantage. The mirror has the ability to move short distances quite rapidly, and this, together with the SNR improvements due to the Fellgett and Jacquinot advantages, make it possible to obtain spectra on a millisecond timescale.(192)

D. Methods of study

6. Prostate Tissue Collection

The samples of prostate tissue selected for the present study were provided by the Laboratory of Signal Transduction of the Center for Cell Biology of University of Aveiro in the context of the project PTDC/QUI-BIQ/118492/2010: "Identification of a novel TGFbeta cascade regulated by a Protein Phosphatase 1 complex" from the research team Margarida Sâncio Da Cruz Fardilha and Sandra Maria Tavares da Costa Rebelo, Luis Korrodi Mineiro Marques Gregório and Joana Vieira Silva. The clinical data was collected by the Urologists António Patrício and Nuno Maio.

With full ethical committee approval of the Infante Dom Pedro Hospital, tissue was collected at routine operating lists at the Urology Service of the Infante Dom Pedro Hospital in Aveiro from 8

consenting patients undergoing radical prostatectomy. After surgery, six to eight biopsy cores were collected from 8 patients with prostate cancer (PCa). A portion of normal prostate tissue and a portion of PCa tissue, with approx. 5 mm in thickness each, were sectioned from each patient. A total of sixteen tissue biopsy specimens were included in the present study – see Table 5.

No tissue preparation or fixation was necessary and after the collection the samples were stored in a -80ºC freezer.

Number of patients	Number of samples	Benign	Malignant
8	16	8	8

Table 5 Samples included in this study.

6.1. Sample Characterization

Prostate biopsy samples were collected from radical prostatectomy pieces of 8 patients with ages between 54 and 66 at Infante Dom Pedro Hospital in Aveiro. Patients were attending for radical prostatectomy because they were suspected to have prostate cancer on the basis of either an initial elevated PSA blood test or abnormal digital rectal examination (DRE) or both – see Table 6. All patients gave consent for extra biopsies to be taken and used for purely research purposes. The samples were stored in a -80°C freezer after collection. Besides the initial PSA reported, prior to TRUS biopsy and the DRE results, was also recorded the histologic analysis, including the Gleason grade at the time of the prior biopsy and the Gleason grade of the surgical piece, the TMN staging and further considerations about the prostate characterization and pathology. The Table 6 details the sample characterization for the 8 patients of this study, including the PSA level, the Gleason grade and the final formal TRUS biopsy histology.

Patient	Age	Initial PSA	Gleason (Biopsy)	Gleason (Surgical Piece)	Pathology	TMN staging	Prostate characterization (Surgery)	DRE/Eco	Notes
1 (25/09/12)	64	4,93	7 (3+4) Bilateral	7 (3+4) Bilateral	- 25% of the gland affected	pT2cN0	- Prostate of 35g - Negative Margins	Eco without alterations	-
2 (02/10/12)	66	8	8 (4+4) Left	8 (4+4) Left	- 20% of the gland affected - Extracapsular extension	pT3aN0	- Prostate of 27g - Negative Margins	Eco with a 7,3 mm nodule at the left	-
3 (16/10/12)	64	7,55	7 (3+4) Right	7 (4+3) Bilateral	- 20% of the gland affected - Extracapsular extension at the right	pT3aN0	- Prostate of 36g - Negative Margins	Eco with a 5 mm nodule of the peripheral zone at the left; heterogeneity at the right	-
4 (23/10/12)	64	6,24	7 (3+4) Right	7 (3+4) Right	- 10% of the gland affected	pT2aN0	- Prostate of 59g - Negative Margins	Eco showing peripheral heterogeneity	-
5 (30/10/12)	58	51,2	7 (4+3) Bilateral	7 (3+4) Bilateral	- 35% of the gland affected	pT2aN0	- Prostate of 32g - Negative Margins	- DRE with prostate hardening at the left (suggesting tumour) - Eco without define nodules	Extremely aggressive tumour, occupying large part of the prostate
6 (06/11/12)	54	9,6	9 (5+4) Right	9 (5+4) Bilateral	- 20% of the gland affected - Focal extracapsular extension	pT3aN0R1	- Prostate of 30g - Positive Margins	Eco showing diffuse heterogeneity of the peripheral zone at the right with 18x10mm	Complementary radiotherapy (RT)
7 (09/01/13)	66	6,41	7 (3+4) Right	7 (3+4) Bilateral	- 5% of the gland affected	pT2cN0	- Prostate of 80g - Negative Margins	Eco showing BPH exceeding 60g and with a 12 mm nodule at the right	Patient in androgen deprivation therapy (Casodex) – initiated 3 months before surgery
8 (28/02/13)	59	4,08	7 (4+3) Right	7 (4+3) Bilateral	- 65% of the gland affected - Focal extracapsular extension	pT3aN0	- Prostate of 30g - Negative Margins	DRE with prostate hardening at the right	-

Table 6 The characteristics of the prostate specimens included in this study.

7. Spectroscopy procedure

Mid-infrared spectroscopy was used to obtain the spectra. Therefore, the prostate sample was placed in the path of the IR beam light between the source and the detector and absorbed only the frequency of mid-IR that coincides with the frequency of the vibration allowing the sample molecules to enter in a resonant vibration status. Mid-IR absorbance spectroscopy plots the recorded intensity of absorption bands versus an interval of wavenumbers, from 4000 to 400 cm^{-1}, which corresponds to changes of vibrational energy levels from the ground level to the first energy level (*E0→E1*) in molecules.(189)
Multivariate analysis was performed in order to infer classification and discrimination between prostate cancer tissue and normal prostate tissue. Also relevant spectroscopic regions and corresponding assignments to chemical functional groups have been identified.

7.1. Spectral acquisition

Before spectroscopic analysis, samples of prostate tissue that were stored at -80ºC were thawed at room temperature. Perkin-Elmer Spectrum BX FT-IR spectrometer was used to acquired spectra in the 4 000 to 900 cm^{-1} range at 8 cm^{-1} resolution with 64 co-added scans. Room temperature and humidity were always controlled and have been kept at ± 25ºC and ± 37% respectively. The acquisition of background single beam was performed against air (with the empty crystal) before each 5 mm thickness prostate tissue specimen has been posed on the ATR diamond crystal. The tissue sample is placed onto the crystal in order to fully cover it. During the spectral acquisition all the samples experienced the same constant pressure, characteristic of the golden gate equipment, which increase the adhesion to the crystal and decrease the spectral artifacts. The crystal was carefully cleaned with water between the spectral acquisitions of each sample.
The strong absorption of mid-infrared radiation by water is always a problem when FTIR is used in biological tissues. In the attempt to reduce this problem the sectioned tissue sample has been dried in order to see the actual biochemical composition of the tissue. The attempt of tissue drying was performed by simply allowing water to evaporate from the sample with the acquisition of six spectra (replicas) for each tissue sample. With this methodology the spectral contribution of water was practically eliminated and the three last acquired spectra obtained, which reached the possible drying stage, were the one chosen for the multivariate analysis.
Figures 11 and 12 show an example of the six replicas obtained from a sample of normal prostate tissue and the six replicas obtained from a sample of prostate cancer tissue, respectively. The regions associated with the presence of proteins, lipids, nucleic acids and carbohydrates are identified in the figures.
Given the high heterogeneity of the prostate tissue samples, replicas with discrepant values were removed from the analysis. The acquisition of replicates increased the confidence of results.

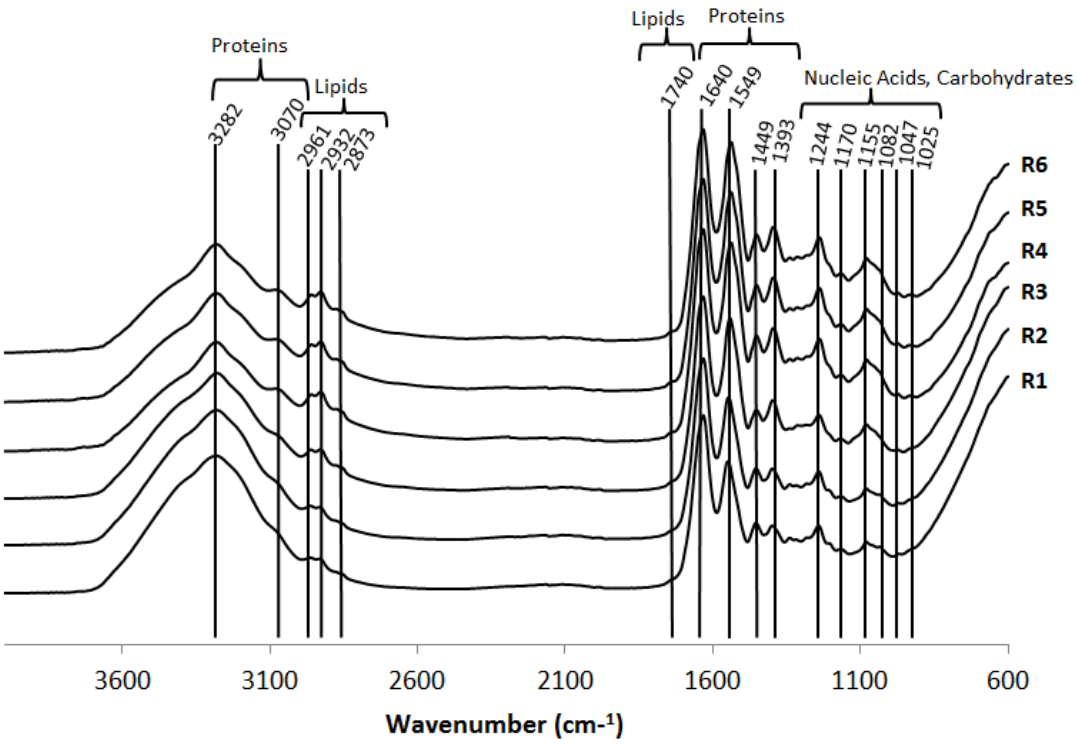

Figure 11 An example of FTIR spectra of the six replicas (R1-R6) obtained from a sample of normal prostate tissue, showing the regions associated with the presence of proteins, lipids, nucleic acids and carbohydrates.(189, 192, 194)

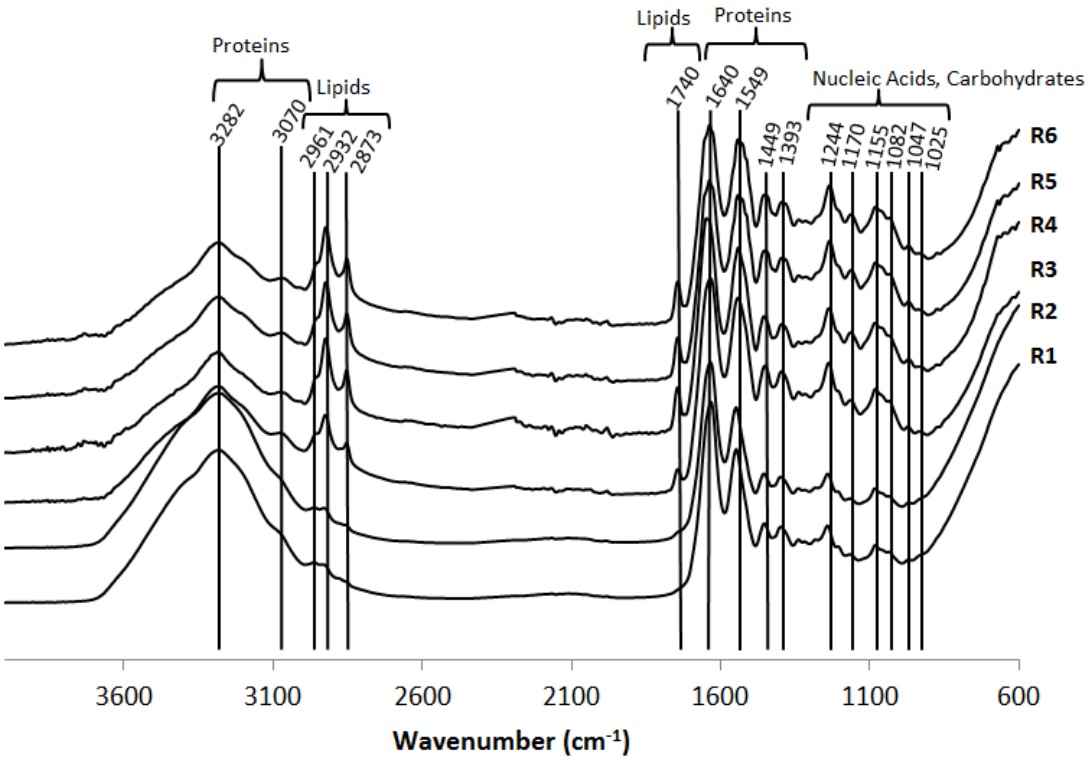

Figure 12 An example of FTIR spectra of the six replicas (R1-R6) obtained from a sample of prostate cancer tissue, showing the regions associated with the presence of proteins, lipids, nucleic acids and carbohydrates.(189, 192, 194)

As mentioned before, in mid-IR spectroscopy bands of water are very intense and may overlap the bands of interest, making the interpretation and identification of differences between spectra very difficult in the direct spectral analysis. Analysing the three first replicas (R1-R3), for both normal prostate tissue and PCa tissue samples, it is easy to visually detect these difficulties. Some important spectroscopic regions are overlapped with H_2O vibrational modes, mainly in the 3600-3200 cm^{-1} region due to O–H stretching bands and near 1645 cm^{-1} due to H–O–H bending band – see Figures 11 and 12.(194)

The problems associated with the water spectrum were minimized by simply allowing water to evaporate from the sample with the acquisition of replicas - tissue drying. In the three last replicas (R4-R6), for both samples, we observe that the bands overlapped with the water spectrum become much sharper as the water evaporates. The dried spectra now show important bands that correspond to vibrations of specific functional groups: proteins in the frequencies range of 3310-3030 cm^{-1} and 1720-1250 cm^{-1}; lipids in the range of 3020-2819 cm^{-1} and 1725-1740 cm^{-1}; carbohydrates and nucleic acids (DNA/RNA) in the range of 1250-900 cm^{-1} – see Figures 11 and 12.(189, 192, 194) The spectra obtained with the tissue drying have more spectroscopic information and allow a better qualitative analysis of the sample by the assignment of the peaks.

8. Data processing

Different methods can be used to analyse mid-IR spectra, from the simple direct spectra analysis to identify the number of peaks to “chemometrics” where mathematical, statistical, and computer sciences methods are applied to improve the understanding of chemical information contained in IR spectroscopic data. (189)

To reduce and correct interferences that may generate irrelevant variances such as atmospheric water vapour and carbon dioxide, variable background absorption profiles, and differences in sample thickness, a pre-processing (data set pre-processing) is required. The choice of normalization is as crucial as the choice of the analysis technique. Rescaling the data, normalization makes different variables and different samples comparable allowing integrating them in a joint analysis. (189, 192, 196)

The identification and assignment of spectral components (marker peaks) is generally performed by the so-called “group frequency approach”. The frequency of vibration of specific functional groups is pre-assigned according to those observed in the mid-IR spectrum of corresponding pure biomolecules or of mixtures of molecules and compared with those already reported in the literature. The application of “functional group analysis" is particularly useful for the type of analysis performed in this study, a qualitative analysis, since the IR spectrum of each molecule is unique and it can serve as a signature to distinguish among different molecules. (189, 196)

However, the unequivocal interpretation of pre-assigned vibrational frequencies is impossible because the vibrations of different molecular components may overlap and the spectrum may reflect only the average biochemical composition.(196)

8.1. Multivariate Analysis

In the results of FTIR studies many variables are observed (i.e. wavenumbers) for a number of individuals (e.g. normal or benign tissues). Each variable may be regarded as constituting a different dimension, such that if there are *n* variables each object may be said to reside at a unique position in an abstract entity referred as *n*-dimensional hyperspace. As this hyperspace is difficult to visualize, multivariate analysis will reduce the data dimensionality, creating a better perception of the data with the least possible loss of information. Therefore, in order to analyse data sets of complex biological matrices such as tissues powerful algorithms of multivariate statistical analysis can be applied. The use of multivariate methods makes possible to compare a large number of variables within a data set. (189)
Multivariate methods can be divided into techniques of multivariate classification (pattern recognition techniques) and of multivariate regression. Multivariate classification can be applied with supervised or unsupervised pattern recognition. In supervised pattern recognition, such as linear discriminant analysis (LDA) and artificial neural networks (ANNS), a substantial amount of information is available regarding the data set. While in unsupervised pattern recognition no "a priori" knowledge about the data set is required. Principal-component analysis (PCA) and cluster analysis (CA) are examples of unsupervised pattern recognition methods which are exploratory for data analysis, while supervised procedures allow for a more precise classification within the class boundaries. Multivariate regression techniques (multivariate calibration methods), such as principal components regression (PCR) and partial least squares regression (PLS), are used to analyse one or multiple constituents in a complex sample that are subject to significantly overlapping analytical signals.(192, 196)

Principal Component Analysis (PCA) is one of the most popular techniques. PCA is a non-parametric method for extracting relevant information from confusing data sets allowing to identify patterns in data and to highlight their similarities and differences. With PCA the large number of initial variables are condensed to only a few new variables or principal components (PCs) those reflecting the most relevant analytical information.(189) This is performed through a transformation of the original data matrix with each wavenumber (variable) being a column and each spectrum (sample) a row. The PCA results consist in two of types of diagrams: diagram of factorial coordinates (scores) and diagram of factorial contributions (loadings). The scores explain how the spectra relate to each other, while loadings explain how the wavenumbers relate to each other justifying the sample distribution along the scores diagram. The first PC (PC1) exhibits the greatest amount of variation, PC2 the second greatest amount of variation and so on. PCA allows as much as possible of the variance in the data set to be described by the first significant PCs, while all subsequent PCs are so low as to be virtually negligible. (189, 199, 201)

8.2. PCA analysis

Before the multivariate analysis, the spectra of the selected replicates were transferred through JCAMP-DX format into the data analysis software developed in the Institut National Agronomique Paris-Grignon in collaboration with the University of Aveiro.

Principal Component Analysis (PCA) was applied to the mid-infrared spectra of prostate samples in order to extract the main sources of variability. PCA analysis of the FTIR-ATR spectra was performed to identify spectral differences between the control and the PCa group. Also some differences within the PCa group will be discussed. PCA was applied to several spectral regions according some specific characteristics related to cancer detection (Table 7).

Two spectral pre-treatment procedures were used in the chosen spectral regions: Standard Normal Deviates (SNV) and second order Savitsky-Golay derivative (2D); the data set was auto-scaled, to put all the spectra to the same scale (standardize) and increase the differences between them (divided by the standard deviation).

All the direct spectral analysis of the spectra and the multivariate analysis PCA performed in this study will be presented and discussed in the next chapter.

Chapter three

This chapter includes the results on the application of FTIR spectroscopy to the samples of prostate cancer (PCa) tissue and normal prostate tissue (controls), in order to detect spectral differences that help in the identification and classification of prostate tumour tissues.

E. Results and discussion

9. Spectral Analysis

Once the infrared spectra have been recorded, the next step is interpretation. Spectral interpretation is simplified by the fact that the bands that appear may be assigned to particular functional groups of the molecule, producing what are known as group frequencies. As already mentioned in the previous chapter the mid-infrared region was the one used in this study. The mid-infrared spectrum can be divided into four regions that are defined as follows: X–H stretching region (4000-2500 cm^{-1}), triple bond region (2500-2000 cm^{-1}), double bond region (2000-1500 cm^{-1}), and the "fingerprint region" (1500-600 cm^{-1}). Table 7 shows the main regions of the mid-infrared spectrum that can be analysed in biological samples and its relation with cancer detection.(189, 192, 202)

Wavenumber (cm^{-1})	Assignment	Assigned biochemical component	Relevant information to cancer detection
3500-2500	X-H stretching (X is C, O or N)		
3300	N-H stretching	Amide A peptide, protein	-
3100	N-H stretching	Amide B peptide, protein	-
2957	CH_3 asymmetrical stretching	Lipids, phospholipids	Dysregulated lipid metabolism; Increased disorder of the methylene chains of membrane lipids
2920	CH_2 asymmetrical stretching		
2872	CH_3 symmetrical stretching		
2851	CH_2 symmetrical stretching		
2000-1500	Stretching of double bonds (e.g. C=O, C=C, C=N)		
1745	C=O stretching	Lipids, Phospholipids esters	Dysregulated lipid metabolism; Membrane lipids (phospholipids) disorder
1655	80% C=O stretching, 10% C-N stretching, 10% N-H bending	Amide I peptide, protein	-
1645	H-O-H bending	Water	-
1545	60% N-H bending, 40% C-N stretching	Amide II peptide, protein	-
1500-600	The "fingerprint region" (many overlapped vibrations)		
1450	CH_3 asymmetrical bending	Lipid, protein	Increased hypomethylation
1395	CH_3 asymmetrical bending, C=O	Lipid, protein	Increased hypomethylation

	stretching		
1378	CH_3 symmetrical stretching	Phospholipid, fatty acid, triglyceride	-
1400-1200	N-H bending, C-N stretching, C=O stretching, C-C stretching and CH_3 stretching	Amide III peptide, protein, collagen	Decreased hydrogen bonding of the C-OH groups of proteins
1245-1230	PO^{2-} asymmetrical stretching	DNA, RNA, phospholipid, phosphorylated protein	Increased hydrogen bonding of the phosphodiester groups of nucleic acids
1170	C-O asymmetrical stretching	Ester	-
1160 and 1120	C-O stretching	RNA ribose	-
1150	C-O stretching, C-O-H bending	Carbohydrates	-
1095, 1084, 1070	PO^{2-} symmetrical stretching	DNA, RNA, phospholipid, phosphorylated protein	Increased hydrogen bonding of the phosphodiester groups of nucleic acids
1078	C-C stretching	Glycogen	Reduced glycogen content
1060, 1050, 1015	C-O stretching	DNA and RNA ribose	-
1050	C-O-P stretching	Phosphate ester	-
1028	C-O-H deformation	Glycogen	Reduced glycogen content
965	PO_3^{2-} stretching	DNA and RNA ribose	-
950	PO_3^{2-} stretching	Phosphorylated protein	-
920	C-O-P stretching	Phosphorylated protein	-

Table 7 Main regions of the mid-infrared spectrum and its relation with cancer detection. Adapted from(189, 192, 202)

The Table 7 reflects a bibliographic review of what have already been described in the IR spectroscopy field about assignments of the mid-IR spectrum related to cancer detection. Therefore, its content will be used to support the direct spectral analysis (Table 8) and the results of the multivariate analysis, presented hereafter.

As we can see in Table 7, the mid-IR spectroscopy is a powerful tool for the study of biological molecules and its application to biological problems is continually expanding, as it can be used in the characterization of complex systems, such as diseased tissues. The main groups of biological molecules that can be studied in the mid-IR spectrum are: Proteins and peptides, Lipids, Carbohydrates and Nucleic acids. (192, 194)

Proteins and Peptides: mid-IR spectroscopy can be used as an effective tool for exploring structural changes and functional mechanisms of bands that can be assigned to the vibrations of amino acids. Amino acids are important components of tissues, playing the role of the building

blocks of proteins. They are involved in metabolic processes at the molecular level and conformational changes of amino acids may modify the proper functioning of vital organs and cellular structure.(203) The IR spectra of proteins exhibit absorption bands associated with their characteristic amide group. In-plane modes are due to C=O stretching, C–N stretching, N–H stretching and O–C N bending and an out-of-plane mode is due to C–N stretching. There are nine amide bands, called amide A, amide B and amides I–VII, in order of decreasing wavenumber.(192, 194) Amide A and B are at approximately 3300 cm^{-1} and 3100 cm^{-1}, respectively, and are due to N-H stretching. The amide I band is the most intense and useful for conformational analysis of proteins, occurring between approximately 1700 and 1600 cm^{-1}. This band represents 80% of the C=O stretching vibration of the amide group coupled to the in-plane N–H bending and C–N stretching modes – see Table 7. The exact wavenumber of this vibration depends on the nature of hydrogen bonding involving the C=O and N–H groups, which is determined by the particular secondary structure adopted by the protein. Proteins generally contain a variety of domains containing polypeptide fragments in different conformations. Therefore, the observed amide I band is usually a complex composite, consisting of a number of overlapping component bands representing helices, β-structures, turns and random structures.(192, 194, 203) The amide II band represents 60% of the N–H bending, with some C–N stretching (40%). The position of the amide II band shifts from 1550 cm^{-1} to 1450 cm^{-1}. The amide III band represents the combination of N-H bending and C–N stretching, with a less intensive contribution from C–C stretching and C=O stretching. It can be found between 1250 and 1300 cm^{-1} – see Table 7. Because the C=O and the N–H bonds are involved in the hydrogen bonding that takes place between the different components of secondary structure, the positions of the amides (I, II, III) bands can be sensitive to the secondary structure content of a protein. The amide IV-VII bands have very low intensities in mid-IR and are not of importance in a mid-IR analysis.(192, 194)

Lipids: lipids, including fatty acids, phospholipids (lipids that contain phosphorus), cholesterol esters and glycerides, can be readily characterized in the mid-IR spectrum. They are important molecular components of membranes and are organized in bilayers of about 40–80 A in thickness, where the polar head group points towards the aqueous phase and the hydrophobic tails point towards the tails of a second layer.(192) The IR spectra of lipids can be divided into the spectral regions that originate from the molecular vibrations of the hydrocarbon tail, the interface region, and the head group. The hydrocarbon tail gives rises to acyl chain modes. The most intense vibrations in the spectra are the CH_2 asymmetric and symmetric stretching, that gives rise to bands at 2920 and 2851 cm^{-1}, respectively. The infrared bands due to the terminal CH_3 groups gives rise at 2957 cm^{-1} (asymmetric stretching) and 2872 cm^{-1} (symmetric stretching) – see Table 7. In the 1500–1350 cm^{-1} region occurs the bands due to methylene and methyl groups. At around 1378 cm^{-1} appears the symmetric deformation mode of the CH_3 group.(192, 194) Spectral bands arising from the head group and interfacial region also provide valuable information. In the interfacial region the important IR bands are the ester group vibrations, particularly the C=O stretching bands in the 1750–1700 cm^{-1} region. In diacyl lipids, this region consists of at least two bands originating from the two ester carbonyl groups. A band at 1742 cm^{-1} is assigned to the C=O mode of the first alkyl chain with a *trans*-conformation in the C–C bond adjacent to the ester

grouping. The band 1728 cm^{-1} C=O wavenumber of the second alkyl chain suggests the presence of a *gauche*-band in that position.
The wavenumber difference observed reflects the structural inequivalence of the chains, with the first alkyl chain initially extending in a direction perpendicular to the second alkyl chain and then developing a *gauche*-bend in order to render the two chains parallel.(194)

Carbohydrates: mid-IR spectroscopy can also be used to identify carbohydrates, including sugars, cellulose, starch, pectins, and carrageenans. The IR bands found for this class of biomolecules are associated with the hydroxyl and carbonyl groups and acetal bonds. In the anomeric region of the mid-IR spectrum at 950–750 cm^{-1} is possible to distinguish the characteristic bands for α and β conformers or pyranoid and furanoid ring vibrations of monosaccharides and polysaccharides. Polysaccharides have strong bands near 3300 cm^{-1} because of O–H stretching. They also show a band near 1650 cm^{-1} associated with a carbonyl group (C=O stretching) and intermolecular water. The region 1400-800 cm^{-1} is associated with coupled C–O and C–C stretching and bending.(194)

Nucleic Acids: the nucleic acids, deoxyribonucleic acid (DNA) and ribonucleic acid (RNA), are vital molecules which carry the genetic code and are responsible for its expression by protein synthesis. The spectra of these molecules can be divided into the modes due to the constituent base, sugar and phosphate groups. The bases (thymine, adenine, cytosine, guanine and uracil) give rise to purinic and pyrimidinic vibrations in the region 1800-1500 cm^{-1}. Bands in the region 1500-1250 cm^{-1} are due to the vibrational coupling between a base and a sugar. In the region 1250-1000 cm^{-1} sugar–phosphate chain vibrations are observed and in the region 1000-800 cm^{-1} are observed sugar/sugar–phosphate vibrations.(192, 194)

9.1. Results and discussion

Peak position can be correlated with known verified tables of key functional group absorbance peak positions. Since differences in key functional group may be directly observed, a direct spectral analysis was performed with the intent to distinguish normal from prostate cancer (PCa) samples.
Figures 13 and 14 show spectra of all samples of normal prostate tissue and PCa tissue, respectively.

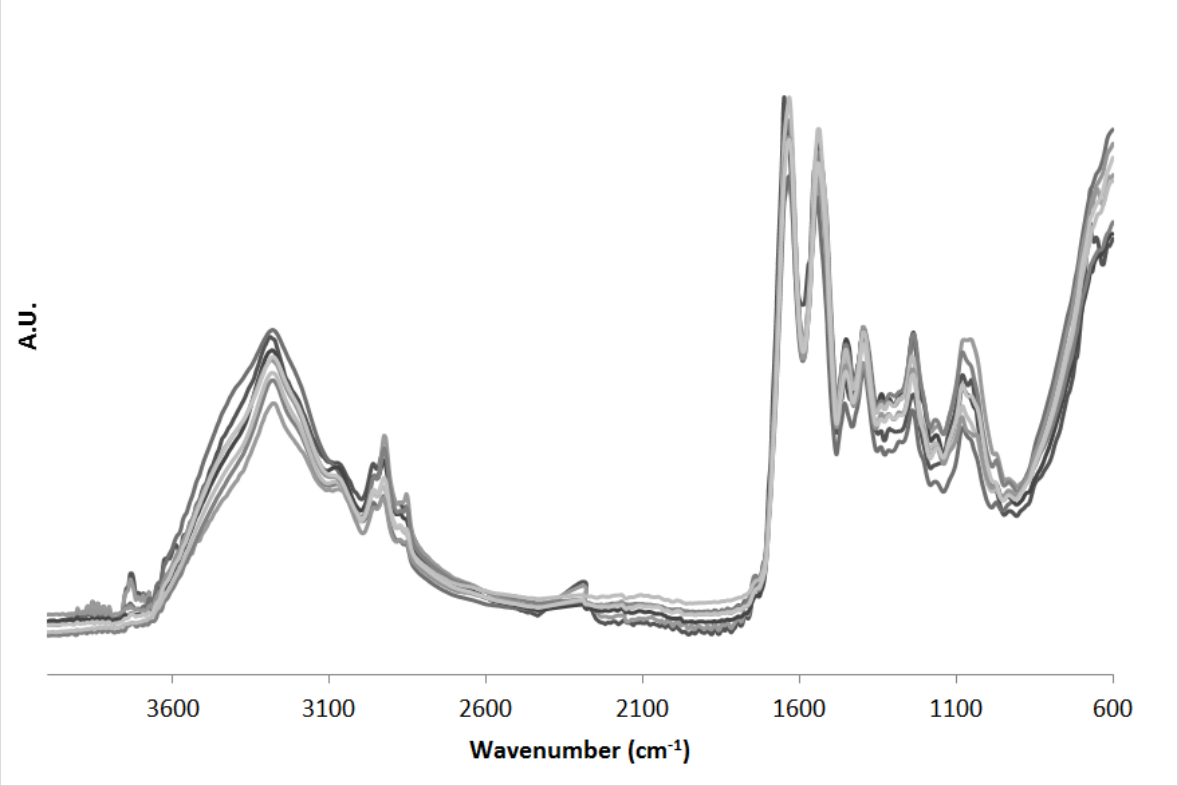

Figure 13 Spectra of all samples of normal prostate tissue (controls). *A.U. Arbitrary Units*

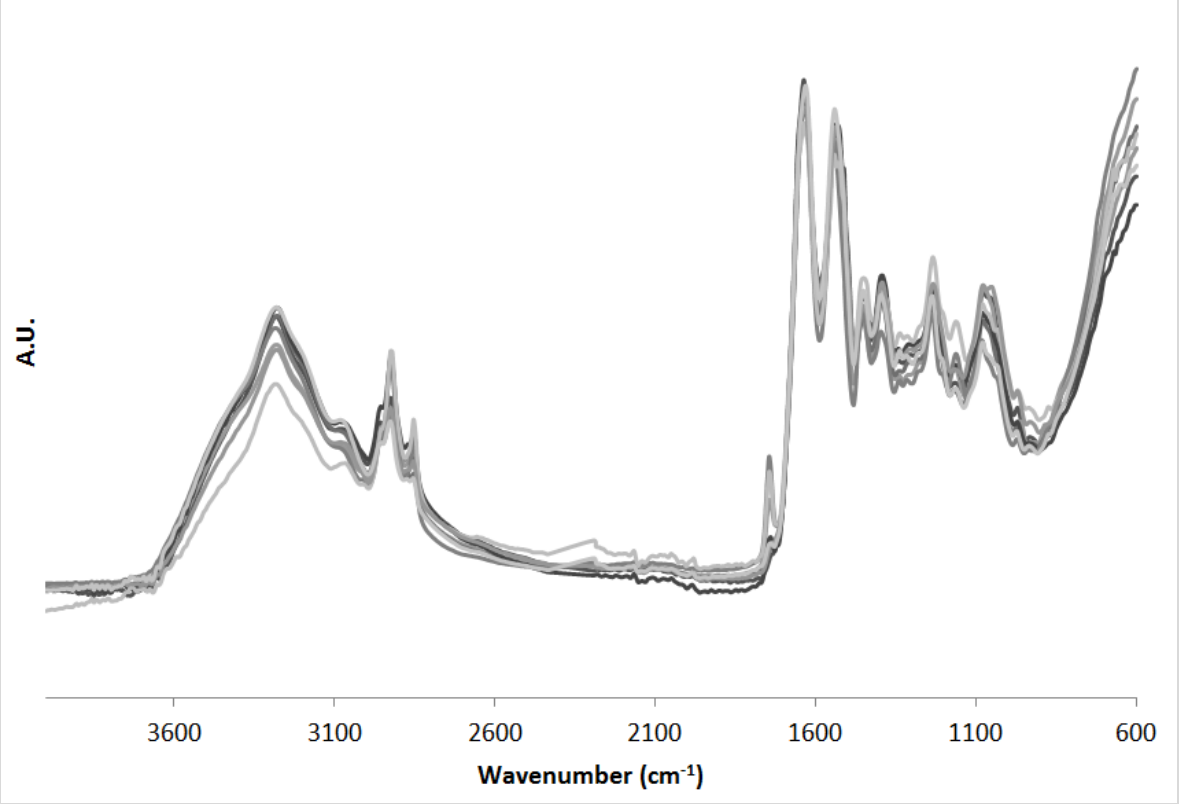

Figure 14 Spectra of all samples of prostate cancer (PCa) tissue. *A.U. Arbitrary Units*

The spectra of all samples of controls (normal prostate tissue) appear to be very similar as it is possible to verify that all spectra overlap, without revealing major differences. On the other hand, at first glance, it is possible to detect some differences when analysing Figure 13, both between the spectra of all samples of PCa and when comparing the spectra of all samples of controls with the spectra of all samples of PCa – Figures 13 and 14. The detected differences between the spectra of PCa may be due to the differences in tumour aggressiveness between patients. In order to understand these differences between the spectra and possibly distinguish the normal prostate samples from the PCa samples a band assignment was performed. Figures 15 and 16 show representative spectra of one control sample and PCa sample of a patient with an aggressive tumour, and representative spectra of one control sample and PCa sample of a patient with a less aggressive tumour, respectively.

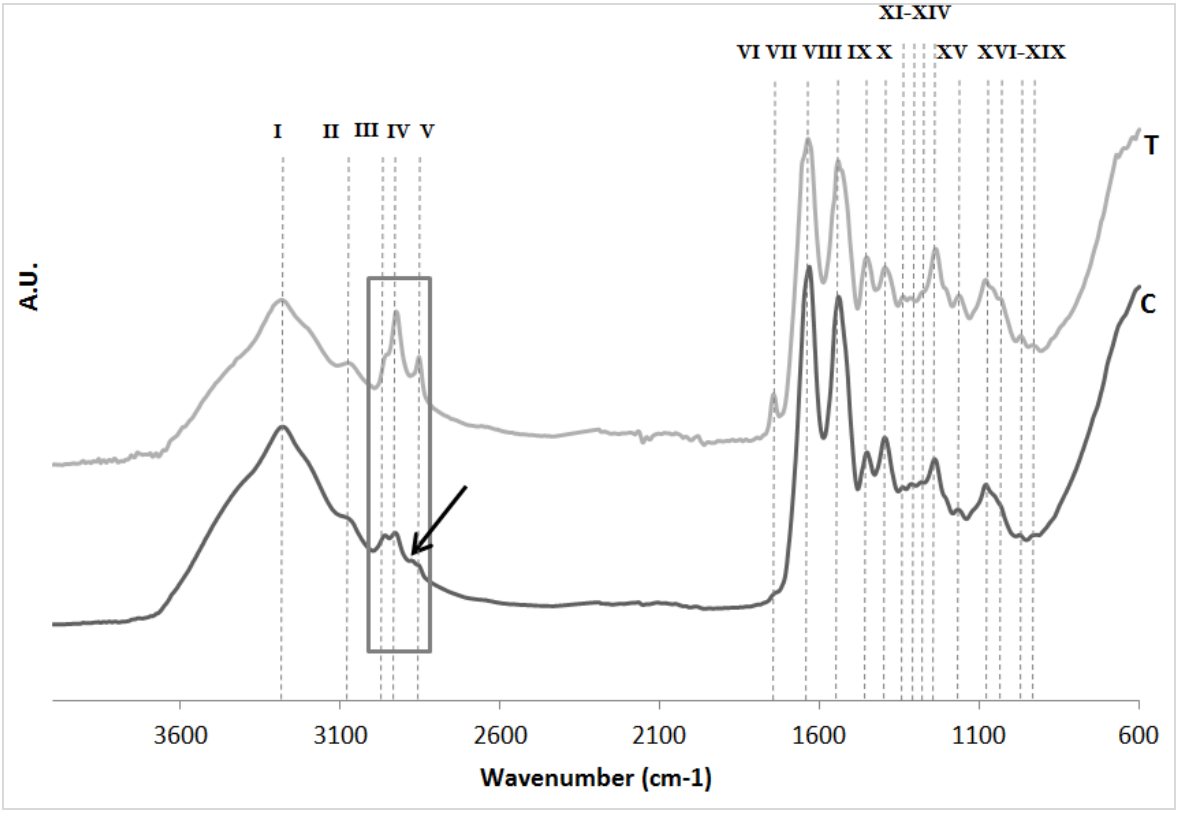

Figure 15 Spectra of one control sample (C) and PCa sample (T) of a patient with an aggressive tumor. *A.U. Arbitrary Units*

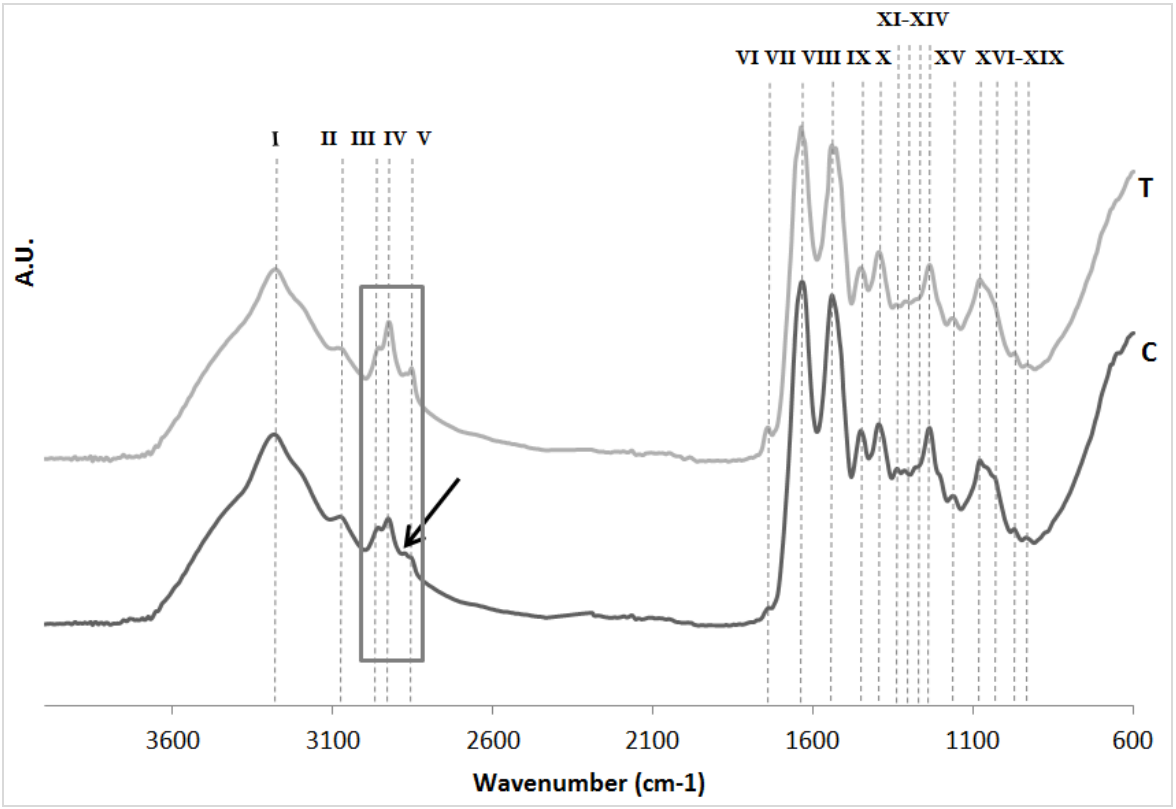

Figure 16 Spectra of one control sample (C) and PCa sample (T) of a patient with a less aggressive tumor. *A.U. Arbitrary Units*

As already mentioned, the identification and assignment of major spectral components by "functional group analysis" is particularly useful in a qualitative analysis since the IR spectrum can serve as a signature to distinguish different samples, by the identification of specific bands of proteins, nucleic acids DNA and RNA, lipids, and carbohydrates. (196)

However, it is evident from the analysis of Figures 15 and 16 that the overall spectra appearance of biological samples such as prostate tissue is complex. Tissues are composed of a mixture of different mid-IR active molecular constituents such as membrane lipids and phospholipids, glycolipids, proteins and nucleic acids (DNA, RNA), and, therefore, their IR spectra contains a large number of bands and many of which will be impossible to confidently assign to vibration of a particular group, in particular analysing the “fingerprinting region”. That fact leads us to conclude that the unequivocal interpretation of pre-assigned vibrational frequencies is impossible because the vibrations of different molecular components of may overlap and the spectrum may reflect only the average biochemical composition.(189, 196)

Table 8 indicate the major FTIR spectra assignments for control and PCa samples. The possible band assignment was made correlating the identified spectra bands with verified tables of key functional group absorbance band positions, and taking in account the information previously presented in Table 7.(164, 189)

Nº	Bands of control and PCa spectra (cm^{-1})	Assignments	Tissue content
I	~3304	N-H stretching	Amide A peptide, protein
II	~3094	N-H stretching	Amide B peptide, protein
III	~2956	CH_3 asymmetrical stretching	Lipids, phospholipids
IV	~2926	CH_2 asymmetrical stretching	
"Arrow" (only in the spectra of control samples)	~2878	CH_3 symmetrical stretching	
V (only in the spectra of PCa samples)	~2860	CH_2 symmetrical stretching	
"Arrow" (only in the spectra of control samples)	~2852	CH_2 symmetrical stretching	
VI	~1750	C=O stretching	Lipids, Phospholipids esters
VII	~1645	80% C=O stretching, 10% C-N stretching, 10% N-H bending	Amide I peptide, protein
VIII	~1548	60% N-H bending, 40% C-N stretching	Amide II peptide, protein
IX	~1464	CH_2 bending	Lipid, protein
X	~1450	CH_3 bending	Lipid, protein
XI	~1372	C-N stretching	Cytosine, guanine
XII	~1362	C-N stretching	Cytosine, guanine
XIII	~1310	N-H bending, C-N stretching, C=O stretching, C-C stretching and CH_3 stretching	Amide III peptide, protein
XIV	~1242	PO_2^- asymmetrical stretching	DNA, RNA, phospholipid, phosphorylated protein
XV	~1200	PO_2^- asymmetrical stretching	Phosphate I
XVI	~1092	PO_2^- symmetrical stretching	DNA, RNA, phospholipid, phosphorylated protein
XVII	~1062	C-O stretching	DNA and RNA ribose
XVIII	~1008	C-O stretching	DNA deoxyribose
XIX	~966	C-O stretching, C-C stretching	DNA deoxyribose

Table 8 Spectral assignments of control and PCa samples, based in the information presented in Table 7.(164, 189)

With the spectral analysis was possible to identify in all spectra of control and PCa samples the contributions of proteins, lipids, carbohydrates and nucleic acids DNA and RNA present in the prostate tissue samples.

At first glance the control and PCa spectra of both patients (aggressive and less aggressive tumour) seem similar, as almost all assign bands are observable in all spectra – see Table 8. However, in a closer look, differences between the control and PCa spectra can be detected, mainly differences in the band intensities. And, analysing both Figures 15 and 16, we detect that these differences are much more evident in the spectra of the patient with an aggressive tumour than in the spectra of the patient with a less aggressive tumour.

The two major bands, which are common for all control and PCa spectra, are the Amide I and Amide II, characterizing the spectrum of proteins. Amide I at ~1645 cm^{-1} identifies the C=O stretching mode and Amide II at ~1548 cm^{-1} refers to the combination of both N–H bending and C–N stretching. As already mentioned, Amide I and II not only identify protein molecule but their positions and shapes reflect the secondary protein structure adopted by the polypeptide chain, reflecting the backbone conformation and hydrogen-bonding pattern.(192, 194) The Amide III is also observable at ~1310 cm^{-1} attributed mainly to N-H bending and C-N stretching. Finally, with the water evaporation and the hydrogen-bonded amino groups dominating the region between 3400 and 3250 cm^{-1}, it is also possible to observe in the spectrum of proteins the Amide A and B at ~3304 cm^{-1} and ~3094 cm^{-1}, respectively, which are due to N-H stretching – see Table 8.(164, 192)

The bands at ~2956 cm^{-1} and ~2926 cm^{-1} attributed to asymmetrical CH_3 and CH_2 stretching, respectively, are present in all spectra and identify the present of lipid molecules – see Table 8. However, there are two bands of the spectrum of lipids at ~2878 cm^{-1} and ~2852 cm^{-1} due to symmetrical CH_3 and CH_2 stretching, respectively, which are only seen in the spectra of control samples; while in the spectra of PCa samples a more intense band at 2860 cm^{-1} probably related to symmetrical CH_2 stretching is observed.(192, 194) Moreover, besides the common present in all spectra of the two referred bands, it is evident that they are more intense in the spectra of PCa samples in both patients – see Figures 15 and 16. It is known that, usually, in biological tissues/cells there are a greater number of methylene groups in phospholipids (lipids of the membrane that contain phosphorus), so the intensity of the CH_2 absorptions is 10-20 times that of the corresponding CH_3 absorption.(202) These differences can be detected in the spectra of control samples. In the spectra of PCa samples is possible to verify an increased disorder of the methylene chains of membrane lipids, which results in the presence of a more intense band at ~2860 cm^{-1} possibly related to symmetrical CH_2 stretching that overlaps the bands at ~2878 cm^{-1} and ~2852 cm^{-1} related to symmetrical CH_3 and CH_2 stretching, respectively. (202, 204)

The presence of lipids is supported by the bands at ~1464 cm^{-1} and ~1450 cm^{-1} attributed to CH_2 and CH_3 bending, respectively.(164)

The band at ~1750 cm^{-1} due to C=O stretching also supports the presence of lipid molecules and its observed higher intensity in the PCa spectra, which is much more evident in the patient with an aggressive tumour, also supports the hypothesis of a disorder in the membrane lipids related to the presence of prostate cancer and suggests that this disorder is in a more advanced stage in patients with a more aggressive tumour – see Figures 15 and 16.(164, 192)

Finally, in the “fingerprint region” is possible identify C-O-C, C-O, C-C, C-O-P, P-O-P vibrations of DNA, RNA, carbohydrates, lipids and proteins. This region presents some specific signatures that enable its rapid identification, however in complex biological samples such as prostate tissue these features are difficult to observe.(189, 192) It was possible to assign some bands common

for all spectra, such as the bands at ~1372 cm^{-1} and ~1362 cm^{-1} due to C-N stretching of cytosine and guanine. The asymmetrical and symmetrical PO^{2-} stretching at ~1242 cm^{-1} and at ~1092 cm^{-1}, respectively, suggest the absorption of O–P=O linkages of the polynucleotide chains in DNA and RNA. The band at ~1200 cm^{-1} due to asymmetrical PO^{2-} stretching is related to phosphate I. The bands at ~1062 cm^{-1} and at ~1008 cm^{-1} are attributed to C-O stretching of DNA/RNA ribose and DNA deoxyribose, respectively, and the band at ~966 cm^{-1} is due to C-O and C-C stretching of DNA deoxyribose – see Table 8.(164, 192)

The direct spectral interpretation reveals some differences between control and PCa samples and between patients and has suggested some hypothesis about the spectral regions and compounds that can be used to distinguish between the control and PCa samples and between PCa samples. However, this analysis is not sufficient to accomplish the proposed goals of identify and characterize prostate tissues.

The visual spectral interpretation has been the backbone of spectroscopic analysis since the establishment of spectrometers but it can be highly subjective, particularly in modern spectroscopy, where a huge amount of spectral data is collected by FTIR. Pattern recognition techniques are now applied to infrared data with the attempt to remove subjectivity and allow realistic processing of large datasets.(189, 192) Therefore, the technique multivariate analysis was used to highlight differences between the study patients and between the study groups (control and PCa).

10. Multivariate Analysis

10.1. Results and Discussion

Principal Component Analysis (PCA) was applied to the mid-infrared spectra of prostate samples in order to extract the main sources of variability and specific spectral regions were chose according to some characteristics related to cancer detection that are possible to identify with FTIR spectroscopy – see Table 7. PCA was applied to the chosen regions at ranges of 3800-3600, 3000-2800, 1800-900, 1500-900, 1300-900, 1200–900 and 1800-1700 cm^{-1}. As previously mentioned in chapter 2, the two spectral pre-treatment procedures applied in the chosen spectral regions were Standard Normal Deviates (SNV) and second order Savitsky-Golay derivative (2D). After testing both data pre-treatments the second order Savitsky-Golay derivative 2D was the one used in all the spectral regions presented below.

The region at 3800-3600 cm^{-1} was tested, despite there was no initial assumption about relevant information to cancer detection in this region – see Table 7. Since it showed no discrimination capable to be explained according to the known sample characterization, the results for this region are not presented. The regions 1800-900, 1500-900 and 1300-900 cm^{-1} were also tested as they could give relevant information (Table 7), mainly about lipid metabolism alterations (1800-1700 cm^{-1}), protein alterations due to increased hypomethylation (1500-1400 cm^{-1}), as well as alterations in the backbone of the nucleic acids and in the glycogen content (1300-900 cm^{-1}). Despite the fact these regions are very information rich and already show some tendency to form two main groups, these results are also not presented. Their loadings proved to

be noisy and very difficult to interpret, and the separation of groups could be better, as the samples still seem a little shuffled. These large range spectral regions do not reveal much relevant information to the aim of the study. Therefore, it seems necessary to reduce the spectral regions and test smaller and more specific spectral ranges according to the assumptions presented in Table 8 and also taking in account the hypothesis suggested by the direct spectral analysis.

Mid-IR region 3000-2800 cm^{-1}

To test the hypothesis of an increased disorder of the methylene chains of membrane lipids associated with the PCa samples, PCA was applied to the region 3000-2800 cm^{-1}, which correspond to the lipid region that includes the C-H, CH_3, CH_2 stretching of lipids and also proteins – see Figure 17. (164)

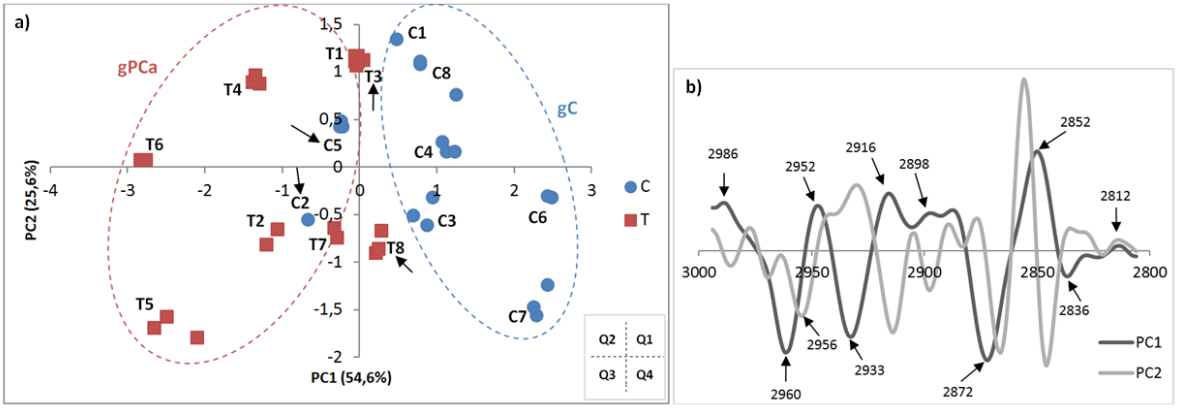

Figure 17 PCA scores (a) and loadings (b) of control and PCa samples at 3000-2800 cm^{-1} range.

Two main groups may be suggested based on the distribution of the samples along PC1, which explains most of the variability. PC2, which could explain the second most important factor of the remaining analysis, do not seem to affect the groups' distribution and, therefore, it had not been taken in account in the loadings interpretation.

It can be observed one group of control samples (gC), which is mainly explained by the positive side of PC1 and, wherefore, distributed in Q1 and Q4. It is constituted by almost all control samples, except C2 and C5. The other group is mainly explained by the negative side of PC1 and distributed in Q2 and Q3. This group of PCa samples (gPCa) includes T1, T2, T4, T5, T6 and T7. The two control samples C2 and C5 are also included in this group. The PCa samples T3 and T8 are not included in the gPCa, however they are distributed close to zero of PC1, which indicates they are less affected by the peaks identified in PCA loadings. The assignments of the peaks selected in the PCA loadings (Figure 17b) are shown in Table 9. The analysis of the loadings is useful to understand the basis of the samples distribution in the PCA scores (Figure 17a).

Bands (cm^{-1})	PC1	Assignments	Group
~2986	+	C-H stretching	gC
~2960	-	Asymmetric CH_3 stretching of lipids and fatty acids	gPCa
~2952	+	Asymmetric CH_3 stretching of acyl chains (lipids)	gC
~2933	-	C-H stretching band in malignant tissues	gPCa

~2916	+	C-H stretching band in normal tissues	gC
~2898	+	Symmetric CH_3 stretching of acyl chains (lipids)	gC
~2872	-	Symmetric CH_3 stretching	gPCa
~2852	+	Symmetric CH_2 stretching of acyl chains (lipids)	gC
~2836	-	N-H stretching (NH_3^+)	gPCa
~2812	+	N-H stretching (NH_3^+)	gC

Table 9 Mid-IR bands at range 3000-2800 cm^{-1} identified in PCA loadings.(164, 192, 194)

The analysis of the PCA scores showed that control samples C1, C3, C4, C6, C7 and C8 are close to each other, suggesting the formation of a group (gC) mainly explained by the positive side of PC1. The distribution and proximity of these control samples is justified by six peaks identified in the PCA loadings profile (2986, 2952, 2916, 2898, 2852 and 2812 cm^{-1}). The peak at 2986 cm^{-1} is an unspecific peak related to the C–H stretching vibration characteristic of this region. The peaks at 2952, 2898, 2852 cm^{-1} are related to asymmetric and symmetric CH_3 stretching and symmetric CH_2 stretching of the acyl chains of lipids, respectively. The peak at 2916 cm^{-1} is related to a band characteristic of normal tissues, due to C-H stretching. The peak at 2812 cm^{-1} is related to the N-H stretching of the NH_3^+. As there is another peak with the same assignment in the negative side of PC1 (2836 cm^{-1}), and so even related to the opposite group, these two peaks do not seem to justify the formation of the groups. (164, 192)

The analysis of the PCA scores also suggested the formation of another group (gPCa), which is explained by the negative side of PC1 and include the PCa samples T1, T2, T4, T5, T6 and T7. Four peaks identify in the PCA loadings can justify the proximity of these samples and the formation of this group: the peak at 2960 cm^{-1} due to asymmetric CH_3 stretching of lipids and fatty acids may suggest differences in fatty acids related to the gPCa, that can be in high concentration or modified; the peak at 2933 cm^{-1} is related to a band only present in malignant tissues; the peak at 2872 cm^{-1} is an unspecific peak related to symmetric CH_3 stretching and the already refereed peak at 2836 cm^{-1} is related to the N-H stretching of the NH_3^+.(164)

As already mentioned, the region 3000-2800 cm^{-1} is the lipid region and includes the stretching vibrations of CH_2 and CH_3 of phospholipids, cholesterol and creatine, which are compounds that, according to the literature, are higher in normal tissues.(164) Therefore, the identification in this region of a higher number of peaks (six) related to the gC was expected and suggest a higher content of these compounds in the control samples in comparison to the PCa samples.

Moreover, the PCA analysis also corroborates the hypothesis of an increased disorder of the methylene chains of membrane lipids associated with the gPCa. Notice that a band related to the asymmetric CH_2 stretching of acyl chains of lipids, which is usually at 2926-2931 cm^{-1}, was not identify in the PCA loadings, probably because of the appearance of a peak at 2933 cm^{-1} characteristic of malignant tissues, which suggest a disorder in membrane methylene chains.(164, 202) Other authors have already concentrated their studies on examining the spectral characteristics of prostate tissue in the region 3000-2800 cm^{-1}. They have also performed a quantitative analysis and have concluded that by using the CH_2/CH_3 ratio it was possible to differentiate between normal and cancerous tissues using FTIR, suggesting a membrane lipid disorder related to the malignant tissues.(202, 204) As the cancer cells divide rapidly, the new membrane biogenesis also has to occur rapidly, which may result in differences in the membrane synthesis and lead to the suggested disorder of the chains of membrane lipids.

The suggested alterations in fatty acids in the gPCa can also be related to an accelerated cancer cells division, which can lead to an increased fatty acid synthesis.(205) These alterations are further investigated in the PCA analysis of the region 1800-1700 cm^{-1}.

The PCa samples T3 and T8 are out of pattern and are not included in the gPCa. As they are located close to zero, they are less affected by the peaks identified in PCA loadings, which may indicate that the identified alterations characteristics of the gPCa are not yet present in these patients; they may be in a more initial stage of PCa where a membrane lipid disorder is not yet evident.
The two control samples, C2 and C5, included in the gPCa are control samples of patients with aggressive tumours. Therefore, their localization close to the PCa samples, especially C2 that is very close to T2, may be a result of errors in the sample collection. These errors may lead to the collection of PCa tissue along with the collection of the normal prostate tissue for these control samples.

Mid-IR region 1200-900 cm^{-1}

PCA was applied to the region 1200-900 cm^{-1}, which correspond to the phosphodiester region, including the phosphodiester stretching bands for absorbances due to glycogen – see Figure 18.(164)

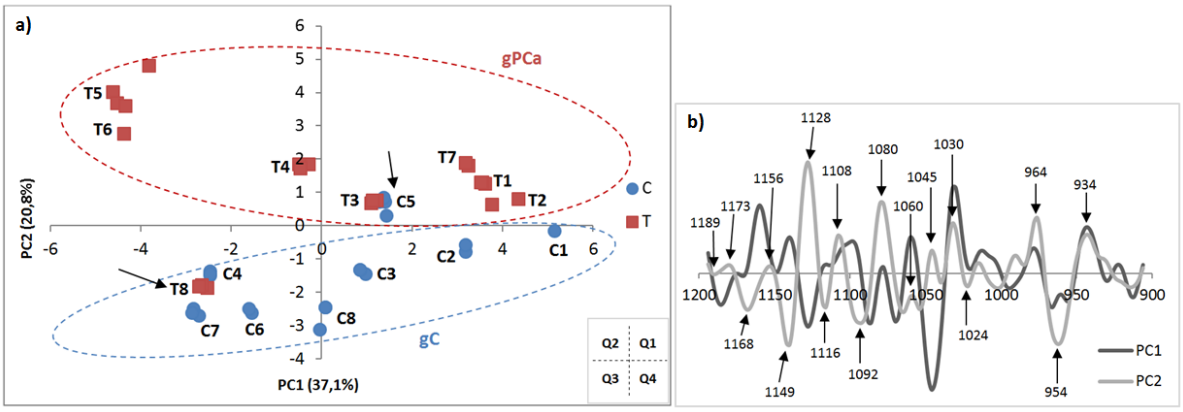

Figure 18 PCA scores (a) and loadings (b) of control and PCa samples at 1200-900 cm^{-1} range.

In this region is also possible to identify in the PCA scores (Figure 18a) two groups based, in this case, on the distribution of the samples along PC2. PC1 do not seem to affect the groups' distribution and, therefore, it had not been taken in account in the loadings interpretation.
Again, one group of control samples (gC) can be observed, which is mainly explained by the negative side of PC2 and distributed in Q3 and Q4. It is constituted by almost all control samples, with the exception again of C5. The group of PCa samples (gPCa) is mainly explained by the positive side of PC2 and distributed in Q1 and Q2. This group includes T1, T2, T3, T4, T5, T6 and T7. The control sample C5 is also included in this group and the PCa sample T8 are again not included. Table 10 shows the assignments of the peaks selected in the PCA loadings (Figure 18b).

Bands (cm^{-1})	PC2	Assignments	Group
~1189	-	Deoxyribose	gC
~1173	+	C-O stretching in malignant tissues	gPCa
~1168	-	C-O stretching in normal tissues; C-O stretching of C-OH groups of serine, threosine and tyrosine of proteins	gC
~1156	+	C-O stretching of proteins and carbohydrates	gPCa
~1149	-	Glycogen absorption due to C-O and C-C stretching and C-O-H deformation	gC
~1128	+	Symmetric phosphodiester stretching of RNA	gPCa
~1116	-	Symmetric P-O-C stretching	gC
~1108	+	Symmetric P-O-C stretching	gPCa
~1092	-	Symmetric PO^{2-} stretching (phosphate II); Symmetric PO2 stretching of RNA and DNA; Symmetric stretching of phosphate groups in phospholipids	gC
~1080	+	Symmetric PO^{2-} stretching of RNA and DNA; Phosphate I in RNA (one of the triad peaks of nucleic acids (along with 1060 and 1030)	gPCa
~1060	+	C-O stretching of deoxyribose (one of the triad peaks of nucleic acids)	gPCa
~1045	+	C-O stretching coupled with C-O bending frequencies of the C-OH groups of carbohydrates (glucose, fructose, glycogen, etc); Glycogen band	gPCa
~1030	+	C-O stretching coupled with C-O bending (one of the triad peaks of nucleic acids)	gPCa
~1024	-	C-O stretching associated of glycogen	gC
~964	+	C-C and C-O stretching in deoxyribose of DNA in malignant tissues	gPCa
~954	-	C-C and C-O stretching of deoxyribose	gC
~934	+	Left-handed helix DNA	gPCa

Table 10 Mid-IR bands at range 1200-900 cm^{-1} identified in PCA loadings.(164, 192, 194)

The analysis of the PCA scores at the region 1200-900 cm^{-1} approximates the samples C1, C2, C3, C4, C6, C7 and C8, proposing the constitution of the group of control samples, gC, explained by the negative side of PC2. Seven peaks identified in the PCA loadings characterize this group: the peaks at 1189 cm^{-1} and 954 cm^{-1} are due to C-C and C-O stretching of deoxyribose; the peak at 1168 cm^{-1} is related to the C-O stretching of the C-OH groups of serine, threosine and tyrosine of proteins and hydrogen-bonded stretching of the C-OH groups, this is a C-O stretching band only present in normal tissues; two peaks associated to C-O and C-C stretching and C-O-H deformation of the glycogen at 1149 cm^{-1} and 1024 cm^{-1}; the peak at 1116 cm^{-1} is due to symmetric P-O-C stretching, as there is another peak with the same assignment and related to the opposite group in the positive side of PC2 (1108 cm^{-1}), these to peaks do not seem to justify the formation of the groups; finally the peak at 1092 cm^{-1} related to symmetric PO^{2-} stretching of phosphate II, symmetric PO^{2-} stretching of RNA and DNA and symmetric stretching of phosphate groups in phospholipids. (164, 192)

The positive side of PC2 in the PCA scores suggest the formation of the group of PCa samples, gPCa, which includes the samples T1, T2, T3, T4, T5, T6 and T7. The distribution of the gPCa is justified by ten peaks identified in the PCA loadings (1173, 1156, 1128, 1108, 1080, 1060, 1045,

1030, 964 and 934 cm^{-1}). The peak at 1173 cm^{-1} is a C-O stretching band only present in malignant tissues. The peak at 1156 cm^{-1} is due to C-O stretching of proteins and carbohydrates and the peak at 1128 cm^{-1} is due to symmetric phosphodiester stretching of RNA. The already refereed peak at 1108 cm^{-1} is related to symmetric P-O-C stretching. The peaks 1080, 1060 and 1030 cm^{-1} are the triad peaks of nucleic acids; the first one is related to symmetric PO^{2-} stretching of RNA and DNA (phosphate I in RNA), the second is due to C-O stretching of deoxyribose and the last one is due to C-O stretching coupled with C-O bending. The peak at 1045 cm^{-1} is a glycogen band and is related to C-O stretching coupled with C-O bending frequencies of the C-OH groups of carbohydrates. The peak at 964 cm^{-1} is a band characteristic of malignant tissues and is due to C-C and C-O stretching in deoxyribose of DNA. Finally, the peak at 934 cm^{-1} is related to the left-handed helix of the DNA.(164, 192)

It has been previously suggested by other authors that the glycogen content can be used to differentiate benign from malignant tissues.(201, 204) Cancer cells have a high metabolic turnover and use up all the glucose for their fast replication. Thus, there is no storage of excess glucose as glycogen and lower glycogen content is characteristic of malignant tissues in comparison to normal tissues.(204) The identification in the PCA loadings of two glycogen bands at 1149 cm^{-1} and 1024 cm^{-1} associated with the gC and of only one glycogen band at 1045 cm^{-1} associated with the gPCa support this hypothesis, suggesting a higher glycogen content in the control samples than in the PCa samples.

Furthermore, in cancer cells, the nuclear compaction reduces due to decrease in hydrogen bonding in DNA, leading to increased nucleus/ cytoplasm ratio.(204) The identified band at 1080 cm^{-1}, due to symmetric PO^{2-} stretching of RNA and DNA, characterized the gPCa (positive side of PC2) and is a band that suggests this increase in the nucleic acids in malignant tissues.

Out of pattern sample T8: The sample T8 is included in the gC and is a PCa sample of a patient with a less aggressive tumour. Its location in the gC may indicate that the identified alterations characteristics of the gPCa are not yet present in this patient.

The control sample C5 is again included in the gPCa. Its localization again close to the PCa samples intensify the possibility of errors in the sample collection, which lead to the collection of PCa tissue along with the collection of the normal prostate tissue for this control sample.

Mid-IR region 1800-1700 cm^{-1}

The region 1800-1700 cm^{-1} corresponds to the region of the fatty acid esters. Also includes the range 1715-1700 cm^{-1}, which corresponds to the region of the bases.(164) PCA was applied to this specific region also to test again the hypothesis of a lipid disorder, but mostly to explore the observances of the direct spectral analysis that highlight a band near 1750 cm^{-1}, related to C=O stretching, which is more intense in the PCa spectra and its higher intensity is much more evident in the spectra of patients with more aggressive tumours - see Figure 19.

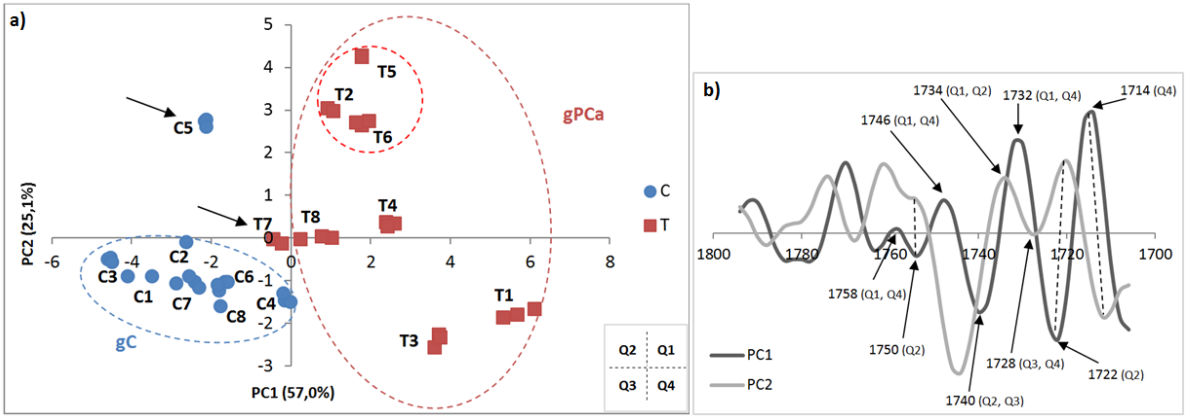

Figure 19 PCA scores (a) and loadings (b) of control and PCa samples at 1800-1700 cm^{-1} range.

Based on the distribution of the samples along PC1, which explains most of the variability, two main groups may be identified. However, PC2, which explains about 25% of the variability, also seems to affect the samples distribution, mainly the positive side of PC2 that seems to explain the distribution of the three PCa samples T2, T5 and T6 distributed in Q1 and the control sample C5 distributed in Q2 – see Figure 19a. Therefore, in a first analysis the examination of the PCA loadings was only based on the PC1 distribution to form the two main groups. After this first interpretation another one based on the PC2 distribution was made.

Based on the distribution of the samples along PC1, one group of only PCa samples (gPCa) can be observed, which is mainly explained by the positive side of PC1 and located in Q1 and Q4. The other group is constituted with only control samples (gC) and is mainly explained by the negative side of PC1 and distributed in Q2 and Q3. The PCa sample T7 are not included in any group as it is distributed close to zero of both PCs, which indicates it is not affected by the peaks identified in PCA loadings. Noticed that the control sample C5, despite being on the negative side of PC1 as all control samples, it is located alone in Q2 and not close to the other control samples. The assignments of the PC1 peaks selected in the PCA loadings (Figure 19b) are shown in Table 11.

Bands (cm^{-1})	PC1	Assignments	Group
~1758	+	C=C stretching of lipids and fatty acids	gPCa
~1750	-	Ester C=O stretching of triglycerides, C=O stretching of polysaccharides	gC
~1746	+	C=O stretching of lipids, Ester C=O stretching of phospholipids	gPCa
~1740	-	C=O stretching of polysaccharides	gC
~1732	+	C=O stretching of the fatty acid ester band	gPCa
~1722	-	C=O stretching	gC
~1714	+	C=O stretching of DNA and RNA, C=O stretching of purine base, C=O stretching of thymine	gPCa

Table 11 Mid-IR bands at range 1800-1700 cm^{-1} identified in PCA loadings, only based in PC1 distribution.(164, 192, 194)

In the region 1800-1700 cm^{-1} all the control samples are in the negative side of PC1 in the PCA scores, forming a group, gC, whose distribution is explained by three peaks in the PCA loadings – see Table 11. The peak at 1750 cm^{-1} due to ester C=O stretching of triglycerides and C=O stretching of polysaccharides and the peak at 1740 cm^{-1} also due to C=O stretching of

polysaccharides. The peak at 1722 cm^{-1} is an unspecific peak related to the C=O stretching vibration characteristic of this region.(164, 192)
The analysis of the PCA scores also showed that all the PCa samples form a group, gPCa, mainly explained by the positive side of PC1. Four peaks identify in the PCA loadings justify the formation of this group: the peak at 1758 cm^{-1} due to C=C stretching of lipids and fatty acids; the peak at 1746 cm^{-1} due to C=O stretching of lipids and ester C=O stretching of phospholipids; the peak at 1732 cm^{-1} due to the C=O stretching of the fatty acid ester band; and finally the peak at 1714 cm^{-1} related to C=O stretching of DNA and RNA, C=O stretching of purine base and C=O stretching of thymine.(164, 192)

The role of lipid metabolism has gained particular interest in prostate cancer research. Many studies have already outlined the unique upregulation of de novo lipid synthesis in prostate cancer.(205-207) Besides the lipogenic phenotype, there is also a metabolic shift in which cancer cells use alternative enzymes and pathways to facilitate the production of fatty acids. The new synthesized lipids can support a number of cellular processes to promote cancer cell proliferation and survival.(205)
Cancer cells are characterized by a large number of metabolic alterations and the shift from catabolic to anabolic metabolism is a hallmark of cancer cells. Normally, by the catabolic pathway, each molecule of glucose consumed by a cell is metabolized through glycolysis to two molecules of pyruvate. Pyruvate is then converted to acetyl-CoA in the mitochondria where it enters the tricarboxylic acid (TCA) cycle to produce redox substrates for oxidative phosphorylation. In cancer cells a unique phenomenon of aerobic glycolysis occurs, whereby they consume a large quantity of glucose, metabolize it via glycolysis, and release the majority as lactic acid into the extracellular space, under normal oxygen conditions.(206, 207)
Therefore, cancer cells seem to consume an excessive quantity of glucose. They utilize it catabolically but also anabolically, whereby the carbons are used as a source to synthesize and fulfil the macromolecular demand of their proliferative phenotype.(205) Thus, lower polysaccharide (glucose) content is expected in malignant tissues. The identified peaks at 1750 cm^{-1} and 1740 cm^{-1}, due to C=O stretching of polysaccharides, characterized the gC (negative side of PC1) and suggest this higher polysaccharide content in the control samples in comparison to the PCa samples.

Furthermore, with the exception of brain, liver, adipose and lung tissues, fatty acid synthesis in normal and differentiated adult cells is relatively low. In the other tissue types, cells utilize circulating fatty acids derived from dietary sources to fulfil their fatty acid requirements. However, it is now recognized that cancer cells exhibit increased production of de novo fatty acids. Because of the fast division of cancer cells, one major purpose for increased fatty acid synthesis is to supply the heavy demand for new membrane biogenesis.(205, 207) Swinnen et al. already demonstrated that de novo fatty acids used for membrane biogenesis also preferentially localize in the membrane's signaling raft domains. Thus, de novo fatty acids may play a significant role in propagating oncogenic signals from the plasma membrane.(205)
The peak at 1758 cm^{-1} due to C=C stretching of lipids and fatty acids and the peak at 1732 cm^{-1} due to the C=O stretching of the fatty acid ester band, which characterized the gPCa (positive side of PC1), suggest an increased content in fatty acids in the PCa samples.

Out of pattern patient T7: the PCa sample T7 is not included in any group and as it is distributed close to zero of both PCs, it is not affected by the peaks identified in PCA loadings. Accordingly to the sample histopathological information the patient number 7 is the only one with an Eco showing benign prostatic hyperplasia (BPH). Also this patient initiated 3 months before surgery an androgen deprivation therapy (Casodex). These characteristics may have affected the tumour tissue content and cause the out of pattern distribution of this sample.

With the attempt to characterize the three samples T2, T5 and T6 and the control sample C5, the PC2 peaks selected in the PCA loadings (Figure 19b) were assigned and are presented in Table 12.

Bands (cm^{-1})	PC2	**Assignments**
~1750	+	Ester C=O stretching of triglycerides; C=O stretching of polysaccharides
~1734	+	Fatty acid ester band
~1728	-	C=O band
~1722	+	C=O stretching
~1714	-	C=O stretching of DNA and RNA, C=O stretching of purine base, C=O stretching of thymine

Table 12 Mid-IR bands at range 1800-1700 cm^{-1} identified in PCA loadings, only based in PC2 distribution.(164, 192, 194)

Based in the PC2 distribution, three peaks characterizing the group T2, T5, T6 and the sample C5 (positive side of PC2) can be identified in the PCA loadings: the peak at 1750 cm^{-1} due to ester C=O stretching of triglycerides and C=O stretching of polysaccharides, the peak at 1734 cm^{-1} related to the fatty acid ester band and the unspecific peak at 1722 cm^{-1} related to C=O stretching.(164) Unfortunately, this new PCA analysis of the PC2 distribution do not give much more new information to the characterization of the group T2, T5 and T6, which accordingly to the sample histopathological information are the three more aggressive tumours.

Out of pattern sample C5: peaks at 1750 cm^{-1} and 1722 cm^{-1} present in PC2+ are also present in the negative side of PC1, thus, they seem to be more related to the distribution of the sample C5 – see Table 12. The sample C5 has always behaved as an out of pattern sample in the previous PCA analysis performed in this study. Therefore, besides the identified peaks do not helped much in the characterization of this sample, there is a strong possibility that this is actually a sample of PCa tissue from the patient number 5, and not a sample of normal prostate tissue. Accordingly to the histopathological information the tumour of the patient number 5 is extremely aggressive, occupying large part of the prostate, thus, it is highly possible that a less developed part of the tumour was collected as being normal prostate tissue of the patient.

Another PCA analysis at the range 1800-1700 cm^{-1} was performed **without the samples T2, T5 and T6**. This analysis was performed in order to test if the contribution of this group of patients with more aggressive tumours were somehow affecting the others samples distribution and therefore masking some important characteristics. The PCA results are shown in Figure 20.

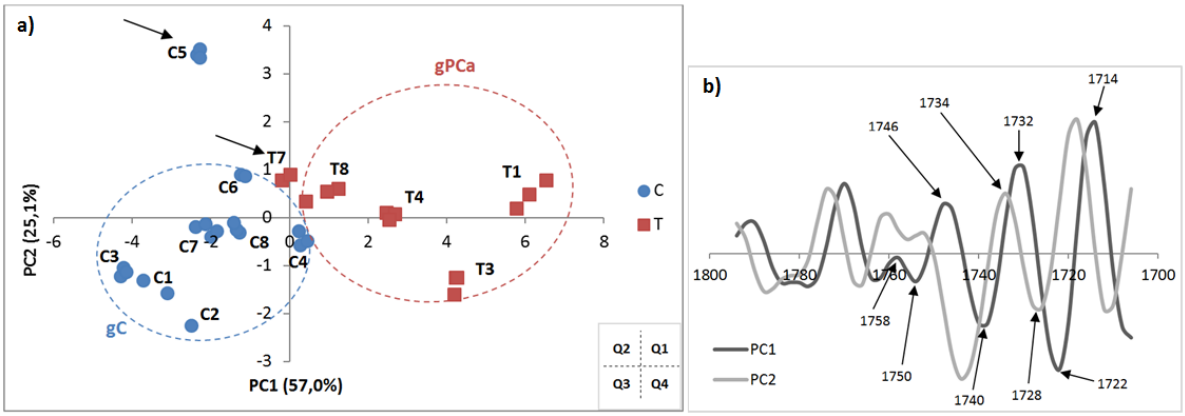

Figure 20 PCA scores (a) and loadings (b) of control and PCa samples at 1800-1700 cm^{-1} range (without T2, T5 and T6)

With this new analysis is possible to identify again the two initially proposed groups (gPCa and gC). The disposition of both groups was not affected, as the distribution of the PCa samples (gPCa) is still explained by the positive side of PC1 and located in Q1 and Q4; and the distribution of the control samples still mainly explained by the negative side of PC1 and distributed in Q2 and Q3. The PCa sample T7 still not being included in any group and the control C5 still located in Q2, distant from the other control samples. The loadings profile remains the same and the distribution of both groups still justified by the same peaks already analyzed above. Therefore, we can conclude that the PCa samples T2, T5 and T6 were not significantly affecting the other samples distribution at the range 1800-1700 cm^{-1}.

Finally, another **PCA analysis of only PCa samples** was also performed at the range 1800-1700 cm^{1}, with the attempt to classify and characterize the PCa samples, taking in account the clinical and histopathological information about the patients – see Table 6, chapter 2. The PCA results are shown in Figure 21.

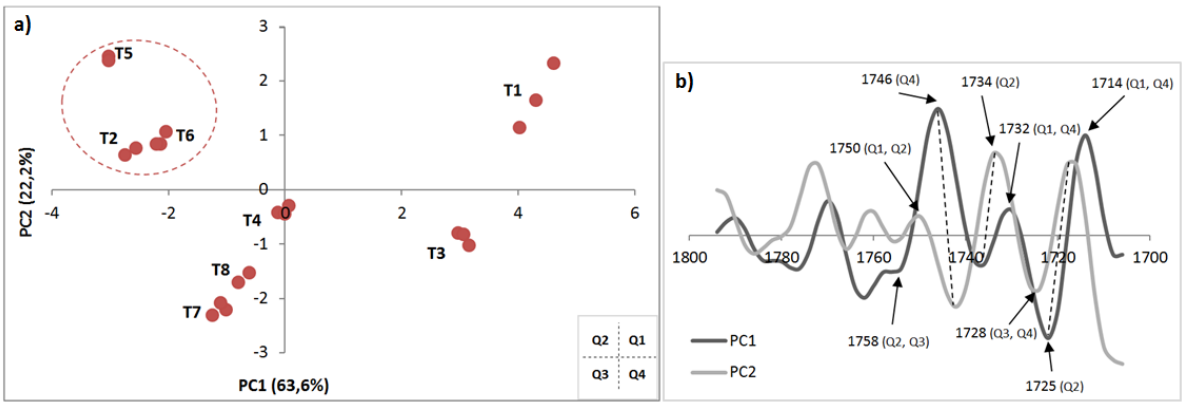

Figure 21 PCA scores (a) and loadings (b) of the PCa samples at 1800-1700 cm^{-1} range.

In a first analysis of the PCA scores the distribution of the samples T2, T5 and T6 alone in Q2, being explained by the negative side of PC1 and the positive side of PC2, is highlighted. The assignments of the peaks selected in the PCA loadings (Figure 21b) are shown in Table 13.

Bands (cm^{-1})	PC1	PC2	Assignments
~1758	-	+ -	C=C stretching of lipids and fatty acids
~1750	+ -	+	Ester group C=O stretching of triglycerides; C=O stretching of polysaccharides
~1746	+	-	C=O stretching of lipids, Ester C=O stretching of phospholipids
~1734	-	+	Fatty acid ester band
~1732	+	+ -	C=O stretching
~1728	+ -	-	C=O band
~1725	-	+	C=O stretching of the fatty acid ester band
~1714	+	+ -	C=O stretching of DNA and RNA, C=O stretching of purine base, C=O stretching of thymine

Table 13 Mid-IR bands at range 1800-1700 cm^{-1} identified in PCA loadings of the PCa samples.(164, 192, 194)

Two peaks identified in the PCA loadings can unequivocally characterize the samples T2, T5 and T6: the peak at 1734 cm^{-1} related to the fatty acid ester band and the peak at 1725 cm^{-1} due to C=O stretching of the fatty acid ester band.(164)

This PCA analysis of only PCa samples support the hypothesis of a lipid disorder characteristic of PCa tissue samples. Furthermore, the two peaks that explained the distribution of the samples T2, T5 and T6 suggest an increased content in fatty acids in these PCa samples, which may indicate that these more aggressive tumours have a more demanding proliferation rate and, therefore, require more *de novo* synthesis of fatty acids in comparison to the samples of patients with less aggressive tumours (T3, T7, T8).
However, the results of the PCA analysis of only PCa samples at the range 1800-1700 cm^{-1} do not give enough information and an in-depth classification of the PCa samples has not been possible.

F. Conclusions

With the direct analysis of the spectra the main bands of the spectra of control and PCa samples between 4000-600 cm^{-1} were assigned. This analysis shows some distinction between control and more aggressive PCa samples, as it allows the identification of perceptive differences between the spectra, mainly in the lipid region. Thereby, besides not being sufficient to distinguish the spectra of control samples from the spectra of PCa samples, the direct spectral interpretation suggested some important hypothesis about spectral regions and compounds that orientate and support the multivariate analysis. The complexity associated to biological tissues, which lead to the overlap of important bands in the IR spectra, along with the highly dimensional data of this study, makes mandatory that an appropriate multivariate analysis was performed.

The multivariate analysis reveals important differences between control and PCa samples. The PCA analysis of three spectral regions (3000-2800 cm^{-1}, 1200-900 cm^{-1}, 1800-1700 cm^{-1}) suggested the formation of two groups, a group of control samples and a group of PCa samples, according to the biochemical modifications characteristics of each region. The analysis of the PCA loadings profiles of the three regions propose that prostate cancer tissues can be probably identify and distinguished from normal prostate tissues based on dysregulations in lipid metabolism, mainly a higher content in fatty acids and an increased disorder of the chains of membrane lipids. Also a lower polysaccharide (glucose) and glycogen content and an increase in the nucleic acids seem to characterize the PCa tissues, which are pathologic findings expected in malignant tissues.
The attempt to classify and distinct between PCa tissues has not been accomplished, as the small sample size do not give enough information and an in-depth classification has not been possible.

The best FTIR conditions for the analysis of tissues have been established: spectra was acquired in the 4000 to 900 cm^{-1} range at 8 cm^{-1} resolution with 64 co-added scans at a room temperature of ± 25ºC and humidity ± 37%. No tissue preparation or fixation influenced the procedure, the radical prostatectomy specimens stored at -80ºC were thawed at room temperature and placed onto the crystal, fully covering it, and during the spectral acquisition all the samples experienced the same constant pressure, increasing the adhesion to the crystal and decreasing the spectral artifacts. The tissue drying was performed by allowing water to evaporate from the sample with the acquisition of six spectra (replicas) for each tissue sample and the three last replicas, which have reached the maximum drying stage, were the ones used in the multivariate analysis. Radical prostatectomy pieces have been identified as a potential gold standard specimen for FTIR prostate tissue analysis.

The biological relevance of the results has been affected by the small sample size; however, there is no doubt that this pilot study served as a first step to caught the attention and the interest for further confirmatory investigations in the future. Prostate cancer diagnostic strategies must evolve and FTIR has clearly demonstrated in this study that it is a powerful bioanalytical technique which when associated with appropriate statistical data analysis methods, such as different multivariate analysis techniques, has the ability to discriminate prostate cancer tissue from normal prostate tissue. The FTIR analysis has proved to be robust and versatile and can enable moving toward diagnosing neoplastic changes at progressively earlier stages. Furthermore, this

pilot study reveals the potential of FTIR to be used as a pathology laboratory tool as it seems to be an ideal diagnostic test that would provide rapid, non-invasive diagnosis at the point-of-care with high throughput and without prior tissue processing.

G. Limitations and Future Remarks

The promising findings of this pilot study merited further investigation of FTIR in tissue studies and it is clear that the challenges of achieving a universal FTIR classification model are significant. A thorough understanding of how FTIR may discriminate between prostate tissues is still necessary to judge its clinical niche and thus requires an increase in the sample size to continue.

The prostate tissue characterization based on the histopathology is subjective, which makes the diagnosis of prostate cancer in individual patients to be problematic. This subjectivity associated with the histopathological sample characterization along with the possibility of sampling errors, may have restricted and awry orientate this study. Furthermore, prostate tissue is characteristically heterogeneous which may have led to the overlap of important FTIR absorptions and masked important biochemical changes of the spectral dataset. Therefore, future experiments validated with an independent and unequivocally classified data set are necessary to deeply understand and identify the molecular changes that may precede the morphological changes, thus enabling earlier diagnosis of prostate cancer. Also a closer approach to analyse specific molecules demonstrated to be associated with prostate cancer, such as fatty acids and glycogen, should be conducted. The results could be supplement with more specific metabolomics techniques, such as Mass Spectrometry or Tissue Microarrays.

In order to further enhance the credibility of FTIR analysis and its potential for automation, the next challenge is to pursue future investigations with the attempt to create a FTIR spectral and biochemical representation of a whole prostate, including all the pathology contained within the specimen. It could be possible with the association of a microscope to the FTIR equipment. The application of vibrational microspectroscopy will enable fine detail analysis of prostate tissue allowing new investigations, such as the correlation of the FTIR spectra of prostate tissue with Gleason score and clinical stage of the PCa at the time of biopsy.

H. References

1. Amin M, Khalid A, Tazeen N, Yasoob M. Zonal Anatomy of Prostate. Annals of King Edward Medical University. 2011;16(3).
2. Hammerich KH, Ayala GE, Wheeler TM. Anatomy of the prostate gland and surgical pathology of prostate cancer. Cambridge University, Cambridge. 2009:1-10.
3. Moore KL. Clinically oriented anatomy: Lippincott Williams & Wilkins; 2013.
4. Moore KL, Agur AM, Dalley AF. Essential clinical anatomy: Lippincott Williams & Wilkins Philadelphia; 2011.
5. Winslow T. Prostate Anatomy. 2005; Medical and Scientific Illustration]. Available from: www.teresewinslow.com.
6. Harvey C, Pilcher J, Richenberg J, Patel U, Frauscher F. Applications of transrectal ultrasound in prostate cancer. British Journal of Radiology. 2012;85(Special Issue 1):S3-S17.
7. McNeal JE. The zonal anatomy of the prostate. The Prostate. 1981;2(1):35-49.
8. McNeal JE. Normal histology of the prostate. The American journal of surgical pathology. 1988;12(8):619.
9. McLaughlin PW, Troyer S, Berri S, Narayana V, Meirowitz A, Roberson PL, et al. Functional anatomy of the prostate: implications for treatment planning. International Journal of Radiation Oncology, Biology and Physics. 2005;63(2).
10. McNeal J. Regional morphology and pathology of the prostate. American journal of clinical pathology. 1968;49(3):347.
11. McNeal J, Price H, Redwine E, Freiha F, Stamey T. Stage A versus stage B adenocarcinoma of the prostate: morphological comparison and biological significance. The Journal of urology. 1988;139(1):61.
12. Cancer Research UK (2008). Prostate Cancer Incidence Statistics: In Europe and worldwide - 2008. http://www.cancerresearchuk.org
13. International Agency for Research on Cancer. GLOBOCAN 2008 database: Cancer Incidence, Mortality and Prevalence Worldwide in 2008. http://globocan.iarc.fr
14. Jemal A, Siegel R, Ward E, Murray T, Xu J, Smigal C, et al. Cancer statistics, 2006. CA: a cancer journal for clinicians. 2006;56(2):106-30.
15. Pinheiro P, Tyczyński J, Bray F, Amado J, Matos E, Parkin D. Cancer incidence and mortality in Portugal. European Journal of Cancer. 2003;39(17):2507-20.
16. Potter SR, Horniger W, Tinzl M, Bartsch G, Partin AW. Age, prostate-specific antigen, and digital rectal examination as determinants of the probability of having prostate cancer. Urology. 2001;57(6):1100-4.
17. Steinberg GD, Carter BS, Beaty TH, Childs B, Walsh PC. Family history and the risk of prostate cancer. The Prostate. 1990;17(4):337-47.
18. Johns L, Houlston R. A systematic review and meta-analysis of familial prostate cancer risk. BJU international. 2003;91(9):789-94.
19. Kheirandish P, Chinegwundoh F. Ethnic differences in prostate cancer. British journal of cancer. 2011;105(4):481-5.
20. Allen NE, Appleby PN, Roddam AW, Tjønneland A, Johnsen NF, Overvad K, et al. Plasma selenium concentration and prostate cancer risk: results from the European Prospective Investigation into Cancer and Nutrition (EPIC). The American journal of clinical nutrition. 2008;88(6):1567-75.
21. Key TJ, Appleby PN, Allen NE, Travis RC, Roddam AW, Jenab M, et al. Plasma carotenoids, retinol, and tocopherols and the risk of prostate cancer in the European Prospective Investigation into Cancer and Nutrition study. The American journal of clinical nutrition. 2007;86(3):672-81.
22. Allen NE, Key TJ, Appleby PN, Travis RC, Roddam AW, Rinaldi S, et al. Serum insulin-like growth factor (IGF)-I and IGF-binding protein-3 concentrations and prostate cancer risk: results

from the European Prospective Investigation into Cancer and Nutrition. Cancer Epidemiology Biomarkers & Prevention. 2007;16(6):1121-7.
23. Heinlein CA, Chang C. Androgen receptor in prostate cancer. Endocrine reviews. 2004;25(2):276-308.
24. Lee H-J, Chang C. Recent advances in androgen receptor action. Cellular and Molecular Life Sciences CMLS. 2003;60(8):1613-22.
25. Saraon P, Jarvi K, Diamandis EP. Molecular alterations during progression of prostate cancer to androgen independence. Clinical chemistry. 2011;57(10):1366-75.
26. Taplin M-E. Androgen receptor: role and novel therapeutic prospects in prostate cancer. 2008.
27. Taplin ME, Balk SP. Androgen receptor: a key molecule in the progression of prostate cancer to hormone independence. Journal of cellular biochemistry. 2004;91(3):483-190.
28. Lin H-K, Hu Y-C, Yang L, Altuwaijri S, Chen Y-T, Kang H-Y, et al. Suppression versus induction of androgen receptor functions by the phosphatidylinositol 3-kinase/Akt pathway in prostate cancer LNCaP cells with different passage numbers. Journal of Biological Chemistry. 2003;278(51):50902-7.
29. Lavery DN, Bevan CL. Androgen receptor signalling in prostate cancer: the functional consequences of acetylation. Journal of Biomedicine and Biotechnology. 2010;2011.
30. Edwards J, Bartlett J. The androgen receptor and signal-transduction pathways in hormone-refractory prostate cancer. Part 2: androgen-receptor cofactors and bypass pathways. BJU international. 2005;95(9):1327-35.
31. Lattouf J-B, Srinivasan R, Pinto PA, Linehan WM, Neckers L. Mechanisms of disease: the role of heat-shock protein 90 in genitourinary malignancy. Nature Clinical Practice Urology. 2006;3(11):590-601.
32. Gleason DF. Histologic grading of prostate cancer: a perspective. Human pathology. 1992;23(3):273-9.
33. Egevad L, Allsbrook Jr WC, Epstein JI. Current practice of Gleason grading among genitourinary pathologists. Human pathology. 2005;36(1):5-9.
34. Oyama T, Allsbrook Jr WC, Kurokawa K, Matsuda H, Segawa A, Sano T, et al. A comparison of interobserver reproducibility of Gleason grading of prostatic carcinoma in Japan and the United States. Archives of pathology & laboratory medicine. 2005;129(8):1004-10.
35. Kronz JD, Silberman MA, Allsbrook WC, Epstein JI. A web-based tutorial improves practicing pathologists' Gleason grading of images of prostate carcinoma specimens obtained by needle biopsy. Cancer. 2000;89(8):1818-23.
36. Mikami Y, Manabe T, Epstein JI, Shiraishi T, Furusato M, Tsuzuki T, et al. Accuracy of Gleason grading by practicing pathologists and the impact of education on improving agreement. Human pathology. 2003;34(7):658-65.
37. Mulay K, Swain M, Jaiman S, Gowrishankar S. Gleason scoring of prostatic carcinoma: impact of a web-based tutorial on inter-and intra-observer variability. Indian Journal of Pathology and Microbiology. 2008;51(1):22.
38. Garnick MB. Prostate cancer: screening, diagnosis, and management. Annals of Internal Medicine. 1993;118(10):804-18.
39. Heyns C, Naude A, Visser A, Marais D, Stopforth H, Nyarko J, et al. Early diagnosis of prostate cancer in the Western Cape. 2001.
40. Tenke P, Horti J, Balint P, Kovacs B. Prostate cancer screening. Prostate Cancer. 2007:65-81.
41. Brawer MK. The diagnosis of prostatic carcinoma. Cancer. 1993;71(S3):899-905.
42. Humphrey P, Andriole G. Prostate cancer diagnosis. Missouri medicine. 2010;107(2):107.
43. Catalona W, Richie J, Ahmann F, Hudson M, Scardino P, Flanigan R, et al. Comparison of digital rectal examination and serum prostate specific antigen in the early detection of prostate

cancer: results of a multicenter clinical trial of 6,630 men. The Journal of urology. 1994;151(5):1283.
44. Ellis W, Chetner M, Preston S, Brawer M. Diagnosis of prostatic carcinoma: the yield of serum prostate specific antigen, digital rectal examination and transrectal ultrasonography. The Journal of urology. 1994;152(5 Pt 1):1520.
45. Jewett HJ. Significance of the palpable prostatic nodule. Journal of the American Medical Association. 1956;160(10):838-9.
46. ALSIKAFI NF, BRENDLER CB. Surgical modifications of radical retropubic prostatectomy to decrease incidence of positive surgical margins. The Journal of urology. 1998;159(4):1281-5.
47. Malavaud B, Villers A, Ravery V, Tollon C, Rischmann P, Charlet J-P, et al. Role of Preoperative Positive Apical Biopsies in the Prediction of Specimen–Confined Prostate Cancer after Radical Retropubic Prostatectomy: A Multi–Institutional Study. European urology. 2000;37(3):281-8.
48. Lodding P, Aus G, Bergdahl S, Frösing R, Lilja H, Pihl C-G, et al. Characteristics of screening detected prostate cancer in men 50 to 66 years old with 3 to 4 ng./ml. prostate specific antigen. The Journal of urology. 1998;159(3):899-903.
49. Partin A, Yoo J, Carter HB, Pearson J, Chan D, Epstein J, et al. The use of prostate specific antigen, clinical stage and Gleason score to predict pathological stage in men with localized prostate cancer. The Journal of urology. 1993;150(1):110-4.
50. Rao AR, Motiwala HG, Karim O. The discovery of prostate-specific antigen. BJU international. 2008;101(1):5-10.
51. Segawa N, Gohji K, Iwamoto Y, Ueda H, Katsuoka Y. Prostate cancer detection by prostate-specific antigen-related parameters. Hinyokika kiyo Acta urologica Japonica. 2003;49(7):405-10. Epub 2003/09/13.
52. Wang M, Valenzuela L, Murphy G, Chu T. Purification of a human prostate specific antigen. The Journal of urology. 2002;167(2):960-4.
53. Kirby R, Fitzpatrick J. Prostate-specific antigen testing for the early detection of prostate cancer. BJU international. 2004;94(7):966-7.
54. Donovan JL, Hamdy FC, Neal DE. Screening for prostate cancer. The case against. Annals of the Royal College of Surgeons of England. 2005;87(2):90.
55. Kirby RS, Fitzpatrick JM, Irani J. Prostate cancer diagnosis in the new millennium: strengths and weaknesses of prostate-specific antigen and the discovery and clinical evaluation of prostate cancer gene 3 (PCA3). BJU international. 2009;103(4):441-5.
56. Brawer MK. Prostate-specific antigen: Current status. CA: a cancer journal for clinicians. 1999;49(5):264-81.
57. Catalona WJ, Smith DS, Ornstein DK. Prostate cancer detection in men with serum PSA concentrations of 2.6 to 4.0 ng/mL and benign prostate examination. JAMA: the journal of the American Medical Association. 1997;277(18):1452-5.
58. Stenman U-H, Abrahamsson P-A, Aus G, Lilja H, Bangma C, Hamdy FC, et al. Prognostic value of serum markers for prostate cancer. Scandinavian journal of urology and nephrology. 2005;39(S216):64-81.
59. de la Taille A, Katz A, Bagiella E, Olsson CA, O'Toole KM, Rubin MA. Perineural invasion on prostate needle biopsy: an independent predictor of final pathologic stage. Urology. 1999;54(6):1039-43.
60. ORNSTEIN DK, SMITH DS, HUMPHREY PA, CATALONA WJ. The effect of prostate volume, age, total prostate specific antigen level and acute inflammation on the percentage of free serum prostate specific antigen levels in men without clinically detectable prostate cancer. The Journal of urology. 1998;159(4):1234-7.

61. Yuan J, Coplen D, Petros J, Figenshau R, Ratliff T, Smith D, et al. Effects of rectal examination, prostatic massage, ultrasonography and needle biopsy on serum prostate specific antigen levels. The Journal of urology. 1992;147(3 Pt 2):810.
62. Guess HA, Heyse JF, Gormley GJ, Stoner E, Oesterling JE. Effect of finasteride on serum PSA concentration in men with benign prostatic hyperplasia. Results from the North American phase III clinical trial. The Urologic clinics of North America. 1993;20(4):627.
63. Partin AW, Kattan MW, Subong EN, Walsh PC, Wojno KJ, Oesterling JE, et al. Combination of prostate-specific antigen, clinical stage, and Gleason score to predict pathological stage of localized prostate cancer. JAMA: the journal of the American Medical Association. 1997;277(18):1445-51.
64. Brössner C, Bayer G, Madersbacher S, Kuber W, Klingler C, Pycha A. Twelve prostate biopsies detect significant cancer volumes (> 0.5 mL). BJU international. 2000;85(6):705-7.
65. Presti Jr J, Chang JJ, Bhargava V, Shinohara K. The optimal systematic prostate biopsy scheme should include 8 rather than 6 biopsies: results of a prospective clinical trial. The Journal of urology. 2000;163(1):163.
66. Aus G, Damber J-E, Khatami A, Lilja H, Stranne J, Hugosson J. Individualized screening interval for prostate cancer based on prostate-specific antigen level: results of a prospective, randomized, population-based study. Archives of internal medicine. 2005;165(16):1857.
67. Hessels D, Verhaegh GW, Schalken JA, Witjes JA. Applicability of biomarkers in the early diagnosis of prostate cancer. Expert review of molecular diagnostics. 2004;4(4):513-26.
68. Pelzer AE, Tewari A, Bektic J, Berger AP, Frauscher F, Bartsch G, et al. Detection rates and biologic significance of prostate cancer with PSA less than 4.0 ng/mL: observation and clinical implications from Tyrol screening project. Urology. 2005;66(5):1029-33.
69. Thompson IM, Ankerst DP, Chi C, Lucia MS, Goodman PJ, Crowley JJ, et al. Operating characteristics of prostate-specific antigen in men with an initial PSA level of 3.0 ng/ml or lower. JAMA: the journal of the American Medical Association. 2005;294(1):66-70.
70. Lilja H. Significance of different molecular forms of serum PSA. The free, noncomplexed form of PSA versus that complexed to alpha 1-antichymotrypsin. The Urologic clinics of North America. 1993;20(4):681.
71. Clements J, Merritt T, Devoss K, Swanson C, Hamlyn L, Scells B, et al. Inactive free: total prostate specific antigen ratios in ejaculate from men with suspected and known prostate cancer, compared with young control men. BJU international. 2000;86(4):453-8.
72. Sävblom C, Malm J, Giwercman A, Nilsson JÅ, Berglund G, Lilja H. Blood levels of free-PSA but not complex-PSA significantly correlates to prostate release of PSA in semen in young men, while blood levels of complex-PSA, but not free-PSA increase with age. The Prostate. 2005;65(1):66-72.
73. Carter HB, Pearson JD. PSA velocity for the diagnosis of early prostate cancer. A new concept. The Urologic clinics of North America. 1993;20(4):665.
74. Saema A, Kochakarn W, Lertsithichai P. PSA density and prostate cancer detection. Journal of the Medical Association of Thailand= Chotmaihet thangphaet. 2012;95(5):661.
75. Seaman E, Whang M, Olsson CA, Katz A, Cooner WH, Benson MC. PSA density (PSAD). Role in patient evaluation and management. The Urologic clinics of North America. 1993;20(4):653.
76. Sheikh M, Al-Saeed O, Kehinde E, Sinan T, Anim J, Ali Y. Utility of volume adjusted prostate specific antigen density in the diagnosis of prostate cancer in Arab men. International urology and nephrology. 2005;37(4):721-6.
77. Thompson IM, Pauler DK, Goodman PJ, Tangen CM, Lucia MS, Parnes HL, et al. Prevalence of prostate cancer among men with a prostate-specific antigen level≤ 4.0 ng per milliliter. New England Journal of Medicine. 2004;350(22):2239-46.

78. Quinn DI, Henshall SM, Sutherland RL. Molecular markers of prostate cancer outcome. European Journal of Cancer. 2005;41(6):858-87.
79. Kurek R, Nunez G, Tselis N, Konrad L, Martin T, Roeddiger S, et al. Prognostic value of combined "triple"-reverse transcription-PCR analysis for prostate-specific antigen, human kallikrein 2, and prostate-specific membrane antigen mRNA in peripheral blood and lymph nodes of prostate cancer patients. Clinical cancer research. 2004;10(17):5808-14.
80. Chiang C-H, Hong C-J, Chang Y-H, Chang LS, Chen K-K. Human kallikrein-2 gene polymorphism is associated with the occurrence of prostate cancer. The Journal of urology. 2005;173(2):429-32.
81. Lintula S, Stenman J, Bjartell A, Nordling S, Stenman UH. Relative concentrations of hK2/PSA mRNA in benign and malignant prostatic tissue. The Prostate. 2005;63(4):324-9.
82. Stephenson S-A, Verity K, Ashworth LK, Clements JA. Localization of a new prostate-specific antigen-related serine protease gene, KLK4, is evidence for an expanded human kallikrein gene family cluster on chromosome 19q13. 3–13.4. Journal of Biological Chemistry. 1999;274(33):23210-4.
83. Ang J, Lijovic M, Ashman LK, Kan K, Frauman AG. CD151 protein expression predicts the clinical outcome of low-grade primary prostate cancer better than histologic grading: a new prognostic indicator? Cancer Epidemiology Biomarkers & Prevention. 2004;13(11):1717-21.
84. Epstein JI, Amin M, Boccon-Gibod L, Egevad L, Humphrey PA, Mikuz G, et al. Prognostic factors and reporting of prostate carcinoma in radical prostatectomy and pelvic lymphadenectomy specimens. Scandinavian journal of urology and nephrology. 2005;39(S216):34-63.
85. Varambally S, Dhanasekaran SM, Zhou M, Barrette TR, Kumar-Sinha C, Sanda MG, et al. The polycomb group protein EZH2 is involved in progression of prostate cancer. nature. 2002;419(6907):624-9.
86. Foster CS, Falconer A, Dodson AR, Norman AR, Dennis N, Fletcher A, et al. Transcription factor E2F3 overexpressed in prostate cancer independently predicts clinical outcome. Oncogene. 2004;23(35):5871-9.
87. Chung L, Baseman A, Assikis V, Zhau HE. Molecular insights into prostate cancer progression: the missing link of tumor microenvironment. The Journal of urology. 2005;173(1):10.
88. Williams TM, Lisanti MP. Caveolin-1 in oncogenic transformation, cancer, and metastasis. American Journal of Physiology-Cell Physiology. 2005;288(3):C494-C506.
89. Yang G, Timme TL, Frolov A, Wheeler TM, Thompson TC. Combined c-Myc and caveolin-1 expression in human prostate carcinoma predicts prostate carcinoma progression. Cancer. 2005;103(6):1186-94.
90. Blancher C, Harris AL. The molecular basis of the hypoxia response pathway: tumour hypoxia as a therapy target. Cancer and Metastasis Reviews. 1998;17(2):187-94.
91. Hrouda D, Nicol D, Gardiner R. The role of angiogenesis in prostate development and the pathogenesis of prostate cancer. Urological research. 2003;30(6):347-55.
92. Chang S. Monoclonal antibodies and prostate-specific membrane antigen. Current opinion in investigational drugs (London, England: 2000). 2004;5(6):611.
93. Belldegrun A, Bander NH, Lerner SP, Wood DP, Pantuck AJ. Society of Urologic Oncology Biotechnology Forum: new approaches and targets for advanced prostate cancer. The Journal of urology. 2001;166(4):1316-21.
94. Chang SS, Reuter VE, Heston W, Bander NH, Grauer LS, Gaudin PB. Five different anti-prostate-specific membrane antigen (PSMA) antibodies confirm PSMA expression in tumor-associated neovasculature. Cancer research. 1999;59(13):3192-8.
95. Burger MJ, Tebay MA, Keith PA, Samaratunga HM, Clements J, Lavin MF, et al. Expression analysis of δ-catenin and prostate-specific membrane antigen: Their potential as diagnostic markers for prostate cancer. International journal of cancer. 2002;100(2):228-37.

96. Leek J, Lench N, Maraj B, Bailey A, Carr I, Andersen S, et al. Prostate-specific membrane antigen: evidence for the existence of a second related human gene. British journal of cancer. 1995;72(3):583.
97. Rajasekaran AK, Anilkumar G, Christiansen JJ. Is prostate-specific membrane antigen a multifunctional protein? American Journal of Physiology-Cell Physiology. 2005;288(5):C975-C81.
98. Landers KA, Burger MJ, Tebay MA, Purdie DM, Scells B, Samaratunga H, et al. Use of multiple biomarkers for a molecular diagnosis of prostate cancer. International journal of cancer. 2005;114(6):950-6.
99. Downing S, Russell P, Jackson P. Alterations of p53 are common in early stage prostate cancer. The Canadian journal of urology. 2003;10(4):1924.
100. Quinn DI, Henshall SM, Head DR, Golovsky D, Wilson JD, Brenner PC, et al. Prognostic significance of p53 nuclear accumulation in localized prostate cancer treated with radical prostatectomy. Cancer research. 2000;60(6):1585-94.
101. Augustin H, Hammerer PG, Graefen M, Palisaar J, Daghofer F, Huland H, et al. Characterisation of biomolecular profiles in primary high-grade prostate cancer treated by radical prostatectomy. Journal of cancer research and clinical oncology. 2003;129(11):662-8.
102. Rubio J, Ramos D, Lopez-Guerrero J, Iborra I, Collado A, Solsona E, et al. Immunohistochemical expression of Ki-67 antigen, cox-2 and Bax/Bcl-2 in prostate cancer; prognostic value in biopsies and radical prostatectomy specimens. European urology. 2005;48(5):745-51.
103. Kaur P, Kallakury BS, Sheehan CE, Fisher HA, Kaufman Jr RP, Ross JS. Survivin and Bcl-2 expression in prostatic adenocarcinomas. Archives of pathology & laboratory medicine. 2004;128(1):39-43.
104. TULUNAY Ö, Orhan D, BALTACI S, GÖĞÜŞ Ç, MÜFTÜOĞLU YZ. Prostatic ductal adenocarcinoma showing Bcl-2 expression. International journal of urology. 2004;11(9):805-8.
105. Rosser CJ, Reyes AO, Vakar-Lopez F, Levy LB, Kuban DA, Hoover DC, et al. Bcl-2 is significantly overexpressed in localized radio-recurrent prostate carcinoma, compared with localized radio-naive prostate carcinoma. International journal of radiation oncology, biology, physics. 2003;56(1):1-6.
106. Scaltriti M, Bettuzzi S, Sharrard R, Caporali A, Caccamo A, Maitland N. Clusterin overexpression in both malignant and nonmalignant prostate epithelial cells induces cell cycle arrest and apoptosis. British journal of cancer. 2004;91(10):1842-50.
107. Scaltriti M, Brausi M, Amorosi A, Caporali A, D'Arca D, Astancolle S, et al. Clusterin (SGP-2, ApoJ) expression is downregulated in low-and high-grade human prostate cancer. International journal of cancer. 2004;108(1):23-30.
108. GLEAVE M, JANSEN B. Clusterin and IGFBPs as antisense targets in prostate cancer. Annals of the New York Academy of Sciences. 2003;1002(1):95-104.
109. Caccamo A, Scaltriti M, Caporali A, D'Arca D, Corti A, Corvetta D, et al. Ca2+ depletion induces nuclear clusterin, a novel effector of apoptosis in immortalized human prostate cells. Cell Death & Differentiation. 2004;12(1):101-4.
110. Dhanasekaran SM, Barrette TR, Ghosh D, Shah R, Varambally S, Kurachi K, et al. Delineation of prognostic biomarkers in prostate cancer. nature. 2001;412(6849):822-6.
111. Srikantan V, Valladares M, Rhim JS, Moul JW, Srivastava S. HEPSIN inhibits cell growth/invasion in prostate cancer cells. Cancer research. 2002;62(23):6812-6.
112. Herter S, Piper DE, Aaron W, Gabriele T, Cutler G, Cao P, et al. Hepatocyte growth factor is a preferred in vitro substrate for human hepsin, a membrane-anchored serine protease implicated in prostate and ovarian cancers. Biochemical Journal. 2005;390(Pt 1):125.
113. Kirchhofer D, Peek M, Lipari MT, Billeci K, Fan B, Moran P. Hepsin activates pro-hepatocyte growth factor and is inhibited by hepatocyte growth factor activator inhibitor-1B (HAI-1B) and HAI-2. FEBS letters. 2005;579(9):1945-50.

114. Reiter RE, Gu Z, Watabe T, Thomas G, Szigeti K, Davis E, et al. Prostate stem cell antigen: a cell surface marker overexpressed in prostate cancer. Proceedings of the National Academy of Sciences. 1998;95(4):1735-40.
115. Zhigang Z, Wenlv S. Prostate stem cell antigen (PSCA) expression in human prostate cancer tissues and its potential role in prostate carcinogenesis and progression of prostate cancer. World Journal of Surgical Oncology. 2004;2(1):13.
116. Hara N, Kasahara T, Kawasaki T, Bilim V, Obara K, Takahashi K, et al. Reverse Transcription-Polymerase Chain Reaction Detection of Prostate-specific Antigen, Prostate-specific Membrane Antigen, and Prostate Stem Cell Antigen in One Milliliter of Peripheral Blood Value for the Staging of Prostate Cancer. Clinical cancer research. 2002;8(6):1794-9.
117. Han K-R, Seligson DB, Liu X, Horvath S, Shintaku PI, Thomas GV, et al. Prostate stem cell antigen expression is associated with gleason score, seminal vesicle invasion and capsular invasion in prostate cancer. The Journal of urology. 2004;171(3):1117-21.
118. de Kok JB, Verhaegh GW, Roelofs RW, Hessels D, Kiemeney LA, Aalders TW, et al. DD3PCA3, a very sensitive and specific marker to detect prostate tumors. Cancer research. 2002;62(9):2695-8.
119. Hessels D, Klein Gunnewiek JM, van Oort I, Karthaus HF, van Leenders GJ, van Balken B, et al. DD3< sup> PCA3</sup>-based Molecular Urine Analysis for the Diagnosis of Prostate Cancer. European urology. 2003;44(1):8-16.
120. Tinzl M, Marberger M, Horvath S, Chypre C. DD3< sup> PCA3</sup> RNA Analysis in Urine–A New Perspective for Detecting Prostate Cancer. European urology. 2004;46(2):182-7.
121. Fradet Y, Saad F, Aprikian A, Dessureault J, Elhilali M, Trudel C, et al. uPM3, a new molecular urine test for the detection of prostate cancer. Urology. 2004;64(2):311-5.
122. Commentary A. Prostate-specific antigen best practice policy. Oncology. 2000;14(2):267.
123. Daneshgari F, Taylor GD, Miller GJ, Crawford ED. Computer simulation of the probability of detecting low volume carcinoma of the prostate with six random systematic core biopsies. Urology. 1995;45(4):604-9.
124. Djavan B, Ravery V, Zlotta A, Dobronski P, Dobrovits M, Fakhari M, et al. Prospective evaluation of prostate cancer detected on biopsies 1, 2, 3 and 4: when should we stop? The Journal of urology. 2001;166(5):1679.
125. GORE JL, SHARIAT SF, MILES BJ, KADMON D, JIANG N, WHEELER TM, et al. Optimal combinations of systematic sextant and laterally directed biopsies for the detection of prostate cancer. The Journal of urology. 2001;165(5):1554-9.
126. Schröder F, Albertsen P, Boyle P, Candas B, Catalon A, Cheng C, et al. Early Detection and Screening for prostate cancer. Prostate cancer, 3rd International Consultation Eds: L Denis, G Bartsch, S Khoury, M Murai, A Partin Editions. 2003;21.
127. Epstein JI, Herawi M. Prostate needle biopsies containing prostatic intraepithelial neoplasia or atypical foci suspicious for carcinoma: implications for patient care. The Journal of urology. 2006;175(3):820-34.
128. ENLUND AL, Varenhorst E. Morbidity of ultrasound-guided transrectal core biopsy of the prostate without prophylactic antibiotic therapy. A prospective study in 415 cases. British journal of urology. 1997;79(5):777-80.
129. RODRIGUEZ LV, TERRIS MK. Risks and complications of transrectal ultrasound guided prostate needle biopsy: a prospective study and review of the literature. The Journal of urology. 1998;160(6):2115-20.
130. Rodríguez LV, Terris MK. Risks and complications of transrectal ultrasound. Current opinion in urology. 2000;10(2):111-6.
131. Goto Y, Ohori M, Scardino PT. Use of systematic biopsy results to predict pathologic stage in patients with clinically localized prostate cancer: a preliminary report. International journal of urology. 1998;5(4):337-42.

132. Sebo TJ, Bock BJ, Cheville JC, Lohse C, Wollan P, Zincke H. The percent of cores positive for cancer in prostate needle biopsy specimens is strongly predictive of tumor stage and volume at radical prostatectomy. The Journal of urology. 2000;163(1):174.
133. Stamey TA, Freiha F, McNeal J, Redwine E, Whittemore A, Schmid H. Localized prostate cancer. Cancer. 1993;71(S3):933-38.
134. Javidan J, Wood DP, editors. Clinical interpretation of the prostate biopsy. Urologic Oncology: Seminars and Original Investigations; 2003: Elsevier.
135. Barry MJ, Fowler Jr F, O'Leary MP, Bruskewitz R, Holtgrewe H, Mebust W, et al. The American Urological Association symptom index for benign prostatic hyperplasia. The Measurement Committee of the American Urological Association. The Journal of urology. 1992;148(5):1549.
136. Thorpe A, Neal D. Benign prostatic hyperplasia. The Lancet. 2003;361(9366):1359-67.
137. Barry MJ, Collins MM. 131 - Benign Prostatic Hyperplasia and Prostatitis. Goldman's Cecil Medicine (Twenty-Fourth Edition). Philadelphia: W.B. Saunders; 2012. p. 805-10.
138. Untergasser G, Madersbacher S, Berger P. Benign prostatic hyperplasia: age-related tissue-remodeling. Experimental gerontology. 2005;40(3):121-8.
139. Perry B, Langenstroer P. Benign Prostatic Hyperplasia. In: Editors-in-Chief: SJE, David BB, editors. xPharm: The Comprehensive Pharmacology Reference. New York: Elsevier; 2007. p. 1-3.
140. Bostwick DG. Prostatic intraepithelial neoplasia (PIN): current concepts. Journal of cellular biochemistry. 1992;50(S16H):10-9.
141. Bostwick DG, Brawer MK. Prostatic intra-epithelial neoplasia and early invasion in prostate cancer. Cancer. 1987;59(4):788-94.
142. Sakr W, Grignon D, Crissman J, Heilbrun L, Cassin B, Pontes J, et al. High grade prostatic intraepithelial neoplasia (HGPIN) and prostatic adenocarcinoma between the ages of 20-69: an autopsy study of 249 cases. In vivo (Athens, Greece). 1994;8(3):439.
143. Bostwick DG, Meiers I. Atypical small acinar proliferation in the prostate: clinical significance in 2006. Archives of pathology & laboratory medicine. 2006;130(7):952-7.
144. Iczkowski KA, MacLennan GT, Bostwick DG. Atypical small acinar proliferation suspicious for malignancy in prostate needle biopsies: clinical significance in 33 cases. The American journal of surgical pathology. 1997;21(12):1489.
145. Wang W, Bergh A, Damber JE. Morphological transition of proliferative inflammatory atrophy to high-grade intraepithelial neoplasia and cancer in human prostate. The Prostate. 2009;69(13):1378-86.
146. Heinisch M, Dirisamer A, Loidl W, Stoiber F, Gruy B, Haim S, et al. Positron emission tomography/computed tomography with F-18-fluorocholine for restaging of prostate cancer patients: meaningful at PSA< 5 ng/ml? Molecular Imaging and Biology. 2006;8(1):43-8.
147. Kelloff GJ, Choyke P, Coffey DS. Challenges in clinical prostate cancer: role of imaging. American Journal of Roentgenology. 2009;192(6):1455-70.
148. Thornbury JR, Ornstein DK, Choyke PL, Langlotz CP, Weinreb JC. Prostate Cancer What Is the Future Role for Imaging? American Journal of Roentgenology. 2001;176(1):17-22.
149. Bouchelouche K, Turkbey B, Choyke P, Capala J. Imaging prostate cancer: an update on positron emission tomography and magnetic resonance imaging. Current urology reports. 2010;11(3):180-90.
150. Brassell SA, Rosner IL, McLeod DG. Update on magnetic resonance imaging, ProstaScint, and novel imaging in prostate cancer*. Current opinion in urology. 2005;15(3):163.
151. Heidenreich A, Bellmunt J, Bolla M, Joniau S, Mason M, Matveev V, et al. EAU guidelines on prostate cancer. Part 1: screening, diagnosis, and treatment of clinically localised disease. European urology. 2011;59(1):61-71.

152. Edge SB, Compton CC. The American Joint Committee on Cancer: the 7th edition of the AJCC cancer staging manual and the future of TNM. Annals of surgical oncology. 2010;17(6):1471-4.
153. Cote RJ, Taylor CR. Prostate, bladder, and kidney. Immunomicroscopy: A Diagnostic Tool for the Surgical Pathologist Philadelphia, PA: WB Saunders Co. 1994:256-76.
154. Goel A, Abou-Ellela A, DeRose P, Cohen C. The prognostic significance of proliferation in prostate cancer: image cytometric quantitation of MIB-1. JOURNAL OF UROLOGIC PATHOLOGY. 1996;4:213-26.
155. Wiatrowska B, Robertson S, Crook J. Measures of proliferative activity in prostatic adenocarcinoma. JOURNAL OF UROLOGIC PATHOLOGY. 1997;6:131-8.
156. Greenlee RT, Hill-Harmon MB, Murray T, Thun M. Cancer statistics, 2001. CA: a cancer journal for clinicians. 2001;51(1):15-36.
157. Bolla M, Collette L, Blank L, Warde P, Dubois JB, Mirimanoff R-O, et al. Long-term results with immediate androgen suppression and external irradiation in patients with locally advanced prostate cancer (an EORTC study): a phase III randomised trial. The Lancet. 2002;360(9327):103-8.
158. Lamb DS, Denham JW, Mameghan H, Joseph D, Turner S, Matthews J, et al. Acceptability of short term neo-adjuvant androgen deprivation in patients with locally advanced prostate cancer. Radiotherapy and oncology: journal of the European Society for Therapeutic Radiology and Oncology. 2003;68(3):255.
159. Pilepich MV, Winter K, Lawton CA, Krisch RE, Wolkov HB, Movsas B, et al. Androgen suppression adjuvant to definitive radiotherapy in prostate carcinoma—long-term results of phase III RTOG 85–31. International Journal of Radiation Oncology* Biology* Physics. 2005;61(5):1285-90.
160. van den OUDEN D, Hop W, SCHRODER FH, Klein E. Progression in and survival of patients with locally advanced prostate cancer (T3) treated with radical prostatectomy as monotherapy. Commentary. The Journal of urology. 1998;160(4):1392-7.
161. Matthäus C, Bird B, Miljković M, Chernenko T, Romeo M, Diem M. Infrared and Raman microscopy in cell biology. Methods in cell biology. 2008;89:275-308.
162. Liu KZ, Xu M, Scott DA. Biomolecular characterisation of leucocytes by infrared spectroscopy. British journal of haematology. 2007;136(5):713-22.
163. Mostaço-Guidolin LB, Bachmann L. Application of FTIR spectroscopy for identification of blood and leukemia biomarkers: A review over the past 15 years. Applied Spectroscopy Reviews. 2011;46(5):388-404.
164. Movasaghi Z, Rehman S, ur Rehman DI. Fourier transform infrared (FTIR) spectroscopy of biological tissues. Applied Spectroscopy Reviews. 2008;43(2):134-79.
165. Petter C, Heigl N, Rainer M, Bakry R, Pallua J, Bonn G, et al. Development and application of Fourier-transform infrared chemical imaging of tumour in human tissue. Current medicinal chemistry. 2009;16(3):318-26.
166. Walsh MJ, German MJ, Singh M, Pollock HM, Hammiche A, Kyrgiou M, et al. IR microspectroscopy: potential applications in cervical cancer screening. Cancer letters. 2007;246(1):1-11.
167. Rehman S, Movasaghi Z, Darr JA, Rehman IU. Fourier transform infrared spectroscopic analysis of breast cancer tissues; identifying differences between normal breast, invasive ductal carcinoma, and ductal carcinoma in situ of the breast. Applied Spectroscopy Reviews. 2010;45(5):355-68.
168. Baker MJ, Gazi E, Brown MD, Shanks JH, Clarke NW, Gardner P. Investigating FTIR based histopathology for the diagnosis of prostate cancer. Journal of biophotonics. 2009;2(1-2):104-13.
169. Baker MJ, Gazi E, Brown MD, Shanks JH, Gardner P, Clarke NW. FTIR-based spectroscopic analysis in the identification of clinically aggressive prostate cancer. British journal of cancer. 2008;99(11):1859-66.

170. Kwak JT, Hewitt SM, Sinha S, Bhargava R. Multimodal microscopy for automated histologic analysis of prostate cancer. BMC cancer. 2011;11(1):62.
171. Lewis PD, Lewis KE, Ghosal R, Bayliss S, Lloyd AJ, Wills J, et al. Evaluation of FTIR Spectroscopy as a diagnostic tool for lung cancer using sputum. BMC cancer. 2010;10(1):640.
172. Sahu RK, Mordechai S. Spectral signatures of colonic malignancies in the mid-infrared region: from basic research to clinical applicability. Future Oncology. 2010;6(10):1653-67.
173. Travo A, Piot O, Wolthuis R, Gobinet C, Manfait M, Bara J, et al. IR spectral imaging of secreted mucus: a promising new tool for the histopathological recognition of human colonic adenocarcinomas. Histopathology. 2010;56(7):921-31.
174. Krafft C, Sobottka SB, Geiger KD, Schackert G, Salzer R. Classification of malignant gliomas by infrared spectroscopic imaging and linear discriminant analysis. Analytical and bioanalytical chemistry. 2007;387(5):1669-77.
175. Wehbe K, Pineau R, Eimer S, Vital A, Loiseau H, Déléris G. Differentiation between normal and tumor vasculature of animal and human glioma by FTIR imaging. Analyst. 2010;135(12):3052-9.
176. Eikje NS, Aizawa K, Sota T, Ozaki Y, Arase S. Identification and characterization of skin biomolecules for drug targeting and monitoring by vibrational spectroscopy. The open medicinal chemistry journal. 2008;2:38.
177. Hammody Z, Argov S, Sahu R, Cagnano E, Moreh R, Mordechai S. Distinction of malignant melanoma and epidermis using IR micro-spectroscopy and statistical methods. Analyst. 2008;133(3):372-8.
178. Quaroni L, Casson AG. Characterization of Barrett esophagus and esophageal adenocarcinoma by Fourier-transform infrared microscopy. Analyst. 2009;134(6):1240-6.
179. Le Naour F, Bralet M-P, Debois D, Sandt C, Guettier C, Dumas P, et al. Chemical imaging on liver steatosis using synchrotron infrared and ToF-SIMS microspectroscopies. PloS one. 2009;4(10):e7408.
180. Bird B, Miljkovic M, Romeo MJ, Smith J, Stone N, George MW, et al. Infrared micro-spectral imaging: distinction of tissue types in axillary lymph node histology. BMC Clinical Pathology. 2008;8(1):8.
181. Liu K-Z, Jia L, Kelsey SM, Newland A, Mantsch H. Quantitative determination of apoptosis on leukemia cells by infrared spectroscopy. Apoptosis. 2001;6(4):269-78.
182. Ami D, Neri T, Natalello A, Mereghetti P, Doglia SM, Zanoni M, et al. Embryonic stem cell differentiation studied by FT-IR spectroscopy. Biochimica et Biophysica Acta (BBA)-Molecular Cell Research. 2008;1783(1):98-106.
183. Kelly JG, Nakamura T, Kinoshita S, Fullwood NJ, Martin FL. Evidence for a stem-cell lineage in corneal squamous cell carcinoma using synchrotron-based Fourier-transform infrared microspectroscopy and multivariate analysis. Analyst. 2010;135(12):3120-5.
184. Walsh MJ, Hammiche A, Fellous TG, Nicholson JM, Cotte M, Susini J, et al. Tracking the cell hierarchy in the human intestine using biochemical signatures derived by mid-infrared microspectroscopy. Stem Cell Research. 2009;3(1):15-27.
185. Bhargava R, Fernandez DC, Hewitt SM, Levin IW. High throughput assessment of cells and tissues: Bayesian classification of spectral metrics from infrared vibrational spectroscopic imaging data. Biochimica et Biophysica Acta (BBA)-Biomembranes. 2006;1758(7):830-45.
186. Kendall C, Isabelle M, Bazant-Hegemark F, Hutchings J, Orr L, Babrah J, et al. Vibrational spectroscopy: a clinical tool for cancer diagnostics. Analyst. 2009;134(6):1029-45.
187. Lattouf JB, Saad F. Gleason score on biopsy: is it reliable for predicting the final grade on pathology? BJU international. 2002;90(7):694-8.
188. Mackanos MA, Contag CH. FTIR microspectroscopy for improved prostate cancer diagnosis. Trends in biotechnology. 2009;27(12):661-3.

189. Bellisola G, Sorio C. Infrared spectroscopy and microscopy in cancer research and diagnosis. American journal of cancer research. 2012;2(1):1.
190. Gazi E, Baker M, Dwyer J, Lockyer NP, Gardner P, Shanks JH, et al. A correlation of FTIR spectra derived from prostate cancer biopsies with Gleason grade and tumour stage. European urology. 2006;50(4):750-61.
191. Paluszkiewicz C, Kwiatek WM. Analysis of human cancer prostate tissues using FTIR microspectroscopy and SRIXE techniques. Journal of Molecular Structure. 2001;565:329-34.
192. Stuart B. Infrared Spectroscopy: Fundamentals and Applications. 2004. JohnWiley & Sons, Ltd. 2000.
193. Steele D. Infrared spectroscopy: theory. Handbook of Vibrational Spectroscopy. 2006.
194. Stuart BH. Infrared Spectroscopy of Biological Applications: An Overview. Encyclopedia of Analytical Chemistry: John Wiley & Sons, Ltd; 2006.
195. Niemantsverdriet JW. Spectroscopy in catalysis: John Wiley & Sons; 2007.
196. Pavia DL. Introduction to spectroscopy: CengageBrain. com; 2009.
197. Finkenthal D. Introduction to the electromagnetic spectrum, General atomic. 1996.
198. Smith BC. Fundamentals of Fourier transform infrared spectroscopy: CRC press; 2011.
199. Smith GD, Palmer RA. Fast Time-Resolved Mid-Infrared Spectroscopy Using an Interferometer. Handbook of Vibrational Spectroscopy. 2002.
200. Specac. Golden Gate ATR [Internet]. Available from: www.specac.com
201. Yano K, Sakamoto Y, Hirosawa N, Tonooka S, Katayama H, Kumaido K, et al. Applications of Fourier transform infrared spectroscopy, Fourier transform infrared microscopy and near-infrared spectroscopy to cancer research. Journal of Spectroscopy. 2003;17(2-3):315-21.
202. Othman NH, El-Tawil SG. FTIR Spectroscopy: A New Technique In Cancer Diagnoses.
203. Olsztyńska-Janus S, Szymborska-Małek K, Gąsior-Głogowska M, Walski T, Komorowska M, Witkiewicz W, et al. Spectroscopic techniques in the study of human tissues and their components. Part I: IR spectroscopy. Acta Bioeng Biomech. 2012;14:101-15.
204. Singh B, Gautam R, Kumar S, Kumar VB, Nongthomba U, Nandi D, et al. Application of vibrational microspectroscopy to biology and medicine. Current Science (Bangalore). 2012;102(2):232-44.
205. Suburu J, Chen YQ. Lipids and prostate cancer. Prostaglandins & other lipid mediators. 2012;98(1):1-10.
206. Santos CR, Schulze A. Lipid metabolism in cancer. FEBS Journal. 2012;279(15):2610-23.
207. Zhang F, Du G. Dysregulated lipid metabolism in cancer. World journal of biological chemistry. 2012;3(8):167.